Institute of Translational Medicine

Department of Molecular and Clinical Cancer Medicine

Evaluation of UHRF1 Expression in Pancreatic Cancer

Thesis submitted in accordance with the requirements of the University of Liverpool for the degree of Doctor in Philosophy by

Wafa Abualainin

April 2014

Supervisors: Dr. Eithne Costello and Prof. John P Neoptolemos

Declaration

I certify that this is an original piece of work performed in the Department of Molecular and Clinical Cancer Medicine, University of Liverpool. All of the work included in this thesis was undertaken by myself, except for where it is stated otherwise. This work has not been submitted or used at any other University.

Wafa Abualainin

To my gorgeous daughters Raghad and Layan
and
To the memory of my beloved brother Muhammad

Abstract:

The ubiquitin-like with PHD and ring finger domains 1 (UHRF1) is a DNA binding protein, involved in epigenetic regulation. UHRF1 expression varies in different cancers, and its role in pancreatic ductal adenocarcinoma (PDAC) is unknown. PDAC is a devastating disease with an overall 5-year survival rate of less than 5 %. Here we report that UHRF1 is frequently overexpressed in PDAC and negatively regulates Keap1, an important component of the Nrf2-mediated cellular stress response pathway. UHRF1 was expressed in 114 of 132 (86%) pancreatic tumours, was associated with larger tumour size (p= 0.02) and had higher expression in tumours compared to matched preneoplastic (PanIN) lesions (n=9). UHRF1 expression varied at different phases of the cell cycle with a peak level at G2/M. Moreover, siRNA-mediated depletion of UHRF1 was associated with a G2/M phase block and induced apoptosis. UHRF1 protein expression levels varied in different PDAC cell lines and reflected the DNA methylation levels in examined sequences. UHRF1 knockdown reduced global DNA methylation in *LINE-1* and *Alu-V* repetitive elements and tumour suppressor-specific ($p16^{Ink4a}$ and *RASSF1*) promoter methylation. Combining UHRF1 knockdown with 5-aza-deoxycytidine treatment resulted in restoration of P16 levels compared to controls siRNA samples. KEAP1 expression loss was previously reported in ~70 % of PDAC cases. Here we established that the Keap1 promoter is hypermethylated in pancreatic cancer cells. UHRF1 knockdown was accompanied by a reduction in Keap1 promoter methylation, restoration of KEAP1 protein, loss of NRF2 protein and corresponding loss of NRF2 downstream gene expression. We showed strong evidence that Keap1 expression is regulated by its promoter methylation, as KEAP1 expression was restored following 5-aza-deoxycytidine treatment. In PDAC tumour specimens (n=124), an inverse

relationship between UHRF1 and KEAP1 expression was observed (p=0.002). In summary, we have shown a role for UHRF1 in pancreatic cancer growth and promoter methylation. Moreover, we have discovered an important function for UHRF1 in controlling KEAP1 expression and consequently regulating the KEAP1/NRF2 stress response pathway.

Acknowledgment:

I give thanks to Allah for protection and for strengthening me to do my study from the beginning to the end. My special and heartfelt thanks to my primary supervisor Dr. Eithne Costello for the opportunity to undertake this research in the Department of Molecular and Clinical Cancer Medicine, Institute of Translational Medicine, University of Liverpool (UoL), and for her guidance, support and patience in every step during my study. Without her, my PhD would never have been done. I thank my secondary supervisor Prof. John Neoptolemos.

I give deep thanks to Hamad Medical Corporation (HMC, Doha- Qatar) for funding me for my PhD and for making my dream come true. I thank all who supported me from HMC staff and in particular the Molecular Genetics Laboratory team; Ajayeb Almeri, Ramin Badii, Ali Alavi, Beena Nazer, Nader Aldwaik, Mahmoud Qasim, Mohamad Mansour, Mohamad Erfan, Amr Alsharabasi, Aisha Zyara, Hanan Nasrallah, Rowa Siam and Atiya Saif.

I thank the entire UoL group in the Molecular and Clinical Cancer Medicine Department for supporting me in one way or another in the completion of this thesis. I especially thank Claire Jenkinson and Anthony Evans for sharing their knowledge and never refusing to help me with any simple or difficult laboratory experiments, data analysis and writing my thesis. I also thank them for being wonderful office and Lab mates. I thank Traintafillos Lilglou for his patience and support in supervising the methylation experiments. I warmly thank William Greenhalf, Carlos Rubbi, Joseph Slupsky, Christopher Goldring, Neil Kitteringham, Chris Halloran, Prof. Fiona Campbell, Timothy Andrews, Prof. Paula Ghaneh, Lawrence Barrera, Fran Oldfield, Owain Jones, Sumit Nandi, Elizabeth Garner, Li Yan, James Nicholson, Robert Ferguson, Katharine Hand, Thompson Gana, Asma Sultana, Elizabeth Tweedle, Dammy Olayanju, Ian Copple, Holly Bryan,

Ahmad Al-Khafaji, Victoria Shaw, Paul Sykes, George Nikolaidis, Alexandros Daskalos, Taoufik Nedjadi, Khalid Dijani, Mark Aspinall-O'Dea, Sarah Tonack, Adam Ware and Taha Elmitwally.

I thank Thamir Ismail and his family for their great support and for treating me and my children as family during my study in the UK. I thank my grandmother Samera Mosa, my uncles: Ghassan Baddoura, Hisham Faris, Mahmoud Baddoura, Ibrahim Baddoura, Aziz Baddoura, Naeem Asiri and Adel Saleh, and my aunts: Huda Baddoura, Iman Nasser, Reem Mansour, Maha Shanbor, Samar Bayaa, Rabeha Ebwini and Mhasen Zain Aldeen for their encouragements. Also I would like to thank Ghazi Alkhatib, Mayson Alheyari, Sri Listari Romo and their families.

I deeply thank my amazing cousins: Nada Faris, Yasmine Baddoura, Sawsan Faris, Maram Baddoura, Riham Baddoura, Nadine Baddoura, Yasmeen Faris, Sawsan Abualainin, Hosam Baddoura, Ameen Faris, Ahmad Adel, Marwa Adel, Mona Assem and Noha Adel. I thank my fabulous friends: Ula Kokash, Hadeel Abu-Jalalah, Moza Al-Kowari, Fatima Khan, Asmaa Salman, Mashael Lari, Ghadder Alswaidi, Famita Alobaidli and Rania Attieh, for their support, being thoughtful, and helping me to relieve my stress during my study.

Last but not least, I would like to thank my wonderful family and I hope I have made them proud: my father Mahmoud Abualainin, my mother Laila Baddoura, my sisters and brothers: Nadia, Ali, Ibrahim, Rima Taha, Mostafa, Sara and Areej Alan; who encouraged me and for their love, blessings and good wishes. I would especially like to thank my brother Ali Abualainin again for his great support, encouragement, bigheartedness and for standing beside me in every happy and hard moment during my PhD. I endlessly thank my awesome and beloved children Raghad and Layan for their patience until I ended my PhD; even when they were suffering of homesickness.

Publications and Posters:

Findings of this study have been presented in the following manuscript:

UHRF1 regulates Keap1 expression in pancreatic cancer**,** **Wafa Abu-Alainin**, T Liloglou, Fiona Campbell, Timothy Andrews, Christopher Goldring, Neil Kitteringham, Taoufik Nedjadi, Thompson Gana, William Greenhalf, John P Neoptolemos, and Eithne Costello .*Submitted*

Findings of this study have been presented at the following research meetings:

Nuclear UHRF1 is overexpressed in pancreatic cancer and its depletion from PDAC cell lines leads to cell cycle arrest and increased apoptosis. Authors: **Wafa AbuAlainin**; Adam Ware; Traintafillos Lilglou; Fiona Campbell; William Greenhalf; John Neoptolemos and Eithne Costello.

- Abstract was published in Pancreatology, Volume 13, Issue 3, Pages S27-S28, May 2013.
- Poster presented at 45th Annual Meeting of the European Pancreatic Club June 26–29, 2013 Zurich, Switzerland.

During my study I contributed to the following studies:

Analysis of the effects of K-Ras depletion on the growth characteristics of pancreatic cancer cell lines. Robert Ferguson, **Wafa AbuAlainin**, John Neoptolemos, Eithne Costello, William Greenhalf.

Analysis of the effect of K-Ras depletion on G2 cyclins, in pancreatic cancer cell lines.

Robert Ferguson, Adam Ware, **Wafa AbuAlainin**, John Neoptolemos, Eithne Costello, William Greenhalf. Abstract was published in Pancreatology May 2013 (Vol. 13, Issue 3, and Page S29). Poster presented at 45th Annual Meeting of the European Pancreatic Club June 26–29, 2013 Zurich, Switzerland.

List of abbreviations:

ADP	Adenosine diphosphate
AP	Acute pancreatitis
APS	Adenosine 5' phosphosulfate
ARE	Antioxidant response element
ATP	Adenosine triphosphate
BCA	Bicinchoninic acid
BIO	Biotinylated
BSA	Bovine serum albumin
BTB	Broad complex-tramtrack and bric-a-brac
C1	Protein kinase C conserved region 1
Caspases	Cysteine-dependent aspartate-specific proteases
CdK	Cyclin dependent kinase
CDKN2A	Cyclin dependent kinase inhibitor 2A
CKIs	Cyclin dependent kinase inhibitors
CP	Chronic pancreatitis
CpG	Cytosine-phosphate guanine
CYP2A5	Cytochrome P 450 isoform 2A5
DAB	DiAminobenzidine
DAPI	Diamidino-2-phenylindole
dATPαS	Deoxyadenosine alfa-thio triphosphate
DMSO	Dimethyl sulfoxide
DNA	Deoxyribonucleic acid
DNMT1	DNA methyltransferase 1
dNTP	Deoxyribonucleotide triphosphate
DPC4	Deleted in pancreatic cancer 4
DTT	Dithiothreitol
E	Enzyme
E1	Ub-activating enzyme
E2	Ub-conjugating enzyme
E3	Ub-ligase enzyme
ECL	Enhanced chemiluminescence
EDTA	Ethylenediaminetetraacetic acid
EN	Endonuclease
ERK	Extracellular signal-regulated kinase
FACS	Fluorescence-activated cell sorting
FBS	Fetal bovine serum

GCLC	Glutamate-cysteine ligase catalytic
HCP	Hereditary chronic pancreatitis
HD	Homozygous deletion
HDAC	Histone deacetylase
HO-1	Heme oxygenase 1
HRP	Horseradish peroxidise-conjugated
ICBP 90	Inverted CCAAT box binding protein of 90 kDa
ICC	Immunocytochemistry
IHC	Immunohistochemisty
IVR	Intervening linker domain
Keap1	Kelch-like ECH- associated protein 1
LINE	Long interspersed nuclear element
LOH	Loss of heterozygosity
LTR	Long terminal repeat
MCN	Mucinous cystic neoplasm
Neh	Nrf2-ECH-homology
NP 95	Nuclear Protein of 95 KD
NQO1	NADPH quinone oxidoreductase
NRF2	Nuclear factor erythoid 2-related factor 2
ORF	Open reading frame
PAGE	Polyacrylamide gel electrophoresis
PanIN	Pancreatic intraepithelial neoplasia
PBS	Phosphate buffered saline
PC	Pancreatic cancer
PCR	Polymerase chain reaction
PDAC	Pancreatic ductal adenocarcinoma
PET	Pancreatic endocrine tumor
PHD	Plant homeo domain
PI	Propidium iodide
PPi	Pyrophosphate
RASSF	Ras association domain-containing protein
RING	Really interesting new gene finger domain
ROS	Reactive oxygen species
RT	Reverse transcriptase
S or SUB	Substrate
SAM	S-adenosyl-methionine
SDS	Sodium dodecyl sulfate
SFN	Sulforaphane

SINE	Short interspersed nuclear elements
siRNA	Small Interfering RNA
SRA	Set and Ring Associated domain
TGF-β	Transforming growth factor – beta
TMA	Tissue microarray
TSGs	Tumour suppressor genes
Ub	Ubiquitin.
UBL	Ubiquitin like domain
UHRF1	The Ubiquitin-like with PHD and RING-finger domain 1

Abbreviations of measuring unite:

g	Gram
U	Unit
mL	Millilitre
µL	Microlitre
mM	Millimolar
L	Liter
µg	Microgram
bp	Base pair
h	Hour
sec	Second
min	Minute
pmol	Picomole
kDa	Kilo Dalton

Table of contents:

List of figures:

List of tables:

Chapter 1:

Introduction

1 Introduction:

1.1 Hallmarks of cancer:

Genetic mutations or alterations in the expression of tumour suppressor genes (TSGs) or oncogenes underlie cancer development. These genes are important for normal cell proliferation, differentiation, and homeostasis. Mutations in, or alteration of expression of TSGs most often result in loss of functional proteins, whereas mutation or overexpression of oncogenes result in gain of function and promote tumorigenesis [1]. Although over 200 different types of human cancer have been identified, they share common features. At least six alterations in a cell's physiology, independent of its environment, are required for a cell to become malignant. This includes self-sufficiency from growth factor signals, insensitivity to anti-growth signals, evasion of apoptosis, limitless replicative potential, angiogenesis within the tumour mass and tissue invasion/metastasis [2]. Another four cancer hallmarks have been latterly added to the list including genome instability, inflammation [3], abnormal cellular metabolism and evading immune destruction [4].

1.2 Introduction to pancreatic cancer:

Pancreatic cancer is almost always a lethal disease with a very poor survival rate. The Cancer Research UK (CRUK) statistics in 2010 reported that 157,000 cases were diagnosed with cancer in the UK, and 5 % of these cases were pancreatic cancer (www.cancerresearchuk.org). Thus, pancreatic cancer is rated as the 10^{th} most common cancer. It is the 5^{th} most common cause of death in the UK, with 5 year survival observed in less than 5 % of diagnosed patients. Pancreatic cancer affects males and females equally and most patients diagnosed are aged 60 years old or

above. People develop pancreatic cancer without identifiable symptoms; therefore, most pancreatic cancer cases are diagnosed in very late stages of the disease and frequently have metastasis at the time of diagnosis [5]. Many risk factors play roles in the development of pancreatic cancer, such as age, smoking, excess weight, alcohol and diet. Several medical conditions have been linked to pancreatic cancer development including diabetes, pancreatitis, family history and genetic mutations [6].

Pancreatic cancers mostly develop in the head of the pancreas and less commonly in the body or in the tail. Moreover, there are different types of pancreatic cancer, either exocrine or endocrine. Almost 80 % of pancreatic cancer cases can be classified as exocrine, which primarily develop tumour masses in the duct system of the exocrine pancreas leading to ductal adenocarcinoma (PDAC). The other exocrine cancers are; cystic tumours, cancer of the acinar cells and sarcoma of the pancreas. Endocrine pancreatic cancer is very rare and includes gastrinomas, insulinomas, somatostatinomas, VIPomas and glucogonomas (www.cancerresearchuk.org). In 2010 the World Health Organization (WHO) published a new edition for pancreatic cancer classification, subtypes and grades [7]. Pancreatic cancers are known to be highly resistant to chemotherapy treatment, although chemotherapy has been shown to benefit patients in both the advanced and adjuvant settings [8-11]. Currently surgery offers the best hope of cure. However, only a minority of patients (approximately 20 %) are eligible for surgery [12, 13].

1.3 Pathophysiology of pancreatic cancer:

The normal pancreas is composed of 2 main cell types which have endocrine (hormones) and exocrine (digestive enzymes) functions. Hormones maintain the level of blood sugar and digestive enzymes are released to the duodenum through the ductal system of the pancreas for food digestion and pH maintenance [14]. As the main endocrine function of the pancreas is to regulate the glucose level in the blood, 80 % of pancreatic cancer patients are diagnosed with diabetes. It is still unclear if pancreatic cancer causes diabetes or diabetes promotes pancreatic cancer development [15]. Several clinical and pathological changes arise in the organ as a result of cancer development, and are mainly solid or cystic [16]. The most common pancreatic neoplasm is pancreatic ductal adenocarcinoma, which causes obstruction in the ductal system of the pancreas as well as the bile duct. Obstruction of the bile duct causes jaundice which is one of the complications developed by pancreatic cancer patients. Also steatorrhoea, an excess of fat in stools, may result due to duct obstruction. Patients with metastasis to the liver may have enlarged liver. As most pancreatic cancer develop in the head of the pancreas, most patients develop back pain [17].

1.4 Clinical trials for PDAC treatment:

In general terms, the main approaches for cancer treatment are surgical removal of the tumour mass and irradiation and chemotherapy, depending on the tumour type and stage of the disease. Recently immunotherapy has been proposed as an important cancer treatment [18]. Chemotherapy may be used to improve symptoms and prolong survival of cancer patients; it is also needed following surgery to reduce the risk of recurrent tumour growth. In clinical trials,

combinations of chemotherapy and surgery or radiotherapy have clearly demonstrated improvement in survival compared to surgery or radiotherapy alone in several types of cancers [19]. Generally anti-cancer drugs target distinct pathways to induce tumor cell death. Therefore the cell's response to the anti- cancer drugs differs according to the disturbed pathway. Anti-cancer drugs often target cells by interfering with DNA synthesis and replication within the cell cycle [20]. Many drugs are under validation in clinical trials, to minimize their side effects, and to improve outcome. Examples of chemotherapeutic drugs and their mechanisms of action are reviewed elsewhere [4, 13]. The efficacy of these chemotherapeutic drugs can be significantly reduced due to genetic alteration resulting in drug resistance [20]. Clinical trials have shown survival advantages when several drugs are combined instead of exposing patients to a single specific drug as a first line therapy. Gemcitabine combined with capecitabine (GEM-CAP) showed survival advantages compared to gemcitabine (GEM) alone, in advanced and metastatic pancreatic cancer [9]. FOLFIRINOX is a combination of oxaliplatin, irinotecan, fluorouracil (FU) and leucovorin that resulted in survival benefits in patients with metastatic pancreatic cancer compared to gemcitabine [21]. New biological therapies are undergoing clinical trials in mouse models and in humans. One such example is vandetanib, a tyrosine kinases inhibitor that inhibits cell growth [22]. This drug is currently being evaluated in the VIP trial, the aim of which is to compare GEM treatment alone to GEM combined with vandetanib in advanced pancreatic cancer patients. The Phase III European Study Group for Pancreatic Cancer-3 (ESPAC-3) trial showed that GEM and FU with folic acid were equally effective in the adjuvant setting. Based on ESPAC-3 the most efficient drugs used for pancreatic cancer treatment are GEM, FU and folic acid. In addition, patients in ESPAC-3 who received full six cycles of treatment after surgery

showed improved survival compared to patients who received less than six cycles of treatment. Also there was no significant difference in survival outcome between patients treated early or later after surgery. This study suggests that delaying the start time for chemotherapeutic treatment allows the pancreatic cancer patients to recover from surgery, as patients who feel stronger are more likely to complete the full six cycles of treatment [10].

1.5 Genetics of pancreatic cancer:

The pancreatic cancer tumour mass is multi-cellular, comprising a combination of pancreatic cancer cells, pancreatic cancer stem cells and tumour stroma. The tumour stroma itself contains many cell types. A variety of different cancer pathways are affected in this tumour type [23]. A progression model for pancreatic cancer has been derived, in which the cancer is shown to develop through different stages. Changes in benign epithelial cells and the development of precursor lesions have been documented. The most common pancreatic cancer precursor lesions are the pancreatic intraepithelial neoplasia (PanINs), which arise with many morphological, histological and genetic or epigenetic changes (Figure 1-1) [24].

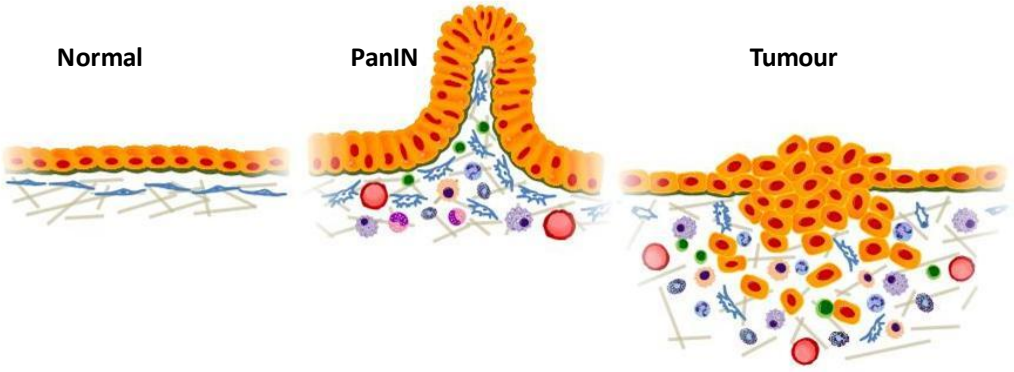

Figure 1-1 : Stages of pancreatic cancer development. The normal pancreatic ductal cell transforms to cancer cells through intermediate stages of PanINs. This figure is taken from [24] with the authors' permission.

Pancreatic cancer development has been associated with over sixty genetic alterations, most of which are point mutations [8]. These alterations result in disruption of 12 cellular pathways; apoptosis, DNA damage, cell cycle transition at G1/S, Hedgehog signaling, homophilic cell adhesion, integrin signaling, c-Jun N-terminal kinase signaling, KRAS signaling, regulation of invasion, small GTPase-dependent signaling, TGF-β signaling and Wnt/Notch signaling. Not all of the 12 pathways are disrupted in every pancreatic cancer and every pathway is linked to a gene mutation [8]. Genomic instability in pancreatic cancer occurs early during tumorigenesis, as over 50 % of genomic rearrangements are detected in both the primary tumour and in metastases [25].

The K-RAS oncogene is the most common mutationally activated oncogene in pancreatic cancer and is activated in 90 % of cases. It plays a role in several signaling pathways that involve cell growth [5, 23, 26-29]. K-Ras mutations result in K-RAS GTPase activation which mediates stimulation of several signaling pathways, such as the RAF-mitogen-activated protein kinase,

phosphoinositide-3-kinase (PI3K) and RalGDS pathways (Figure 1-2). The continuous activation of K-Ras plays a role in the cell growth, proliferation and survival [30].

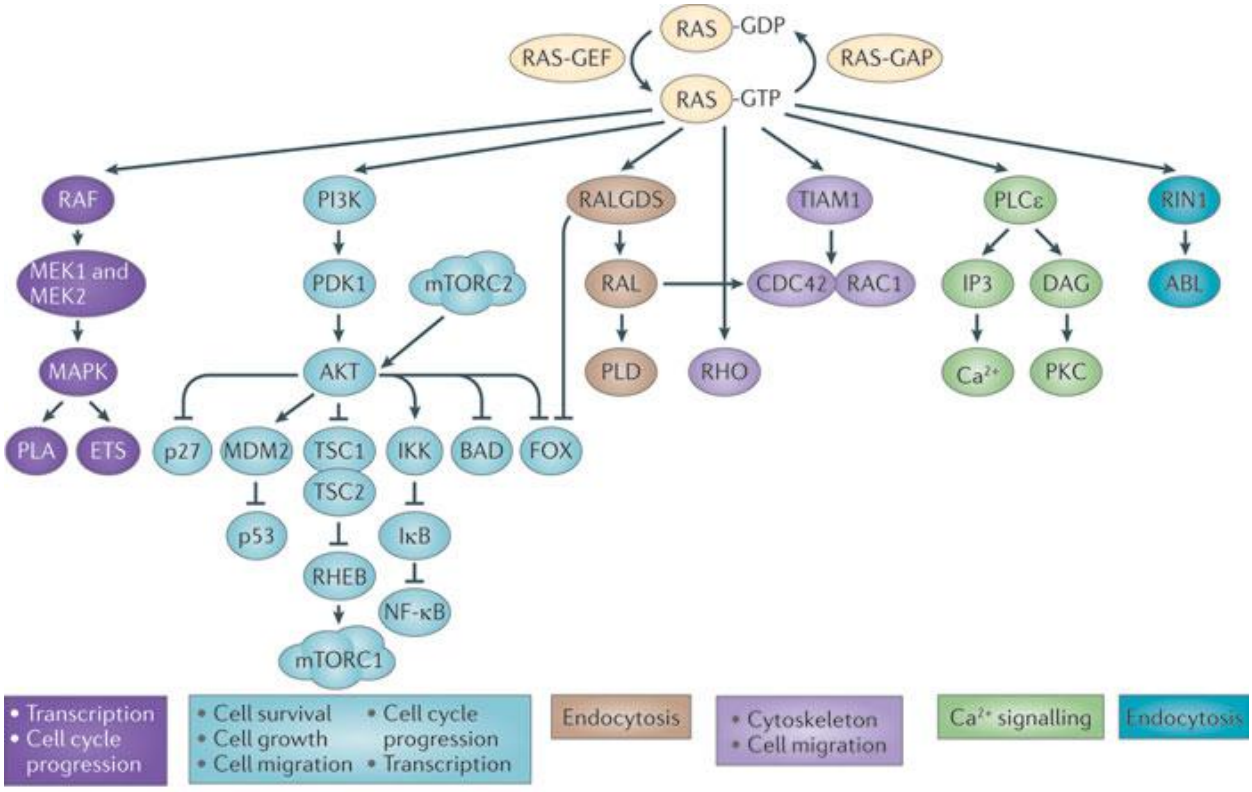

Figure 1-2. RAS signaling pathway. RAS regulates different pathways involved in cell growth. This figure is taken from [31] without permission.

The most commonly inactivated TSG in pancreatic cancer is the cyclin dependent kinase inhibitor 2A gene or Inhibitor of CDK4 (CDKN2A/p16^{INK4a}), which encodes the P16 protein. P16 plays a role in the initiation and progression of pancreatic cancer. Other TSGs are inactivated in pancreatic cancer, such as TP53 and SMAD4. These genetic alterations start early in PDAC and are detected in the precursor lesions [5, 23, 26-29].

1.6 Epigenetic changes in pancreatic cancer:

In addition to the well-characterized genetic changes, epigenetic changes play a fundamental role in pancreatic cancer development and progression [32]. Amongst these, DNA methylation is a well-known epigenetic mechanism which influences pancreatic cancer through the silencing of TSG promoters. The CDKN2A gene [33] and several other genes in pancreatic cancer cells have been activated following treatment with demethylation drugs [34]. UHRF1 (ubiquitin-like, containing PHD and RING finger domains 1), contributes to the maintenance of DNA methylation by recruiting DNMT1 to its hemimethylated DNA substrate [35]. The enzyme DNA methyltransferase 1 (DNMT1) is considered responsible for maintaining methylation patterns of methylated cytosine residues from the parent strand of DNA to the newly synthesised daughter strand [36]. A recent study analyzed proteins from pancreatic cancer specimens and normal pancreas in order to identify new protein markers for pancreatic cancer. This study reported over-expression of UHRF1 in pancreatic cancer but not in normal pancreas [37]. No descriptive or functional studies of UHRF1 in this cancer type have been published. In this thesis we have investigated some of UHRF1's roles in pancreatic cancer.

1.7 Ubiquitin-like, containing PHD and RING finger domains (UHRF1):

UHRF1, also known as ICBP90, is a DNA binding and multi-domain protein [38, 39]. UHRF1 is a member of the UHRF family that comprises 4 members: UHRF1, UHRF2, UHRF3 and UHRF4. The functions of UHRF4 have not been reported, but it is listed in the gene database (gene bank). The structures of UHRF3 and UHRF4 are different from UHRF1 [40]. UHRF2 has the same structure as UHRF1 but it has a different function. It is involved in cell cycle regulation and it has

been reported to interact with UHRF1 [41]. The UHRF1 protein contains different domains in its structure; the ubiquitin-like domain (UBL), 1st Tudor domain, 2nd Tudor domain, Plant Homeo Domain (PHD), Pre-PHD, Set and Ring associated domain (SRA) and the really interesting new gene domain (RING) [42] (Figure 1-3).

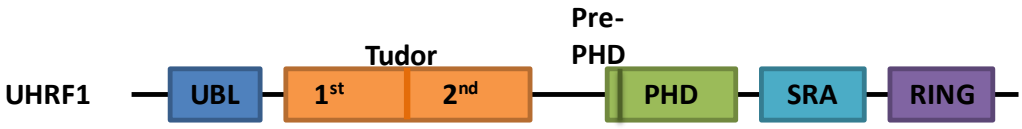

Figure 1-3: UHRF1 protein structure. UHRF1 domains; UBL: ubiquitin-like domain, 1st Tudor domain, 2nd Tudor domain, PHD: Plant Homeo domain, Pre-PHD, SRA: Set and Ring associated domain and RING: really interesting new gene domain.

UHRF1 has a critical role in cell growth and proliferation [38, 40]. UHRF1 is involved in epigenetic regulation during cell division, including DNA methylation maintenance and histone modification. In our study we focused on the role of UHRF1 in DNA methylation maintenance in pancreatic cancer cells. UHRF1 binds to the hemimethylated DNA via its SRA domain, mutations in the SRA domain results in loss of UHRF1 ability to bind to the DNA [43, 44]. Given that histone-modification is an important mechanism for regulation of gene expression, UHRF1 recruits histone methyltransferase to the histone H3 tail [45, 46]. UHRF1 recognizes the H3 tail by either its PHD domain [47, 48] or by the action of both tudor and PHD domains at the same time [49]. The RING domain is responsible for the ubiquitin E3 ligase activity of UHRF1, which reveals the importance of UHRF1 in cell regulation and growth [38]. It is still unknown if UHRF1 domains act in a dependent or independent manner from each other [50]. UHRF1 stability is maintained by protein-protein interaction with ubiquitin specific processing protease 7 (USP7), also known herpes virus-associated ubiquitin specific processing protease 7 (HAUSP), an

important protein required to activate DNMT1. UHRF1 and DNMT1 form a complex with USP7 in-order to successfully methylate the DNA [51]. A recent study showed that UHRF1 phosphorylation in the M-phase, results in USP7-UHRF1 complex dissociation, leading to a reduction of UHRF1 steady-state level. This study suggests that maintained levels of UHRF1 are important for regulating cellular proliferation [52]. UHRF1 stability under normal conditions and in response to DNA damage is controlled by $SCF^{\beta\text{-}TrCP}$ with ubiquitin E3 ligase activity [53]. UHRF1 in mouse is called Np95 and its endogenous expression in normal T-cells shows highest levels at S phase and lowest levels at G2/M, while in tumour T-cells its expression is not changed during cell cycle [39, 54]. UHRF1 is overexpressed in several types of human cancers [55] such as bladder [56, 57], breast [58, 59], colorectal [60, 61] prostate [62] and lung cancer [63, 64]. UHRF1 overexpression induced cancer transformation in hepatic cells [65]. UHRF1 overexpression was observed in pancreatic cancer, but the study lacked any analysis of the functional role of UHRF1 in pancreatic cancer [37].

1.7.1 The mechanism of ubiquitin (UB) enzymatic activity:

The ubiquitination of proteins is an important process for regulating degradation and determining the half-life and expression levels of proteins in the cell. This targeting for degradation depends on a number of enzymes classed as E1, E2 and E3, with each acting to form a cascade reaction. E1 acts as the first activating enzyme in the ubiquitination pathway, activating UB for subsequent transferral to E2 enzymes. E2s act as carriers or conjugating enzymes that mediate E3 action on the targeted protein. E3 UB ligases recognise specific proteins and facilitate ubiquitin conjugation to then target the protein to the 26S proteasome for degradation [66].

1.8 Cell cycle regulation and apoptosis:

1.8.1 Cell cycle regulation:

The cell cycle is the process where cells undergo replication through four different phases including, G1, S, G2 and M; this process is controlled by a complex of many activators or inhibitors. The G1 phase, known as the cell growth phase, is where the cell increases in size. During G1 cells produce crucial proteins for use in subsequent phases of the cell cycle. S phase follows where new DNA synthesis takes place and the cell duplicates its DNA contents. The cell prepares for division during G2 then forms two new cells during M phase, splitting the DNA and cellular components in half. Following M phase, the cells reenters the cycle at G1/G0 [67]. The cell cycle is regulated by enzymes essential for progression beyond specific checkpoints, in particular cyclin dependent kinases (Cdks), cyclins and cyclin dependent kinase inhibitors (CKIs). These are known to regulate transcription, epigenetic regulation, metabolism, stem cell self-renewal neuronal function and spermatogenesis [67, 68]. Cdks are produced in G1, and activate DNA replication resulting in initiation of the G1/S transition and activation of downstream proteins that are involved in later events in the cell cycle. Losing control of cell division, especially at the transition from G1 to S phase, results in cancer development [69, 70]. The members of the cyclin protein family include cyclin E, cyclin D, cyclin A and cyclin B. Cyclin E and D interact with cdK 2 to control G1 and are important for retinoblastoma protein Rb/E2F transcription, which is essential for cell differentiation and growth [68]. Rb/E2F transcription factors are required for cell entry into S phase; furthermore, Rb/E2F proteins have been found to be overexpressed in most types of cancer [70]. Cyclin A also interacts with cdk2 and cdk1 to control S phase, while cyclin B controls progression through M phase [68]. Cyclin B is important

for survival and proliferation of cancer cells [71]. Most of the cyclins are produced during the cell cycle, but cyclin D is regulated by the Ras-signaling pathways after extracellular signal-regulated kinase (ERK) activation [70]. Defects in cyclin expression affect cell cycle progression and result in decreased cell viability; downregulation of cyclin B leads to reduced cyclin A expression, S phase delay and apoptosis [72]. Cyclin E cleavage is associated with apoptosis in tumour cells [73].

1.8.2 Apoptosis:

Apoptosis is programmed cell death which takes place in normal adult tissue regulation and plays a role in normal embryonic development [74]. Apoptosis is regulated by a family of proteases called Caspases (cysteine-dependent aspartate-specific proteases) that are involved in the activation and transduction of apoptotic induction. Caspases are divided into two main groups based on their function. The initiator caspases (caspases 2, 8, 9 and 10) are responsible for activating the activator caspase cascade. Activator caspase (caspases 3, 6 and 7) activation results in cleavage of many structural proteins such as actin, fodrin, lamin and gelsolin, leading to nuclear and cellular morphology alteration. Activator caspase substrates also include members of cellular DNA repair mechanisms including poly ADP-ribose polymerase (PARP) and DNA-PK [75-77]. Caspase 3 cleavage results in the induction of caspases 2 and 6 which drive the cell to complete apoptosis [78].

1.8.3 The role of UHRF1 in cell cycle regulation and apoptosis:

UHRF1 depletion from different cancer cells, including breast and colorectal, results in activation of the DNA damage response pathway, cell cycle arrest at G2/M phase and apoptosis

induction. UHRF1 causes cell cycle arrest and apoptosis in an independent manner to p53 expression [79]. UHRF1-induced apoptosis involves activation of caspase 8 and the downstream effector caspase 3; evidenced by loss of apoptotic induction by UHRF1 depletion in caspase 8 knockdown cells [79]. On the other hand, it has been reported that UHRF1 depletion causes cell cycle arrest at G1 phase in Hela cells [80]. In lung cancer, UHRF1 plays an important role in cell cycle regulation; its depletion from human non-small lung cancer cells resulted in either G1 cell cycle arrest or G2/M phase arrest [38]. The expression level of UHRF1 through the cell cycle is not clear, as in one study UHRF1 showed maintained levels through all cell cycle phases [81] and in another report UHRF1 showed reduction in its steady levels in M phase proliferation [52]. This study suggests that maintained levels of UHRF1 are important for regulating cellular proliferation [52]. Thus, UHRF1 appears to play an important role in cell cycle progression and its depletion results in cell cycle obstruction. In the current study, we examined the role of UHRF1 in cell cycle regulation utilising pancreatic cancer as a model.

1.9 DNA Methylation:

DNA methylation is one of the epigenetic alterations that cause cancer development. Epigenetic modifications of the DNA structure cause changes in gene expression, rather than changes in the primary coding DNA sequence. These changes are heritable and can be reversed with treatment. In DNA, methylation occurs in cytosine residues followed by guanine in the DNA sequence (CpG). In normal cells, DNA methylation is an organised process and the addition of a methyl group to the CpG sites is not random. DNA methylation occurs at specific sites on the genome, including CpG rich regions or islands in the promoter region within the DNA

sequence, which result in gene inactivation. Other sites of DNA methylation include CpG-containing repetitive DNA sequences for the maintenance of DNA stability. Hypomethylation of these sites has been linked to cancer development (Figure 1-4) [82].

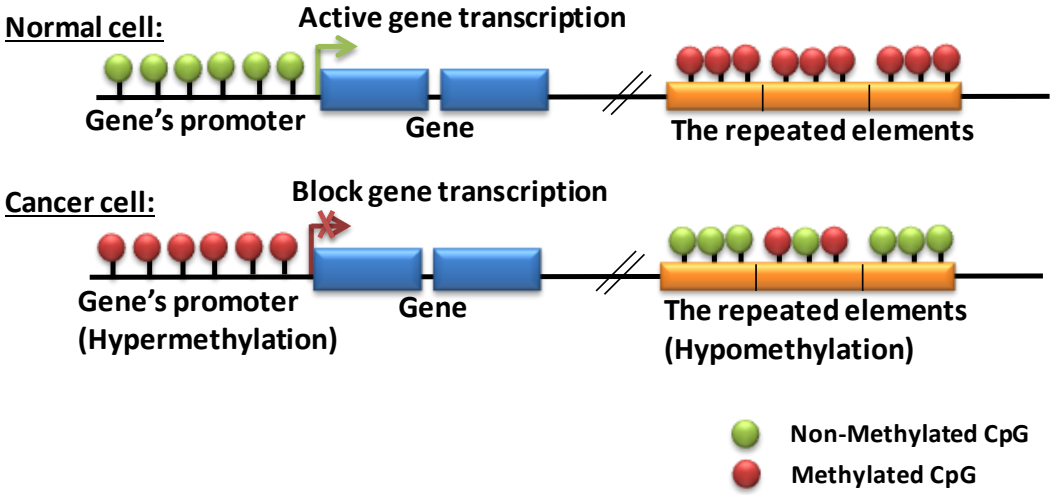

Figure 1-4. A schematic drawing presents the DNA methylation status in normal and cancer cells. In normal cells, gene promoters are non-methylated while the repetitive sequences are heavily methylated. In cancer cells, gene promoters are silenced by DNA methylation (hypermethylation) and the repetitive elements are hypomethylated.

Silencing of many TSGs through promoter methylation and subsequent loss of protein function has been reported in several types of cancers. In normal cells DNA methylation plays an important role in regulating gene expression, for example, the random X inactivation in females [83]. Moreover, DNA methylation is an important process for normal embryonic development and maintaining chromosomal stability [84]. DNA methylation levels vary during the cell cycle with the lowest levels detected during G1 that subsequently increase during S phase [85]. DNA methylation is catalysed by enzymes called DNMTs. As mentioned previously above, UHRF1 contributes to the maintenance of DNA methylation by recruiting DNMT1 to its hemimethylated DNA substrate [35]. The DNA methylation mechanism is regulated by DNMT1

through the addition of a methyl group to carbon five in the cytosine ring to form 5-methylcytosine, using S-adenosyl-methionine (SAM) as a methyl donor as shown in (Figure 1-5) [86].

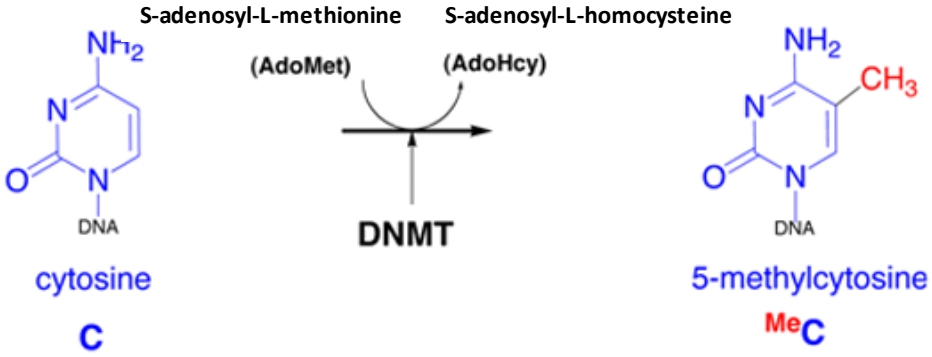

Figure 1-5. The DNA methylation mechanism. DNMT1 adds a methyl group to the carbon number 5 in the cytosine ring to form 5-methylcytosine using S-adenosyl-methionine (SAM) as a methyl donor.

UHRF1 recruits the DNMT1 to the hemi-methylated DNA and together they form a complex with other important proteins, which are required for DNA replication and cell proliferation, to allow successful methylation and inheritance of the methylated DNA to the newly produced daughter cells during cell division (Figure 1-6) [87]. UHRF1 has been found to interact with DNMT1 protein within the S phase of the cell cycle, during DNA synthesis [43].

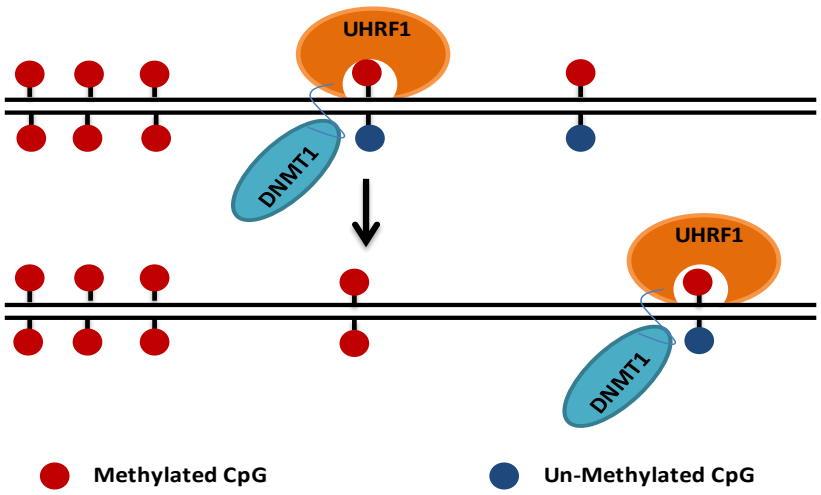

Figure 1-6. UHRF1 binds hemi-methylated DNA and recruits DNMT1 to allow full DNA methylation.

1.10 The role of UHRF1 in DNA methylation:

UHRF1 plays an important role in DNA damage repair, epigenetic regulation and DNA replication. One mechanism by which UHRF1 recruits DNMT1 onto the hemi-methylated DNA sequence has been proposed [88]. Briefly, UHRF1 recognizes the hemi-methylated cytosine in the CpG sites through its SRA domain, forming SRA-DNA complexes. The SRA binding flips the methyl-cytosine base outside of the DNA double strand, allowing UHRF1 to bind DNMT1. Following DNMT1 binding, the non-methylated cytosine is flipped from the other side of the DNA helix to be targeted by DNMT1. DNMT1 adds a methyl group to the targeted cytosine resulting in a fully methylated CpG site (Figure 1-7). DNA methylation maintenance mechanism takes place in S phase of the cell cycle [81].

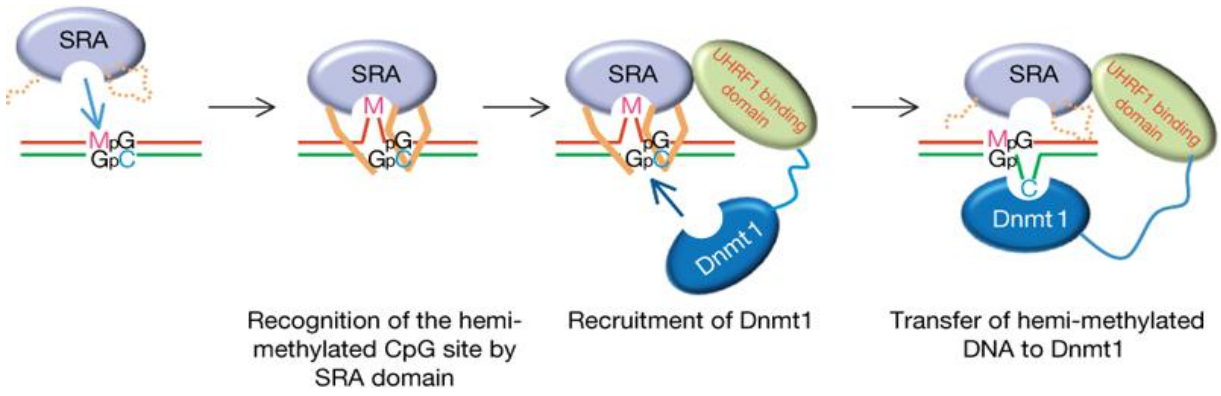

Figure 1-7. DNA methylation maintenance by UHRF1, the Flipping model. UHRF1 recognises hemi-methylated DNA by its SRA domain. The methylated cytosine is flipped to the outside of the DNA helix. Following DNMT1 binding to UHRF1, the non-methylated cytosine is flipped to the other side of the DNA helix and is targeted by DNMT1. This figure is taken [88] without permission.

1.10.1 DNA methylation in cancer:

Global changes in the epigenetic landscape are one of the hallmarks of cancer. Many cancers exhibit changes in their DNA methylation pattern compared to benign cells. DNA hypermethylation refers to an increase in methylation, while the loss of DNA methylation level is referred to as DNA hypomethylation. Both hypermethylation and hypomethylation have been reported in several cancers [89]. DNA hypermethylation in gene-specific promoters leads to the blockade of gene transcription. Promoter silencing of TSGs by DNA hypermethylation is a common epigenetic development in cancer, and has been reported for *CDKN2A, CDKN2B, MGMT, MLH1, BRCA1, CDH1, CDH13 and DAPK1*. Loss of TSG function disturbs many pathways in the cell, including cell cycle regulation, DNA repair and apoptosis as well as tumour metastasis [89, 90]. DNA methylation is a reversible mechanism that occurs early in cancer

development. Epigenetic therapy or de-methylating agents can reverse DNA methylation and prevent cancer progression [91].

DNA hypomethylation of repetitive sequences affects genomic instability and can cause chromosomal re-arrangement or translocation. DNA hypomethylation of silenced oncogenes results in oncogenic reactivation and promotes carcinogenesis [89, 90]. In pancreatic cancer the gene promoters of the *CDKN2A* [92], *RASSF1* [93] and other genes [94] are highly methylated unlike in normal cells.

1.10.2 DNA methylation therapy:

The most common de-methylation agent used in cancer treatment is 5-aza-deoxycytidine. This drug consists of a ring analogue of the pyrimidine nucleoside cytidine, in which a nitrogen atom replaces the carbon group number 5 which interferes with DNMT activity. The drug specifically binds to DNA and blocks DNMT binding, promoting de-methylation and re-expression of silenced genes [83] (Figure 1-8). The free DNMT1 molecules are degraded by ubiquitination thus reducing the DNA methylation level [95].

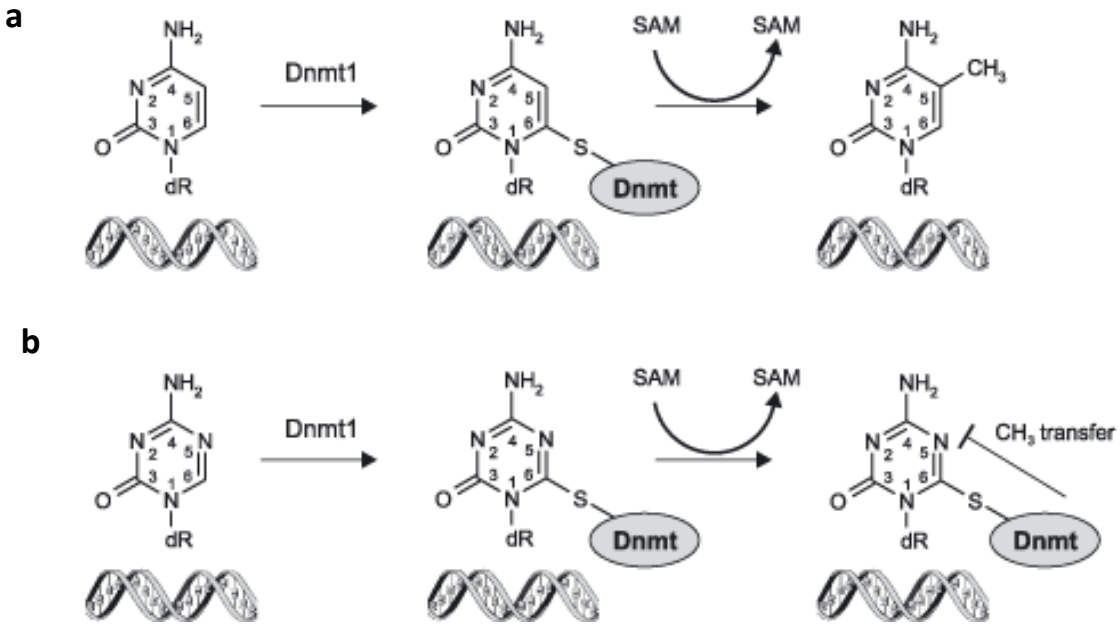

Figure 1-8. The mechanism of action of 5-aza-deoxycytydine. (a). DNMT1 adds a methyl group to the cytosine ring. A methyl group is donated by SAM (adenosyl-methionine) (b) 5-aza-deoxycytidine adds a nitrogen atom to carbon number 5 which blocks DNMT1 activity.

5-aza-deoxycytidine restores gene expression by either de-methylation dependent or independent mechanisms [96]. Treatments with 5-aza-deoxycytidine to reactivate silenced genes, regulate apoptosis and increase sensitivity to radiotherapy have been used in clinical trials in prostate cancer patients [97]. DNMT1 overexpression plays a role in cancer progression by increasing the methylation level and inactivation of certain genes [98].

1.10.3 DNA methylation measurement protocols:

Different methods are available for the measurement of DNA methylation, including methylation specific PCR (MSP) (Taqman and Sybr-green), microarray expression profiling, restriction landmark genomic scanning, CHIP-on-chip and pyrosequencing [99]. Most of these techniques only allow for the analysis of specific CpGs or are time- and cost-intensive, but Pyrosequencing overcomes these limitations [100]. In our study, we used the Pyrosequencing

technique to examine DNA methylation status. Only a small quantity of DNA is needed for each run, so this technique preserves DNA samples from clinical specimens [101]. One advantage of pyrosequencing lies in its simplicity combined with the accuracy of measurements of DNA methylation levels for each CpG in the targeted sequences. Briefly, the protocol begins with DNA bisulfate treatment followed by polymerase chain reaction (PCR) leading to pyrosequencing (Figure 1-9).

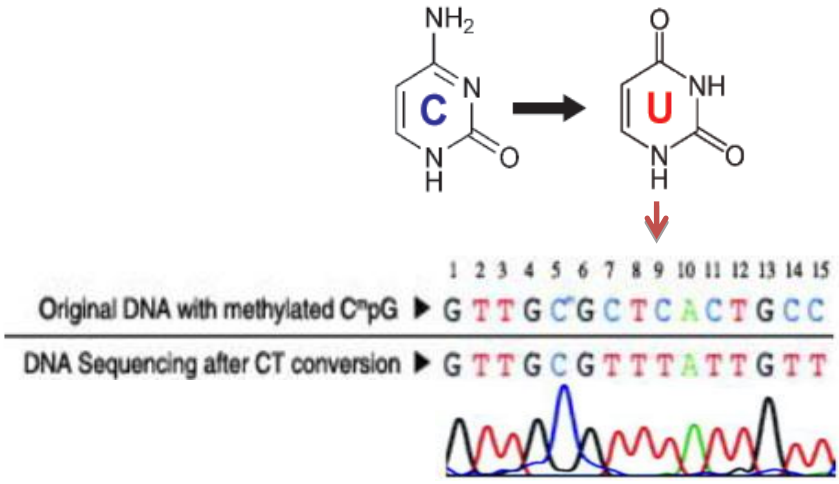

Figure 1-9. DNA sequencing results following bisulfite treatment. The 5th nucleotide in the original DNA sequence is a methylated cytosine, which was not converted to thymine following CT conversion by bisulfite treatment, while the unmethylated cytosines in the original DNA sequence were completely converted into uracil and complemented with thymine following PCR.

The methylation level is calculated by analysing the ratio of C to T in the CpG site [102]. The amplified DNA contains one biotinylated strand that serves as a pyrosequencing template. This template and the sequencing primers are incubated with DNA polymerase, ATP sulfurylase, luciferase, apyrase, substrates adenosine 5' phosphosulfate (APS) and luciferin. Following primer annealing, the primers are extended by DNA polymerase which catalyzes the addition of

complementary deoxyribonucleotide triphosphate (dNTP). This reaction resulted in pyrophosphatase (PPi) release in equivalent amount of each added nucleotide (Figure 1-10).

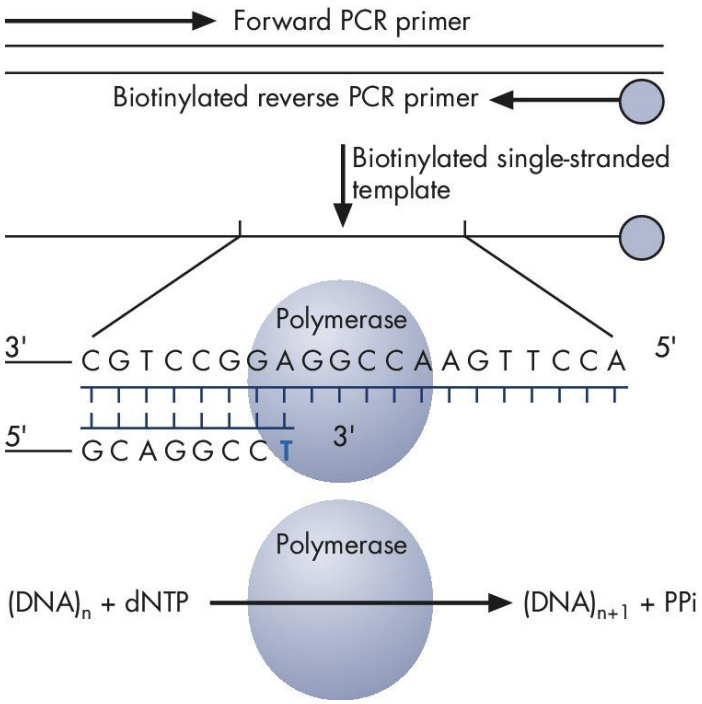

Figure 1-10: The DNA is amplified by PCR and the biotinylated sequence serves as a pyrosequencing template. Following primer annealing the enzyme DNA polymerase facilitates the addition of complementary nucleotides to extent the primer sequence and the PPi is released in each reaction.

The unused dNTPs or ATPs are degraded by an enzyme called apyrase. At the time when degradation at each step is finished, the next set of nucleotides is added for further sequence extension (Figure 1-11).

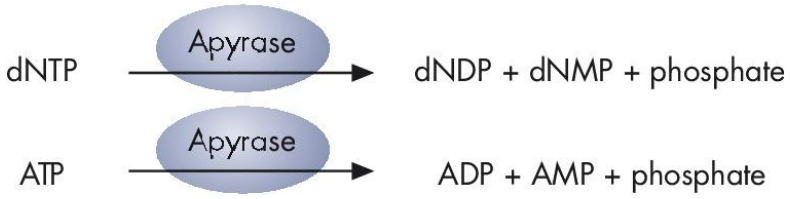

Figure 1-11. Apyrase degrades unused dNTPs or ATPs after each nucleotide addition.

DNA polymerase requires dATP for its activity, and for this initial step the source of dATPs in the reaction is deoxyadenosine alfa-thio triphosphate (dATPαS). Later in the process, the enzyme luciferase does not recognize dATPαS but instead uses ATP produced by an enzyme called sulfurylase that converts PPi to ATP in the presence of adenosine 5' phosphosulfate (APS). Luciferase then mediates the conversion of luciferin to oxyluciferin, resulting in light generation as explained in Figure 1-12a. The amount of generated light is equivalent to ATP used in the reaction. The light is detected by a charge coupled device (CCD) camera provided in the pyrosequencing machine and visualised as a peak (Figure 1-12 a). The nucleotide addition reaction is then repeated, resulting in elongation of the complementary DNA strand and the generation of further peaks. The nucleotides detected by the signal peak raw data output produces a pyrogram (Figure 1-12 b). The global DNA methylation level of repetitive elements LINE1 is widely used as a standard reference of whole genomic methylation when determining new methylation measurement methods or improving existing methods [103-105].

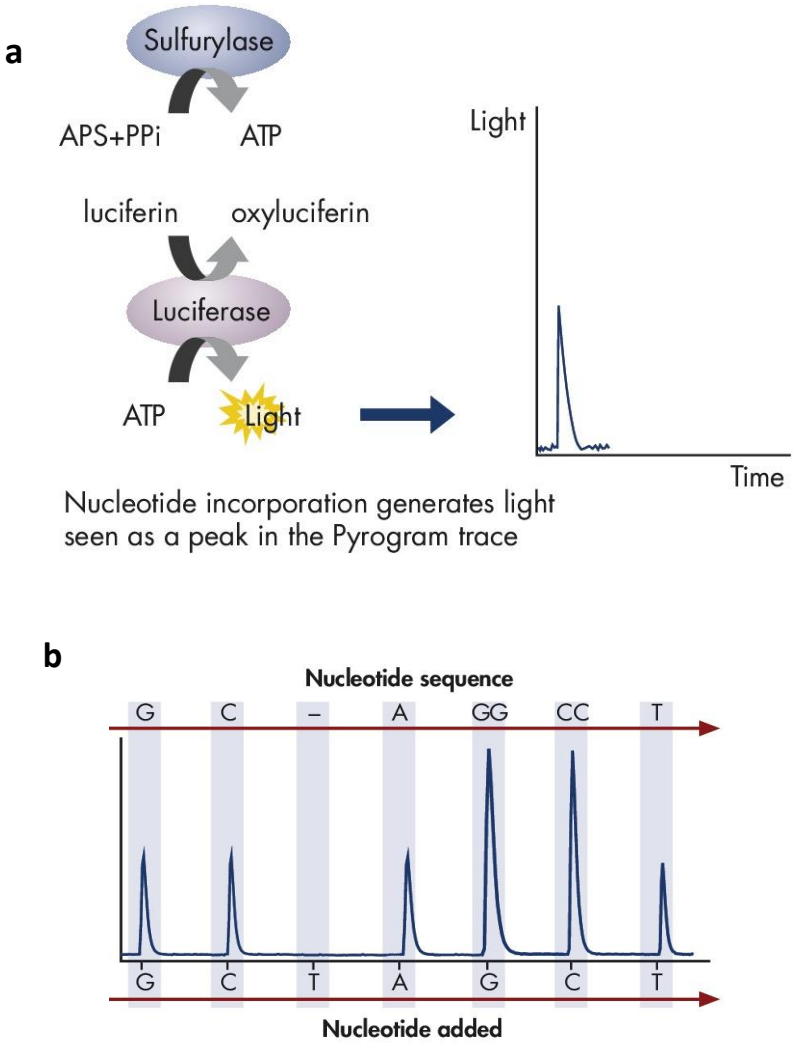

Figure 1-12. Raw data generation in the pyrosequencing reaction. (a). Luciferase uses ATP which is produced by sulfurylase that converts PPi to ATP. Luciferase mediates the conversion of luciferin to oxyluciferin, resulting in light generation. The amount of generated light is equivalent to ATP used in the reaction. The light is then detected as a peak by a CCD camera. (b). Raw data output in the program at the end of the run.

1.10.4 Global DNA hypomethylation:

CpG sites in DNA repetitive elements are highly methylated in normal mammalian cells, to maintain DNA stability. Global de-methylation of these sequences including transposable elements is an early event in cancer development [90]. Repetitive genomic DNA sequences

include long interspersed nuclear elements (LINEs), short interspersed nuclear elements (SINEs) and satellite repeats. Transposable elements form 45 % of the human genome and are classified into DNA transposons and retrotransposons. DNA transposons are inactive in the human genome and are inserted into the DNA sequence by a cut and paste mechanism. Retrotransposons are transcribed into an RNA intermediate followed by amplification through a reverse transcriptase mechanism and insertion into new regions in the human genome. Retrotransposons are grouped into long terminal repeats retrotransposable elements (LTRs) and non-LTRs. LTRs have limited activity in the human genome and containing long-terminal repeats at both ends of their DNA sequence, while non-LTRs are active and contain poly-A sequences at the 3' end of their sequence. The well-known non-LTR elements in the human genome are LINE1 and Alu-V elements. Almost 30% of the human genome is made of these elements, and their activity has been implicated in several diseases [106].

1.10.4.1 LINE1 and *Alu-V* elements:

LINE1 elements form approximately 17 % of the human genome. The full length of *LINE1* is nearly 6 kbp [106]. *LINE1* sequences contain a 5' untranslated region (5'UTR), two open reading frames (ORF) that produce two proteins needed for retrotransposition, and a 3' UTR. Each ORF has its own activity; ORF1 has an RNA binding site and facilitates DNA amplification during the retrotransposition process, while ORF2 has endonuclease (EN) and reverse transcriptase (RT) binding sites. The EN domain causes DNA cleavage at specific sites identified by 5' TTTT AA 3' DNA sequences. The mechanism of how *LINE1* retrotransposes is not fully understood [107].

Alu-V elements comprise about 11 % of the human genome, at a full length of 300 bp and do not code for any protein. It is thought that Alu-V is linked to chromosomal abnormalities and genomic stability [108].

1.10.4.2 LINE1 and *Alu-V* elements in cancer:

LINE1 elements have been widely examined in human cells and in particular how their hypomethylation can cause genomic instability and chromosomal breaks [107]. *LINE1* hypomethylation is detected in several cancer types, including early neoplastic stages of cancer development [109]. Genomic instability due to *LINE1* hypomethylation was detected in early stages of urothelial carcinoma [110]. *LINE1* hypomethylation was also detected in different tumours, compared to matched normal tissues from the same studied organs. It has been reported that *LINE1* methylation is tissue-specific in different cancers, including, breast, colon, lung, head and neck, bladder, esophagus, liver, prostate and stomach. The hypomethylation level in colonic cancer was greater in advanced stages when compared to dysplastic polyps and normal epithelial tissues [105]. Hepatocellular carcinoma patients have been shown to have higher *LINE1* hypomethylation levels in their leukocyte DNA [111]. In breast cancer, *LINE1* and *Alu-V* elements were hypomethylated in tumours compared to normal tissue and white blood cells (WBC) DNA [112]. A recent pilot study evaluated the methylation changes in whole blood with a view to identifying markers for the detection of pancreatic tumors. LINE-1 and Alu repeats were slightly less methylated compared to control blood [113]. In this study, we focused on global DNA methylation regulation by UHRF1 in pancreatic cancer cell lines.

1.11 Tumour suppressor gene hypermethylation:

DNA hypermethylation of TSG promoters is a common epigenetic change in different cancers as described in section 1.10.1. In pancreatic cancer *CDKN2A* [92], *RASSF1* [93] are frequently hypermethylated. Since both of these genes form important components of this thesis, they are described below.

1.11.1 Cyclin dependent kinase inhibitor 2A (CDKN2A):

CDKN2A is the most frequently inactivated TSG in pancreatic cancer. This gene encodes the $p16^{INK4A}$ protein which plays an important role in normal cell cycle regulation by inhibiting cyclin dependent kinases (CDK4 and CDK6) and arresting the cell cycle in late G1 phase. $p16^{INK4A}$ protein function is lost in 95% of pancreatic cancer cases. *CDKN2A* inactivation is an early event in pancreatic cancer and can be detected in PanINs [29]. $p16^{INK4A}$ inactivation by DNA methylation has been reported in several cancers including head and neck squamous carcinoma [114], hepatocellular carcinoma [115], gallbladder cancer [116] and pancreatic cancer [92]. It has been demonstrated that demethylation agents such as 5-aza-deoxycytidine can restore $p16^{INK4A}$ protein expression in cancer cells [20].

1.11.2 Ras association domain family 1 (*RASSF1)*:

Ras association domain family 1 is a member of the RASSF family. The RASSF family consists of ten members and is known to play an important role in cell cycle control and apoptosis. A recent review has shown that eight of ten members are hypermethylated in various cancers [117]. *RASSF1* has been reported to be hypermethylated in pancreatic and other cancers [93, 112]. In different mouse model studies, *RASSF1* plays a role in cell growth, cell cycle regulation,

cell migration and apoptosis [117]. *RASSF1* silencing in pancreatic cancer has been shown to be inversely correlated with K-Ras activation [93].

1.12 The KEAP1 / NRF2 pathway:

K-RAS activation was shown to promote tumorigenesis in pancreatic cancer by activating the KEAP1 (Kelch-like ECH-associated protein 1)/ NRF2 (Nuclear factor erythroid 2-related factor 2) pathway vivo [118]. The KEAP1 / NRF2 pathway protects normal cells from chemical or oxidative stress. KEAP1 interacts with the transcription factor NRF2, directing it for ubiquitination and proteasomal degradation. Disruption of the interaction between NRF2 and KEAP1 occurs under numerous cellular stress conditions mechanism [119], and results in stabilization and nuclear accumulation of NRF2. Subsequently, nuclear NRF2 interacts with antioxidant response elements (AREs) to promote transcription of genes encoding antioxidant proteins, detoxification enzymes and xenobiotic transporters [120]. The nuclear accumulation of NRF2 is thought to protect the cell from chemotherapeutic agents and facilitate cancer progression [120].

1.12.1 NRF2 normal function and structure:

NRF2 plays a major role in cellular homeostasis, differentiation, proliferation, and inflammation. In normal cells, NRF2 is a central regulator of antioxidant enzymes and is responsible for protecting the internal cellular environment whenever the cell is exposed to chemical or oxidative stress. NRF2 plays a major role in cellular homeostasis, differentiation, proliferation, and inflammation [121]. NRF2 mediates the induction of target genes such as heme oxygenase-1 (HO-1) and NAD(P)H:quinone oxidoreductase 1 (NQO1) to protect against

the inflammatory response in human monocytes [122]. Also it has been reported that NRF2 plays a role in the suppression of pro-inflammatory signaling pathways [123]. Therefore, NRF2 is an important target for anti-inflammatory drugs [124, 125]. NRF2 also plays a role in cellular proliferation [126] and tumour development [127]. In pancreatic cancer NRF2 has been reported to increase cell proliferation [128]. NRF2 also regulates the activation of DNA repair pathways in response to exposure to reactive chemical species [129]. NRF2 generally is a key regulator of phase II drug detoxification and antioxidant enzymes or transporters, which can be upregulated to inhibit xenobiotic toxicity [130]. In a mouse model, it has been reported that the expression of multidrug resistance-associated protein transporters is dependent on NRF2 [131]. As a result of these and other functions, dysfunction of NRF2 enhances susceptibility to the onset of various diseases. A summary of the pathways that NRF2 regulates is shown in Figure 1-13.

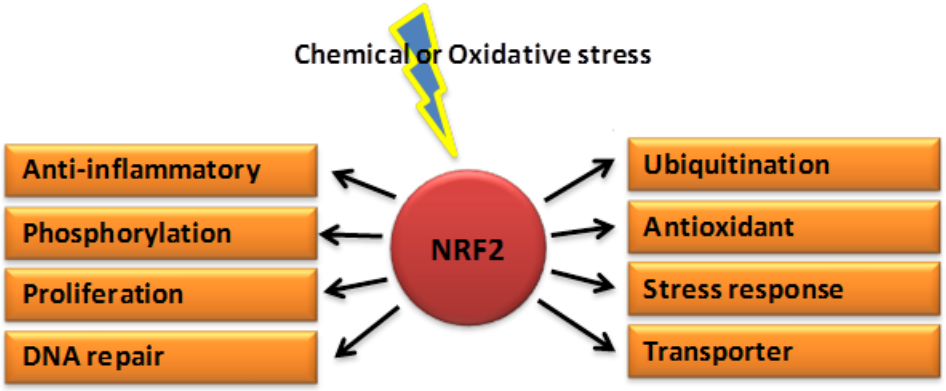

Figure 1-13. A schematic drawing summarising NRF2 responses.

NRF2 protein structure as shown in Figure 1-14 contains 6 different NRF2-ECH-homology (Neh) domains. Neh1 is a DNA binding domain, Neh2 is the KEAP1 binding domain, Neh 3-5 domains

are responsible for transactivation of NRF2 and Neh6 domain is responsible for NRF2 degradation [119, 132]. The Neh2 domain contains 2 important motifs, the low-affinity DLG motif and the high-affinity ETGE motif, this domain is recognised by KEAP1, the repressor of NRF2 [133].

Figure 1-14. A schematic representation of NRF2 protein structure.

1.12.2 KEAP1 normal function and structure:

NRF2 activity is mainly regulated by KEAP1 by direct interaction or through an indirect mechanism [119]. In normal cells, NRF2 interacts with KEAP1 in the cytoplasm and regulates NRF2 levels by ubiquitination [133]. A detailed study showed that KEAP1 recruits NRF2 by the ETGE motif and the DLG motif is required for ubiutination signaling initiation [134]. In a Keap1 deficient mouse model Nrf2 was found to accumulate in the nucleus [135]. KEAP1 has been identified as a substrate-specific adaptor protein of Cul3-based ubiquitin E3 ligase, to target NRF2 for proteasomal degradation, while under oxidative stress conditions this mechanism is inhibited [136, 137]. KEAP1 protein contains different domains as shown in Figure 1-15, including, broad-complex-tramtrack and bric-a-brac (BTB) domain at the N-terminal end, intervening linker domain (IVR), and the double glycine/Kelch repeats at the C-terminal end [119]. The BTB domain binds Cul3 protein and is responsible for NRF2 inhibition, with each Cul3 ligase binding to two KEAP1 proteins [119, 137]. The C-terminal Kelch repeats facilitate NRF2

binding. The IVR is responsible for transmitting signals that affect the ability of the Kelch domain to bind NRF2 and maintain NRF2 stability [138], as it contains reactive cysteine residues that act as sensors for electrophilic and oxidative stress. The IVR domain is rich with cysteine residues [119] but two in particular are important for the maintenance of NRF2 basal level, namely Cys 273 and Cys 288 [133].

Figure 1-15. A schematic representation of KEAP1 protein structure.

1.12.3 KEAP1/NRF2 pathway regulation mechanisms:

In normal cells, KEAP1 traps NRF2 in the cytoplasm and directs it for ubiquitination and proteasomal degradation. NRF2 is released from KEAP1 following exposure to a chemical or oxidative stress, and results in translocation of NRF2 to the nucleus and stimulation of its downstream target genes [136]. Following exposure to oxidative stress, modifications occur in the cysteine residues of KEAP1 that disturb its binding to the DLG and ETGE motifs of NRF2. As a result, NRF2 is not targeted for KEAP1-dependent ubiquitination and accumulates in the nucleus [133] . The activation of NRF2 takes place following signaling by KEAP1 as it is the primary oxidant sensor in this pathway, however NRF2 itself may contain oxidant sensors that cause its activation and nuclear translocation. For example, phosphorylation of NRF2 at serine 40 leads to its activation and dissociation from KEAP1 [121]. This mechanism is summarized in Figure 1-16.

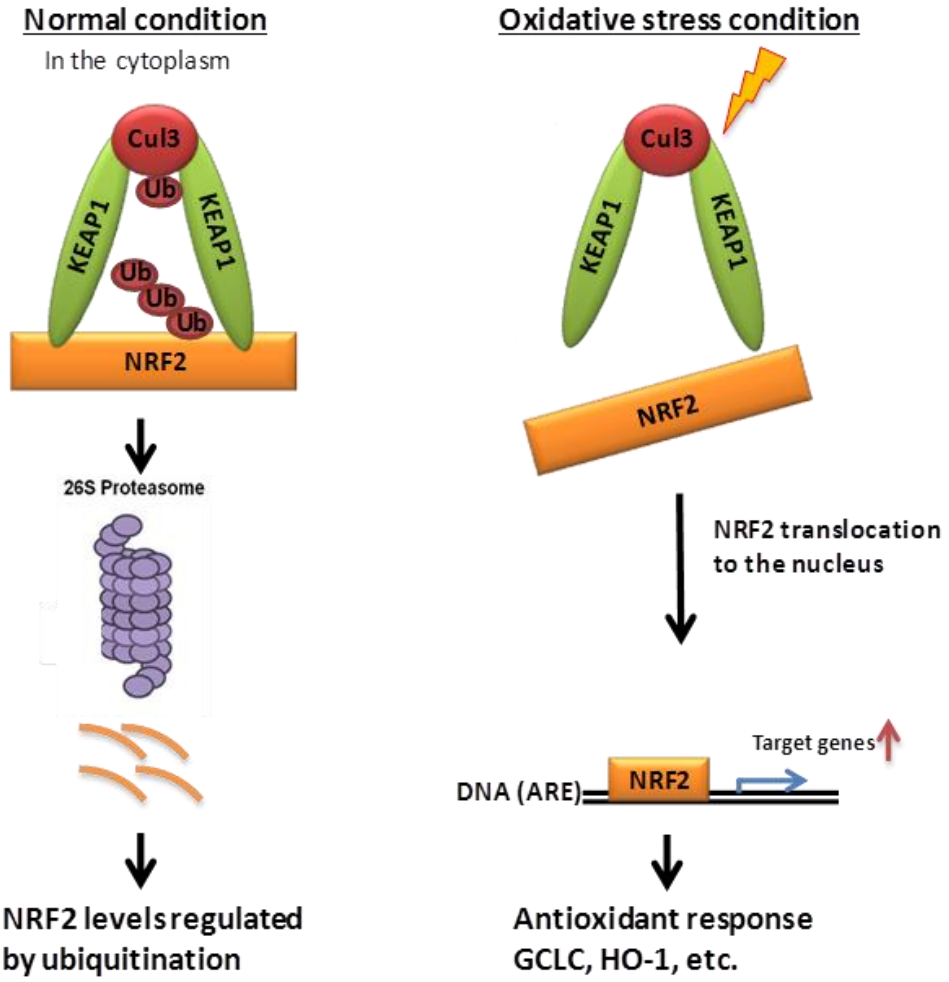

Figure 1-16. A schematic drawing depicting the KEAP1/NRF2 regulatory mechanism. In normal conditions KEAP1 and NRF2 complexes are located in the cytoplasm where KEAP1 negatively regulates NRF2 through ubiquitination and proteasomal degradation. While under oxidative stress, NRF2 dissociates from KEAP1 and translocates to the nucleus to activate downstream genes.

Downstream targets of NRF2 include antioxidant proteins, xenobiotic transporters and phase II drug metabolism enzymes [119]. The best known Nrf2 inducer is sulforaphane (SFN), which reacts with Cys 151 of KEAP1 and inhibits its activity, allowing nuclear translocation of Nrf2 and activation of antioxidant response elements (ARE) [139]. Cys 151 of KEAP1 is needed for the posttranslational modifications of KEAP1 that stimulates oxidative stress [129]. Activation of the KEAP1/NRF2 pathway results in the stimulation of several enzymes. Briefly, the most common targets of Nrf2 are phase II enzymes, such as NADPH quinone oxidoreductase (NQO1) and glutamate-cysteine ligase catalytic (GCLC), redox-active proteins such as heme oxygenase (HO-1), and other enzymes [126, 140]. NRF2 also regulates the induction of cytochrome P450 isoform 2A5 (CYP2A5), a member of the cytochrome P450 superfamily [141]. Moreover, CYP2A5 is the first identified P450 gene that is regulated by NRF2 under stress conditions [142]. Another study has suggested a different mechanism of KEAP1/NRF2 interaction referred to as the shuttling mechanism. Briefly, in normal cells, KEAP1 and NRF2 are located in the cytoplasm, where both are regulated by ubiquitination. When the cell is exposed to oxidative to oxidative or chemical stress, KEAP1 provides transportation of NRF2 to the nucleus, KEAP1 then returns to the cytoplasm without NRF2 or remains in the nucleus and activates the ARE genes as a complex, by a mechanism that is not yet understood [143]. This dynamic shuttling mechanism increases NRF2 stability and prevents NRF2 ubiquitination by KEAP1 in the nucleus [144]. NRF2 is regulated by either KEAP1-dependant or KEAP1-independent mechanisms, where other proteins regulate its activity [119]. Other KEAP1-independent regulators of NRF2 function include mitogen-activated protein kinases (MAPK), phosphatidylinositol-3 kinase and protein kinase C [121]. It has also been reported that KEAP1 is an ARE-dependent gene. KEAP1 protein

expression is down-regulated in both NRF2 positive and NRF2 negative cells as the antioxidant response take place [145].

1.12.4 KEAP1/NRF2 pathway in cancer:

Besides the protection that NRF2 gives to normal cells, it is also thought to have a pathological role in cancer. Here NRF2 has a dual role in that its downstream genes are overexpressed in tumours, assisting neoplastic transformation, whilst also protecting the cells against chemotherapy resulting in longer cell survival [146]. Phase II enzymes are a battery of important detoxifying proteins, which play a role in cell protection against mutagens. The expression of Phase II enzymes is not only disturbed in cancers, but also results in the occurrence of other diseases [147]. NRF2 deficiency leads to defects in cell proliferation and greatly enhances the cell's sensitivity to oxidant-induced cell death [148]. The damage resulting in tissues due to oxidative stress is proportional to the severity of the stress and NRF2 activation [149]. KEAP1 inactivation by gene mutation or loss of heterozygosity in cancer cells results in prolonged activation of NRF2 protein expression and its downstream genes, tumorigenesis and chemoresistance. The expression level of NRF2 is also correlated with resistance to several drugs [146]. Mutations in the reactive cysteine residues result in loss of function of KEAP1 [150]. In lung cancer patients with mutation in the recognition sites of DLG or ETGE motifs, NRF2 overexpression and resistance to chemotherapeutic treatments have been reported [127]. Inhibiting NRF2 and NRF2-dependent proteasome activity in pancreatic cancer resulted in improved response to anticancer drugs. Loss of KEAP1 protein due to promoter hypermethylation has been reported in several cancer types, including prostate, lung [151-155]

and colorectal cancer [147]. Thus, an emerging mechanism has been reported in cancer where the KEAP1/NRF2 pathway is regulated by methylation of the *KEAP1* gene promoter.

1.12.5 KEAP1/NRF2 pathway in pancreatic cancer:

The KEAP1/NRF2 pathway is active in pancreatic cancer. NRF2 is up-regulated in pancreatic cancer cell lines and tissues, and its depletion by small interfering RNA (siRNA) decreases cellular proliferation and reduces resistance to different anticancer therapies (GEM, FU and cisplatin). The *NRF2* gene in pancreatic cancer has no known mutations, while KEAP1 gene has been shown to contain synonymous mutations. One study has reported dysregulation of the KEAP1/NRF2 pathway in pancreatic cancer cells, while no significant correlations were found between KEAP1 expression and NRF2 in tissue specimens [128]. The oncogene K-RAS, which is commonly activated in pancreatic cancer, is also thought to regulate NRF2 expression levels in pancreatic cancer cells. Its depletion causes a decrease in NRF2 mRNA levels and an increase in reactive oxygen species (ROS) which can promote tumorigenesis. Thus, the continuous increase in NRF2 mRNA levels by K-Ras oncogene activation results in increased cellular protection and provides a cell survival advantage and resistance to apoptosis [118].

KEAP1 dysfunction due to its promoter hypermethylation has been reported in prostate, lung [151-155] and colorectal cancer [147]. In pancreatic cancer the KEAP1/NRF2 pathway is dysregulated and the KEAP1 gene has been examined for point mutations. The KEAP1 gene has no mutations in our pancreatic cancer cell lines [128], but the methylation status of its promoter in pancreatic cancer has not been examined. Accordingly, it is possible that DNA methylation controls KEAP1 expression in pancreatic cancer and this is a focal point of the investigation presented here. Additionally, it is notable that DNA methylation is regulated by

UHRF1, which was shown by our group to be overexpressed in pancreatic cancer specimens but not in normal pancreas [37], and as this study nor other studies reported the functional role of UHRF1 in pancreatic cancer, the work presented here has evaluated UHRF1 expression and function in this type of cancer and its effect on DNA methylation status, including frequently methylated TSGs and the KEAP1 promoter.

Chapter 2:

Aims and objective

2 Aims and objectives:

The role of UHRF1 in pancreatic cancer has not previously been reported. In this study we aimed:

- To characterize UHRF1 expression in pancreatic cancer cell lines and patient samples.
- To examine UHRF1 function in pancreatic cancer cells.
- To determine UHRF1's role in the DNA methylation status in pancreatic cancer cells.
- To determine if the KEAP1 promoter is methylated in pancreatic cancer, and whether UHRF1 regulates its methylation.

To address these aims, this study had a number of objectives.

Specific objectives included:

- To measure UHRF1 protein expression levels in different pancreatic cancer cell lines and in pancreatic cancer tissue using a tissue micro-array.
- To investigate UHRF1's functional role in cell cycle regulation, proliferation and apoptosis in pancreatic cancer cells.
- To measure the global DNA methylation levels in pancreatic cancer cells and assess the impact of alteration of UHRF1 expression levels on the DNA methylation levels.
- To investigate the KEAP1 promoter methylation status in pancreatic cancer cells, and examine the associations of UHRF1 and Keap1 regulation.

Chapter 3:

Materials and methods

3 Materials and methods:

3.1 Tissue samples:

A pancreatic ductal adenocarcinoma tissue microarray (TMA) was obtained from the Liverpool Cancer Tissue Bank, Department of Pathology, University of Liverpool. In general, 4 TMA sections with a total number of 132 cases were used in this study of UHRF1 expression in pancreatic cancer patients. Another 4 TMA sections with a total number of 124 samples from the same pancreatic cancer patients were used for KEAP1 scoring (Appendix 1). The TMAs were 5 µm in thickness, paraffin embedded sections containing matched duplicate non-malignant and malignant cores. The TMAs also contain cores of normal colon, sarcoma, kidney and liver tissues used for orientation. Pancreatic cancer sections, with a total number 32, were used for UHRF1 antibody optimization and validation.

3.2 Cell line maintenance:

Pancreatic ductal adenocarcinoma cell lines, MiaPaca-2, CFpac-1, Panc-1, Suit-2 and BxPc-3 (Table 1), were all maintained in RPMI medium supplemented with 10% Fetal Bovine Serum (FBS) (Sigma), 100 U/mL penicillin (Sigma), 100 ug/mL streptomycin (Sigma) and 2 nM L-Glutmamine (Sigma). Cells were grown in vented T75 cell culture flasks (Nunc, NY) at 37 ^{o}C in a 5% CO_2 incubator, sub-cultured when they reached 80 % confluence and the flasks were replaced every 2 weeks. All the cell lines were genotyped prior to use in this thesis. Genotyping was performed using gDNA from each cell line and the PowerPlex-16 HS system (Promega) was used to amplify the DNA fragments according to the manufacturer's instructions. Detection of

the amplified fragments was performed using Genetic Analyzer (3130- Applied Biosystem) and GeneMapper software (Version 4.0) as described in [128].

Cell line	Established by	Source of tumour cells
MiaPaca-2	Yunis (USA)	Primary tumour
CFpac-1	R.A. Shoumacher (USA)	Liver metastasis
Panc-1	M. Lieber (USA)	Primary tumour
Suit-2	T. Iwamura (Japan)	Liver metastasis
BxPc-3	M.H. Tan	Primary tumour

Table 1: Anatomical site of origin of pancreatic ductal adenocarcinoma cell lines.

3.3 Freezing and thawing of cells stocks:

Approximately 2 X10^6 pelleted cells were resuspended in 1 mL freezing medium (70 % RPMI medium (Sigma, 1640), 10 % dimethyl sulfoxide (DMSO) (Sigma) and 20 % FBS) and transferred to 1 mL screw caped cryo-vials (Nunc™, cat: 375418) followed by storage for 2 h at -80 ^oC and then transferred to -140 ^oC liquid nitrogen.

3.4 Culturing cells from frozen stocks:

Cells were carefully defrosted in a 37 ^oC water-bath, centrifuged at 100 g for 5 min and then resuspended and washed with PBS to remove any remaining DMSO. Cells were pelleted from the PBS and resuspended in 1 mL pre-warmed medium followed by transfer into a culture flask containing 20 mL culture medium.

3.5 Western blot analysis:

3.5.1 Protein lysate preparation:

Harvested cells were washed with PBS. Then approximately 100 - 300 µL of ice cold Tris-SDS lysis buffer (10 % 1 M Tris-HCl pH 6.8, 20 % of 10 % sodium dodecyl sulfate (SDS), 70 % dH_2O) or RIPA buffer (2 % 1 M Tris, 5 % 3 M NaCl, 0.5 % SDS, 1 % IGEPAL CA 630 (Sigma, 13021), 0.2 % 0.5 M EDTA, pH 8, 91.3 % dH_2O) and a freshly added tablet of complete mini EDTA-free protease inhibitor cocktail (Roche, cat: 11 836 170 001), was added to the cells followed by incubation overnight in –20 ^{o} C and subsequent disruption by sonication with 30 % intensity for 5 sec. Protein lysates were clarified by centrifugation at 10,000 g at 4 ^{o}C for 10 min. Clear lysates were aliquoted into 20 µg and stored at -20 ^{o}C for short term storage (up to 1 month) and at - 80 ^{o}C for long term storage.

3.5.2 BCA Protein Assay:

Quantification of total protein concentration was determined by Pierce bicinchoninic acid (BCA) protein assay for every lysate sample, following the manufacturer's instructions (Thermo Scientific, 23225). Briefly, 50 µL of sample was added to 1 mL of working solution and incubated for 2 h at room temperature and the protein concentration was measured using a spectrophotometer at 562 nm with reference to a standard curve created by using known Bovine Serum Albumin concentrations (BSA).

3.5.3 Protein sample preparation:

Total protein lysate (20 µg) was mixed with 5 X sample loading buffer (10 % SDS, 50 % glycerol (BDH laboratory supplies), 300 mM Tris-HCl pH 6.8, 0.05 % Bromophenol Blue (Sigma), and 1M

dithiothreitol (DTT) (Sigma) freshly added) to reach final concentration of 1 X loading buffer. Samples were denatured at 95 ^{o}C for 15 min prior to loading on an SDS-PAGE gel.

3.5.4 Gel electrophoresis and protein detection:

Equal quantities of denatured protein (20 µg/sample) and a molecular weight marker were loaded and separated on pre-casted Mini-PROTEAN TGX Any-KD Gels (BIO-RAD, 456-9034) for 25 min at 200 volts using 1 X SDS running buffer (0.3 % trisma base, 1.44 % glycine, 0. 1 % g SDS (Sigma)). Samples were transferred during 7 min from the polyacrylamide gels onto positively charged membranes (0.2 µm PVDF (BIO-RAD, 170-4156)) using Bio-Rad turbo transfer apparatus according to the manufacturer's instructions. The membranes were then blocked with 5 % non-fat milk (Bio-Rad) phosphate buffered saline + 0.04 % tween 20 (PBST) for 1 h at room temperature followed by overnight incubation at 4°C in with the appropriate primary antibody (Table 2) diluted in 5 % milk/PBST. Membranes were then washed with PBST for 1h (4 X 15 min) and incubated with conjugated secondary antibody in 5 % milk/ PBST (Table 2) for 1 h at room temperature. Membranes were then washed with PBST for 1h (4 X 15 min). The protein bands were visualized with enhanced chemiluminescence ECL detection buffer (PerKinElmer) and signals were detected on sensitive x-ray films. This protocol was described in [128].

Antibody	Species	Dilution	Supplier and Catalog number
UHRF1	Mouse	1:1000	abcam, ab57083
UHRF1	Mouse	1:1000	Santa Cruz, sc-136264
KEAP1	Goat	1:1000	Santa Cruz, sc-15246
NRF2	Rabbit	1:1000	abcam, ab137550
P16	Mouse	1:500	Santa Cruz, sc373695
Caspase 3	Mouse	1:1000	abcam, ab13847
Cyclin A	Rabbit	1:2000	Santa Cruz, sc751
Cyclin B	Mouse	1:2000	Santa Cruz, H-433
Cyclin E	Mouse	1:2000	Santa Cruz, sc248
NQO1	Goat	1:3000	Abcam, ab2346
GCLC	Rabbit	1:3000	Abcam, ab53179
HO-1	Rabbit	1:3000	Abcam, ab13243
CYP2A5	Chicken	1:3000	Dr. Ian Copple, University of Liverpool
β-actin	Mouse	1:20,000	Sigma, A5441
Polyclonal anti-mouse HRP	Goat	1:3000	Dako, P 0447
Polyclonal anti-rabbit -HRP	Goat	1:3000	Dako, P 0448
Polyclonal anti- Goat -HRP	Rabbit	1:3000	Dako, P 0449
Polyclonal anti- chicken -HRP	Rabbit	1:5000	Sigma, A9046

Table 2: Primary and secondary antibodies used for immuno-blotting.

3.6 siRNA transfection:

Cells were transfected using lipofectamine 2000 (Invitrogen, cat: 11668-019) in antibiotic-free medium according to the manufacturer's instructions and as described in [128]. Briefly, cells were seeded in 6 well plates (Corning Incorporated 3516, Sterile) and allowed to grow overnight to reach 40 % confluence. At this time, 30 nM siRNA (Table 3 and Table 4) in 200 µL of

Opti-MEM, were added to 200 µL of Opti-MEM containing transfection solution and incubated at room temperature for 20-30 min then added drop-wise to the cells. At least 2 different control siRNAs were used in each experiment including the Non-targeting siRNA pool control 1 (Thermo Scientific Dharmacon, cat: D-001206-13-20), RISC-free siRNA (Thermo Scientific Dharmacon, siGENOME® control siRNA, cat: D-001220-01-20), Scrambled siRNA negative control and Off-target siRNA (Thermo Scientific Dharmacon, cat: D-001810-01-20). Following transfection, cells were incubated for 72 h at 37 °C before harvesting and sample preparation.

Anti-UHRF1 siRNA	
siRNA	**Targeted sequences**
Human UHRF1 targeting siRNA-1	GCCAUACCCUCUUCGACUA
Human UHRF1 targeting siRNA-2	GGAACAGUCUUGUGAUCAG
Human UHRF1 targeting siRNA-3	UGGAGGAGGACGUCAUUUA
Human UHRF1 targeting siRNA-4	GAACGGCGUGGUCCAGAUG

Table 3: siRNA anti- UHRF1 targeting sequences. Dharmacon.

Anti-Keap-1 siRNA	
siRNA	**Targeted sequences**
Human Keap-1 targeting siRNA-2	CAGCAGAACUGUACCUGUU
Human Keap-1 targeting siRNA-4	CGAAUGAUCACAGCAAUGA

Table 4: **siRNA anti-Keap-1 targeting sequences. Dharmacon.**

3.7 Cell cycle analysis:

3.7.1 G1 block using double thymidine block:

We optimized the conditions for this experiment prior to cell treatment, based on the cell cycle of each cell line. Using 6 well plates, 15,000 cells / well were maintained in RPMI medium at 37 ^{o}C in a 5 % CO_2 atmosphere and upon reaching 40 – 50 % confluence were treated with G1 blocking reagent thymidine at a final concentration of 2 mM (Sigma, T1895-1G) for 19 h, followed by washing 3 times using sterile pre-warmed PBS. Two mL of fresh medium was added and the cells were transfected with UHRF1-targetting siRNA in selected sets of cells, and then incubated for a further 9 h at 37 ^{o}C in a 5 % CO_2 incubator followed by the addition of a second dose of thymidine (2 mM). Cells were incubated for a further 16 h at 37 ^{o}C. To release the cells from this double block, cells were washed with warm PBS and 2 mL thymidine-free fresh medium was added, followed by collection either at different intervals (0, 2, 4, 7, 8, 9 and 11 h) or at 24 and 48 h after transfection for lysate preparation and flow cytometry.

3.7.2 G2/M block using thymidine nocodazole block:

We optimized the conditions of this experiment prior to cell treatment. Cells were plated and at 40 % confluence, 100 ng/mL nocodazole was added to the cells and washed after 19 h. At this time, cells were transfected with 30 nM UHRF1-targeting or control siRNA and incubated for further 3 h. At this time, thymidine (2 mM) was added to the cells and incubated for 16 h and collected at 24 h and 48 h for lysate preparation and flow cytometry. The following schematic flow chart summarizes cell cycle block treatments (Figure 3-1).

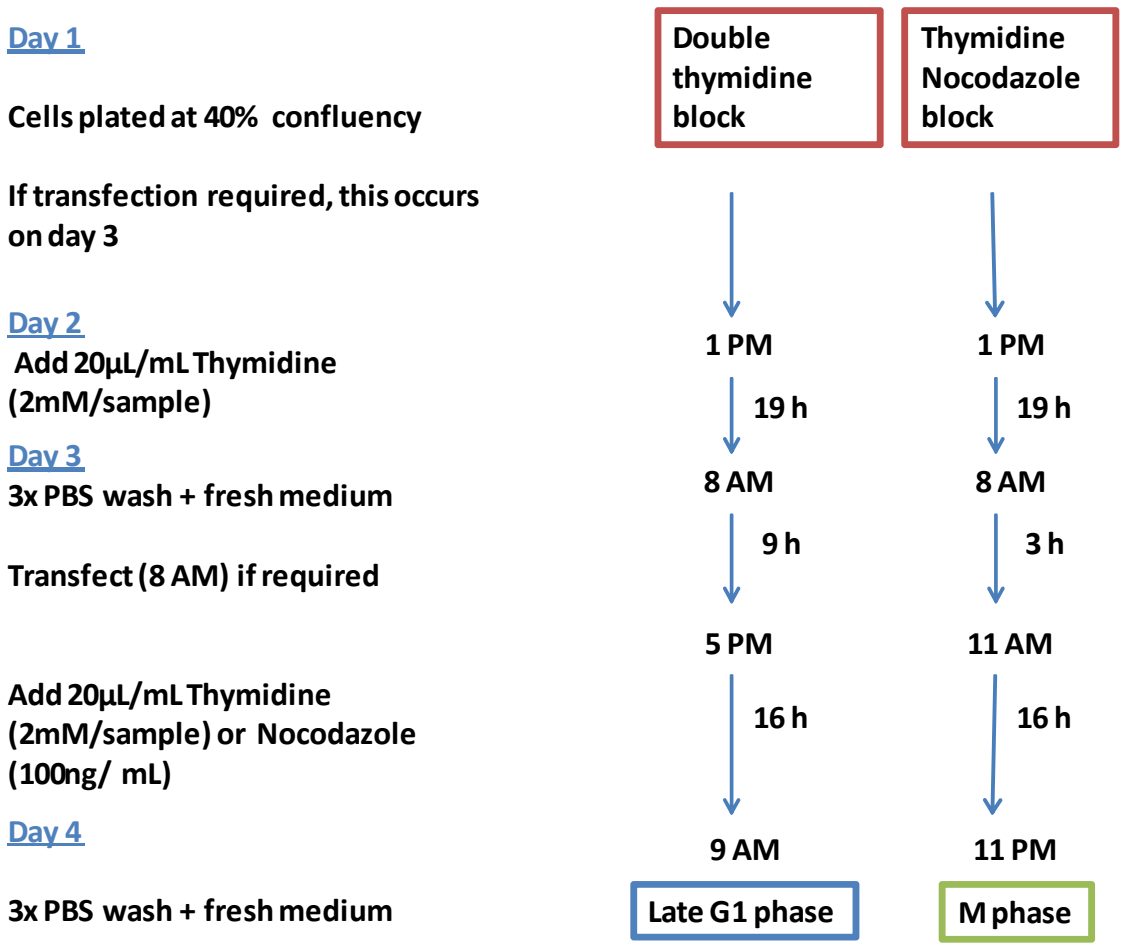

Figure 3-1: Schematic flow chart for cell cycle block protocols.

3.7.3 Propidium Iodide (PI) staining protocol:

The harvested cells were collected, washed with pre-warmed PBS and centrifuged for 5 min at 100 g as described in [128]. Generally 1 X 10^5 cells were re-suspended with 100 µL PBS and fixed with 1 mL ice cold 70 % ethanol added dropwise to the cells with continuous gentle vortexing. Equal number of cells in each sample was kept at 4 ^{o}C for at least 16 h before staining. On the day of analysis, cell pellets were washed with PBS and stained with 1 mL PI buffer (50 µg / mL Sigma), 0.2 % Triton x100 (Sigma) and 1 mg/mL RNase (Sigma, R6513) freshly

added. Cells were incubated in the dark for 15 min at room temperature. Then the stained cells were subjected to flow cytometry using Guava Easy-Cyte flow cytometer (Guava Technology, version 5.3.0.0 and cytosoft PCA96 software) or by BD Biosciences flow cytometer; the best detection of the PI staining (535 – 617 nm) using this machine was achieved by using the PE-Texas Red channel and filter. Results were analysed by Flow Jo software.

3.8 Cell Proliferation assays:

Cells (Table 5), were seeded in triplicate in 96 well plates, and at 40 % confluence, cells were transfected with 30 nM UHRF1- targeting or control siRNA as described earlier in section (3.6). Proliferation was measured 72 h later using the MTS EZ4U kit (Biomedica, Vienna, Austria) according to the manufacturer's instruction and as described in [156]. Briefly, the transfection medium was replaced with 100 µL of fresh medium contains substrate (SUB) and activator solution (ACT) (1: 10) and the absorbance was measured immediately using a Multiskan EX plate reader (Thermo Scientific, UK) at 450 nm and the optimized reading were normalized to the reading at 620 nm. Plates were subsequently read every hour up to 3 h.

Cell line	Incubation Time (h)				
	24	**48**	**72**	**96**	**120**
Suit-2	3	1.5	1.5	1	0.5
MiaPaca-2	4.5	3	3	1.5	1
CFpac-1	4.5	3	3	1.5	1.5
Panc-1	6	4.5	4.5	3	3

Table 5: The initial number of pancreatic cancer cells (n X 10^3) seeded in 96 well plates based on the required incubation time for MTS assay.

3.9 Apoptotic cell analysis:

3.9.1 Annexin V Assay:

Following transfection with UHRF1-targeting and control siRNAs, cell death was analyzed using an Annexin V apoptosis Detection kit II from BD Pharmingen according to the manufacturer's instruction and as described in [128]. Approximately, 1 X 10^6 cells were collected and washed with PBS and resuspended in 1 mL of 1X binding buffer and aliquoted into 1 X 10^5 cells in a 5 mL tube (1 mL) and 3 µL of Annexin V and 2 µL of PI were added to the cells and mixed by gentle vortexing and incubated in dark for 15 min at room temperature. After incubation, 400 µL of 1X binding buffer were added to each tube and analyzed by Cyan flow cytometry within 1 h. To set up the flow cytometry, additional control cells, unstained cells, cells stained with FITC Annexin V only and cells stained with PI only were used as recommended by the kit's instruction. Results were analyzed by Summit software.

3.9.2 Caspase 3/7 activity assay:

Cells were seeded in triplicate in a white walled flat-bottomed 96 well plate at a density of 5,000 cells per well in 100 µL medium, and either transfected with or without UHRF1-targeting siRNA or control siRNA, as described before for 72 h. Transfected cells were either treated with or without the general caspase inhibitor ZVAD to a concentration of 30 µM and incubated at 37^{o}C for 36 h. The activity of caspase 3/7 was then measured using the caspase- Glo 3/7 (Promega, UK) assay kit according to the manufacturer's instructions and as described in [157]. Briefly, 100 µL of caspase reagent was added to the cells and mixed well, followed by

incubation for 1 h in the dark at room temperature. Luminescence was then measured using a 96 well plate luminometer. The results of the luminescent signal are directly proportional to the amount of caspase activity present in each sample.

3.10 Quantification of mRNA levels:

3.10.1 RNA extraction from cultured cells:

RNA was extracted from cultured cells using RNeasy kit (QIAgen) according to the manufacturer's instructions and as described in [128]. Briefly, cell lysate was collected by adding 200 µL of cell lysis buffer directly to the cultured cells and loaded into a QIAshredder spin column placed in a 2 mL collection tube and centrifuged for 2 min at 17,000 g. Cell lysate was mixed with 70% ethanol and transferred to RNeasy spin column placed in 2 mL collection tube and centrifuged for 15 sec at 10,000 g. The spin column was placed in a clean 2mL collection tube and 350 µL of the washing buffer RW1 were added and centrifuged for 15 sec at 10,000 g. DNase mix (RNase-free DNase set, cat no. 79254) was added directly on to the RNeasy silica-membrane, incubated at room temperature for 15 min, washed with 350 µL of RPE buffer and centrifuged for 15 sec at 10,000 g. The washing step was repeated twice and an additional centrifugation step was undertaken to ensure removal of any excess washing buffer. The RNA was collected in a clean 1.5 mL collection tube using RNeasy free water (50-200 µL) and the quality and quantity of the RNA were assessed by nano-drop spectrophotometry.

3.10.2 cDNA synthesis:

cDNA synthesis was performed using Promega Improm II reverse transcriptase (RT) kit (Promega) following the manufacturer's instructions and as described in [128]. Approximately 2 µg of RNA was reverse transcribed by mixing it with the primer mix in a final volume of 20 µL and incubating at 70 °C for 5 min followed by addition of 20 µL of RT mix to each sample (final volume 40 µL). cDNA was synthesised using the polymerase chain reaction (PCR) according to the following cycles: 25°C for 5 min, 42°C for 60 min, 70 °C for 15 min and stored at -80 °C.

3.10.3 Real-Time PCR (RT-PCR):

Quantitative real-time PCR (qRT-PCR) was performed as described in [128] to measure the mRNA levels of the following targeted genes: *KEAP1, NRF2, GCLC, HO-1* and a house keeping gene *GAPDH*. Primers were designed using Primer Express Software (Applied Biosystem, UK) as shown in (Table 6). Sybr green master mix (JumpStart Taq, ready mix, 54438-500 RxN) was used for qPCR following the manufacturer's protocol. Briefly, 50 ng of cDNA was mixed with 2X SYBR master mix buffer and 1 % of primer dilution mix. The RT-PCR reaction was performed in a 96 well plate in a total volume of 20 µL per reaction. Samples were incubated for 2 min at 50 ^{o}C and 10 min at 95 ^{o}C, followed by 40 cycles of denaturation at 95 ^{o}C for 15 sec, and annealing/extension at 60 ^{o}C for 1 min. The mRNA quantification was determined by real-time PCR (Light Cycler machine from Applied Biosystem (ABI PRISM, 7000 sequence detection system) and the outcome data were analyzed using ABI PRISM 7000 SDS software SYBR green template mode. The assay was performed in triplicate and *GAPDH* was used for normalization.

Gene	Primer and nucleotides sequence	
KEAP1	Forward	5' – CAG ATT GGC TGT GTG GAG TT – 3'
	Reverse	5' - GCT GTT CGC AGT CGT ACT TG – 3'
NRF2	Forward	5'- GAG AGC CCA GTC TTC ATT GC – 3'
	Reverse	5' – TTG GCT TCT GGA CTT GGA AC- 3'
GCLC	Forward	5'- AAC CCA AAC CAT CCT ACC CT - 3'
	Reverse	5'- CTC CTC CTT CCA CTG GGT TG - 3'
HO-1	Forward	5'- GCC AGG TGC TCA AAA AGA TT - 3'
	Reverse	5' – CCT GCA ACT CCT CAA AGA GC – 3'
GAPDH	Forward	5'- GGC CTC CAA GGA GTA AGA CC – 3'
	Reverse	5' – AGG GGT CTA CAT GGC AAC TG – 3'

Table 6. Primers used for RT-PCR.

3.11 DNA methylation analysis:

3.11.1 DNA extraction from cultured cells:

DNA extraction from cultured cells was performed using QIAamp DNA mini kit (Qiagen, cat: 51304), using the spin protocol, as recommended by the manufacturer. Briefly, harvested cells were lysed in 200 µL of lysis buffer (AL) followed by the addition of 20 µL of QIAGEN Protease solution. Lysates were then incubated at 56 ^{o}C for 10 min and centrifuged at 6,000 g for 1 min followed by the addition of 200 µL of absolute ethanol and each sample was vortexed for 15 sec. Samples were loaded onto the DNeasy mini spin column, centrifuged at 6,000 g for 1 min, washed with 500 µL of washing buffer (AW1) and centrifuged at 6,000 g for 5 min. This was followed by replacement of the collection tube, addition of 500 µL of washing buffer (AW2) and centrifugation at 17,000 g for 3 min. To ensure removal of any remaining buffer, a further centrifugation at 17,000 g for 2 min was performed using a clean collection tube. The DNA was

eluted from columns using 100 - 200 µL elution buffer (AE) followed by spinning at 17,000 g for 1 min. The DNA purity and quantity were then assessed by the Nanodrop spectrophotometer (Thermo Scientific ND-1000 spectrophotometer). The DNA was stored at -20 ^{o}C.

3.11.2 CT conversion and DNA clean up:

Approximately 1 µg of DNA (in 20 µL solution volume) was treated with EZ DNA methylation-Gold Kit (Zymo Research, Orange, CA, USA), reagent preparation, CT conversion and DNA clean up procedures were carried out according to the manufacturer's instructions. Briefly, 900 µL of dH2O, 300 µL of M-Dilution Buffer and 50 µL M-Dissolving Buffer were mixed together in the CT Conversion Reagent tube and allowed to dissolve at room temperature with continuous shaking for 10 min. In PCR tubes, 130 µL of the CT conversion reagent were added to 20 µL of the DNA and mixed by gentile pipetting. CT conversion reactions were then performed in the thermal cycler according to the following incubation periods: 98 ^{o}C for 10 min, 64 ^{o}C for 150 min and a final hold at 4 ^{o}C. The treated DNA was then added to Zymo-Spin IC column placed in a collection tube containing 600 µL of M-Binding buffer, mixed by gently pipetting and incubated for 1 min at room temperature. Samples were then centrifuged at 17,000 g for 1 min and columns were washed with 200 µL of M-washing buffer followed by centrifugation at 17,000 g for 1 min. Then 400 µL of M-Desulphonation Buffer was added to the column and incubated at room temperature for 15 min then centrifuged for 1 min at 17,000 g. Samples were then washed twice with 200 µL of M-wash buffer and centrifuged for 2 min after the first wash and for 5 min at 17,000 g after the second wash to eliminate any remaining buffer. Columns were placed in 1.5 mL micro-centrifuge tubes and 75 µL of pre-warmed (at 50 ^{o}C) M-elusion buffer was added above the membrane. Treated DNA was collected in 1.5 mL tubes by centrifugation

at 17,000 g for 1 min. The bisulphate treated DNA was used as a template in the amplification of the promoter regions of *KEAP1, CDKN2A, RASSF1, Alu-V and LINE-1* elements by PCR prior to pyrosequencing.

3.11.3 Pyrosequencing Primer Design for *KEAP1*, *CDKN2A*, *RASSF1, Alu-V* and *LINE1* elements:

Primers were designed using Pyromark Assay Design Software by Qiagene (Appendix. 2) and synthesized by Eurofins MWG Operon (Ebersberg, Germany). The following table shows the primers sequences, product size and number of CpGs included in the analysis for each gene.

Region	Primer's	Primer's sequence	Size (bp)	CpGs
KEAP1a	Forward	5' BIO- AAA GGA GAA TAG TAG ATG GTG G -3'	87	6
	Reverse	5'- TCC CTA TCA CTC TTC CCC -3'		
	Pyrosequencing	5'- CCT TCC CTA TCA CTC TT -3'		
KEAP1b	Forward	5'- GGG TAG GTT ATT ATG TTA AGT AGA -3'	97	5
	Reverse	5'BIO- CCC AAA ACC AAA ATC CTC CA -3'		
	Pyrosequencing	5'- ATTATGATTAAGTAGAGT -3'		
LINE-1	Forward	5'BIO- TAG GGA GTG TTA GAT AGT GGG -3'	89	7
	Reverse	5'- CTT CCC AAA TAA AAC AAT ACC -3'		
	Pyrosequencing	5'- CCA AAT AAA ACA ATA CCT C -3'		
RASSF1	Forward	5'- AGT ATA GTA AAG TTG GTT TTT AGA AA -3'	117	9
	Reverse	5'- BIO-CCC TTC CTT CCC TCC TT -3'		
	Pyrosequencing	5'- AAG TTG GTT TTT AGA AAT A -3'		
CDKN2A	Forward	5'- AGG GGT TGG TTG GTT ATT AG -3'	75	7
	Reverse	5'-BIO- CTA CCT ACT CTC CCC CTC TC -3'		
	Pyrosequencing	5'- GGT TGG TTA TTA GAG GGT -3'		
ALU-V	Forward	5'-GAG GTT GAG GTA GGA GAA - 3'	85	4
	Reverse	5'- BIO-CCC AAA CTA AAA TAC AAT AAC-3'		
	Pyrosequencing	5'- GTT GAG GTA GGA GAA- 3'		

Table 7 . Primers used for PCR amplification and Pyrosequencing.

3.11.4 PCR amplifications:

PCR reactions were amplified in a final volume 25 µL using Qiagene Hotstart Plus Master Mix Kit (Qiagen). Briefly, 200 nM biotinylated primers, 400 nM non-biotinylated primers and 100 ng of bisulphite-treated DNA were mixed together and the Applied Biosystems PCR GeneAmp 9700 Thermocycler was used to amplify the targeted sequences according to the following cycles (All PCR programs required initial denaturation and *Taq* activation 95 ^{o}C, 5 min for 1 cycle, Final extension: 72 ^{o}C for 7 min for 1 cycle and a final hold at 6 ^{o}C). The *LINE1* PCR programme was 40 cycles of 94 ^{o}C for 30 sec, 58 ^{o}C for 45 sec, 72 ^{o}C for 45 sec. The *Alu-V* PCR programme was 40 cycles of 94 ^{o}C for 30 sec, 49 ^{o}C for 45 sec, 72 ^{o}C for 45 sec. The *CDKN2A* PCR programme was 10 cycles of 94 ^{o}C for 30 sec, 56 ^{o}C for 40 sec, 72 ^{o}C for 30 sec followed by 30 cycles of 94 ^{o}C for 30 sec, 55 ^{o}C for 30 sec, 72 ^{o}C for 30 sec. The *RASSF1* PCR program was 40 cycles of 94 ^{o}C for 30 sec, 50 ^{o}C for 30 sec, 72 ^{o}C for 30 sec. The *KEAP1a* and *KEAP1b* PCR programme was 40 cycles of 94 ^{o}C for 20 sec, 56 ^{o}C for 30 sec, 72 ^{o}C for 30 sec. The quality and quantity of PCR products were confirmed by examining 3 µL of the PCR reactions in 2% agarose gel electrophoresis (Fisher Scientific, BP: 1356-500). The DNA was stained with special nucleic acid stain (Safe View, Code: NBS-SVI, NB Biologicals) and visualised by a UVP VisionWorks LS instrument prior to Pyrosequencing analysis.

3.11.5 Pyrosequencing assay:

Pyrosequencing was performed using PSQA kit (Biotage, Uppsala, Sweden) according to the manual instruction. Briefly, a mixture of streptavidin sepharose beads and binding buffer dilution (Qiagen) were added to the PCR products in 96 well plates and mixed well by vortexing for 20 min. Using the PyroMark vacuum station (Figure 3-2A), the filter probes were placed in

sterile water for 30 sec and inserted into the 96 well-plate containing the PCR product-streptavidin mixture for double stranded PCR binding, followed by washing with 70 % ethanol for 10 sec and denaturation by 0.2 M NaOH for 20 sec. The single-stranded biotinylated template was then washed in washing buffer for 10 sec and released by incubation at 80 °C for 2 min with continuous shaking in a Pyromark Q96 plate containing sequencing primers followed by a cooling down for 2 min and then the plate was placed in the PSQ instrument. The PyroMark Q96 cartridge, cartridge 5 (Figure 3-2 B), was loaded with PyroGold Q96 reagents (PyroMark Gold Q96, Cat: 972804, Reagents: 5X96), according to pre-run information (PSQ™ 96 MA software). Each run contained at least 1 internal bisulphate conversion control and a no template control. The proportion of DNA methylation at each CpG site was automatically calculated by the PSQ™ 96 MA software and given as a percentage. The methylation index for each promoter was calculated as the mean value of mC/(mC+C) where C is unmethylated cytosine and mC is 5’ methyl-cytosine. The DNA methylation analysis including DNA extraction, CT conversion, PCR amplification and pyrosequencing was described in [64].

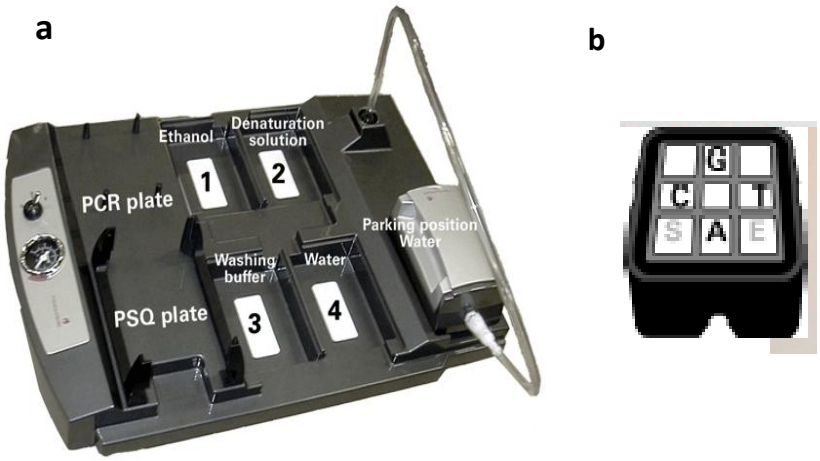

Figure 3-2: The pyrosequencing station. (a). The PyroMark vacuum station. (b). The pyrosequencing cartridge. S: substrate. E: enzyme. G, T, A and C: dNTPs.

3.12 Cell treatment with siRNA and 5-aza-2'-deoxycytidine:

In 6 well / plates, 1 X 10^5 cells were seeded and incubated overnight to achieve 40 % confluence. The next day the culture medium was changed and cells were treated with 100 µM 5-aza-2'-deoxycytidine (Decitabine, Sigma-Aldrich, cat no11390) in the presence or absence of UHRF1-targeting or control siRNA for 72 h, with culture medium replaced with fresh medium containing 100 µM 5-aza-2'-deoxycytidine every 24 h. Cells were harvested and DNA extraction was used in DNA methylation analysis by pyrosequencing in addition to protein analysis. The summary of this protocol is shown in Figure 3-3.

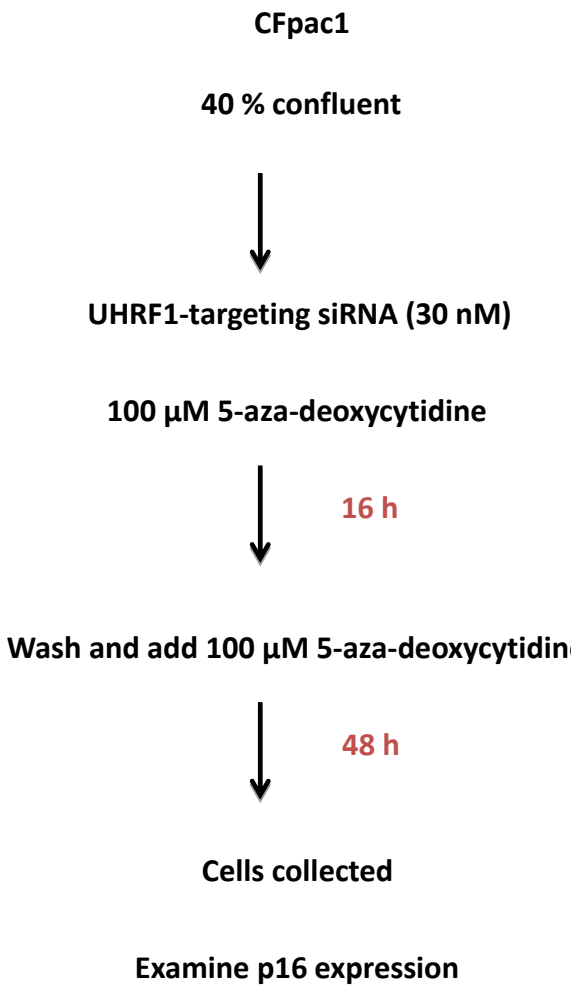

Figure 3-3: Schematic flow chart of siRNA and 5-aza-deoxycytidine cell treatments.

3.13 Cell treatment with sulforaphane:

In 6 well / plates, 1 X 10^5 cells were seeded and incubated overnight to achieve 40 % confluence. The next day the culture medium was changed and cells were treated with 5 µM sulforaphane in the presence or absence of UHRF1-targeting or control siRNA for 72 h. Cells were harvested for protein analysis.

3.14 Immunohistochemistry (IHC) for UHRF1 detection:

IHC conditions were optimized by evaluating two different antigen retrieval buffers (10 mM EDTA buffer pH: 8 and Citrate Buffer pH: 6) and demonstrating the best primary antibody concentration (1:50, 1:100, 1:200, 1:300) using different cells lines and tissue sections. IHC staining was performed on tissue sections and TMA as described in [128]. Generally, the sections were incubated in Xylene for 30 min followed by re-hydration in graded ethanol, 100 %, 90 %, 70 % and 30 %, for 3 min and final 5 min incubation in dH_2O. Antigen retrieval was obtained by pressure cooking the slides for 5 min in 10 mmol EDTA (pH: 8) following by cooling down for 15 min and washing with PBST (0.04 % Tween 20) for 15 min (3 X 5 min). The sections were then blocked using peroxidise blocking reagent (Dako, ref: 4006) for 10 min then washed with PBST for 15 min (3 X 5 min) and further blocked by 5% filtered Bovine Serum Albumin (BSA) for 30 min prior to primary antibody incubation. Anti-UHRF1 (1:200) and KEAP1 (1:100) were incubated at 4˚C overnight. The slides were then rinsed in TBST and incubated with a relevant conjugated secondary anti-body (Dako) for 1h at room temperature followed by 3 washes in PBST for 15 min. The staining was developed in DiAminoBenzidine (DAB) reagent (Dako, liquid DAB and substrate chromogen system, code: K3467) and washed with PBST and counterstained with Haematoxylin (Hematoxylin solution according to Mayer, Sigma, 51275) for 1 min following washing with running water for 5 min and slides were dehydrated in graded ethanol concentrations, 30 %, 70 % and 100 %, for 1 min and a final 3 min in Xylene (Fisher Scientific, code: X/0250/17) and mounted with DPX (VWR, ref: 360292F) for microscopic examination and scoring.

3.15 Immunocytochemistry (ICC) for UHRF1 detection:

Routinely 10,000 cells / well were seeded and incubated for 24 h at 37˚C in 5 % CO_2 using chamber slides (154534, lab Tek II, chamber slide with cover, size 8 well, RS glass slide sterile). The next day medium was removed and cells were washed with PBS and fixed using 500 µL of 4 % formalin solution (DPH laboratory supplies, 28794, 295) and incubated at room temperature for 30 min. Following washing with 500 µL PBST containing 0.2 % Triton X-100 (Sigma) for 5 min, slides were washed with PBS for 3 X 5 min and blocked with peroxidase blocking reagent (Dako, ref: 4006) for 10 min. Cells were incubated with primary antibody (1:400) overnight at 4° C, then washed with PBST for 3 X 5 min and incubated with secondary antibody at room temperature for 1 h, and then washed with PBST for 3 X 5 min. The staining was developed in DiAminoBenzidine (DAB) reagent (Dako, liquid DAB and substrate chromogen system, code: K3467) followed by 3 washes and counterstained by incubation with with Haematoxylin (Hematoxylin solution according to Mayer, Sigma , 51275) for 1 min, washed with running water for 5 min, followed by dehydration in a graded ethanol concentrations, 30%, 70% and 100%, for 1 min in each and a final 3 min in Xylene (Fisher Scientific, code: X/0250/17). The chamber boarders were removed and mounted with DPX (DPX mount for microscopy, VWR, ref: 360292F) for microscopic examination.

3.16 Immunofluorescence detection of UHRF1 in pancreatic cancer cells:

Prior to seeding cells, coverslips were cleaned in ethanol-HCl solution (200 mL 70 % ethnol + 6 mL concentrated HCl) by soaking for at least 1 h. The coverslips were then rinsed with sterile PBS and placed in sterile dishes with 70 % ethanol before being placed in the tissue culture

plates. One coverslip was used in each well of a 24 well dish and 70,000 cells / well were seeded onto each coverslip and incubated for 24 h. Cells were then washed with PBST and fixed using 500 µL of 4 % formalin solution for 15 min with gentle shaking at room temperature. Following washing with 1 mL PBST containing 0.02% Triton X-100 (Sigma) for 5 min, slides were washed with PBST for 3 X 5 min and blocked with 3 % BSA for 20 min. Cells were incubated with UHRF1 primary antibody (1:400) overnight at 4° C and then washed with PBST for 3 X 5 min and incubated with secondary antibody (Donkey anti-mouse Cy3, 715-165-151, Stratech Scientific) at room temperature for 1h in the dark. Cells were washed with PBST for 3 X 5 min and mounted with 4 µL of the mounting medium (Mowiol 4-88/DABCO with addition of DAPI, 0.1 µg / mL).

3.17 Scoring and statistical analysis:

Scoring of the IHC slides was reviewed by 2 pathologists (Prof Fiona Campbell and Dr Timothy Andrews). The information recorded for UHRF1 included the nuclear intensity (graded 0 = negative, 1 = weak, 2 = moderate and 3 = strong). KEAP1 staining was patchy and granular throughout the tumour, therefore scored as either positive or negative. All statistical analyses were performed using StatView version 5.0.1 (SAS Institute Inc., Cary, North Carolina). To obtain associations between UHRF1 nuclear protein expression and clinical parameters, data were cross-tabulated and Fisher's two-sided exact tests applied or Mann-Whitney U-tests performed. Survival analysis was performed using Kaplan-Meier analysis. Spearman's rank correlation was used to correlate the agreement of the nuclear UHRF1 staining percentage

between Abcam antibody and Santa Cruz antibodies. Results were considered significant for p values < 0.05.

Generally, the analysis of continuous data that were normally distributed was tested by t-test and for data that were not normally distributed a non-parametric test was used such as Mann-Whitney. The methylation index for each promoter was calculated as the mean value of mC/(mC+C) by the PSQ™ 96 MA software and given as a percentage. To assess the association between the control siRNA treated cell sets and the UHRF1 depleted cell sets for the DNA methylation analysis and between cells treated or not treated with 5-aza-deoxycytidine, an un-paired t-test was used to analyze methylation values among each group. The caspase 3/7 activity assay and MTS assay data analysis were performed by un-paired t-test. All statistical analyses were performed using StatView version 5.0.1 (SAS Institute Inc., Cary, North Carolina). Results were considered significant for p values < 0.05.

Chapter 4:

Results and data analysis

4 Results and data analysis:

4.1 Measurement of UHRF1 protein expression levels in different pancreatic cancer cell lines and in pancreatic cancer tissue:

4.1.1 UHRF1 expression in tumour cells:

UHRF1 is overexpressed in several types of human cancers [55, 56]. A study in this laboratory had reported overexpression of UHRF1 in pancreatic cancer but not in normal pancreas [37]. However, no descriptive or functional studies of URF1 in this cancer type have been published. Therefore, UHRF1 expression in pancreatic tumors and pancreatic cancer cell lines was investigated.

4.1.2 UHRF1 antibody validation:

Prior to immunohistochemcial staining (IHC) of a pancreatic cancer TMA, two different lysis buffers were evaluated for UHRF1 detection and two independent UHRF1 antibodies, from Abcam and Santa Cruz. As shown in Figure 4-1 a, western blotting analysis of total protein lysate from Panc-1 cells revealed a band of approximately 90 kDa when whole cell lysate was prepared using Tris-SDS lysis buffer (the protein was not detectable when RIPA buffer was used), equivalent to the expected size for UHRF1. This observation was also made for CFpac-1 and Suit2 cells, therefore Tris-SDS lysis buffer was used for subsequent experiments. We examined for specificity for UHRF1 detection using western blotting as in Figure 4-1 b, MiaPaca-2 cells using the Abcam antibody showing single band at the expected molecular weight of UHRF1. Furthermore, no UHRF1 protein expression was detected in cells treated with specific UHRF1-targeting siRNA, where expression was detected in cells treated with the off-target

control siRNA. This validation was also made in Suit-2, CFpac-1 and Panc-1. Moreover, as shown in Figure 4-1 c, the two independent antibodies successfully detected UHRF1 as confirmed by loss of expression in cells treated with the UHRF1 siRNA but not the off-target control siRNA. In this study we used 4 different UHRF1-targeting siRNA sequences for UHRF1 depletion, these siRNA were evaluated prior to use and all resulted in considerable UHRF1 depletion (Figure 4-1 d).

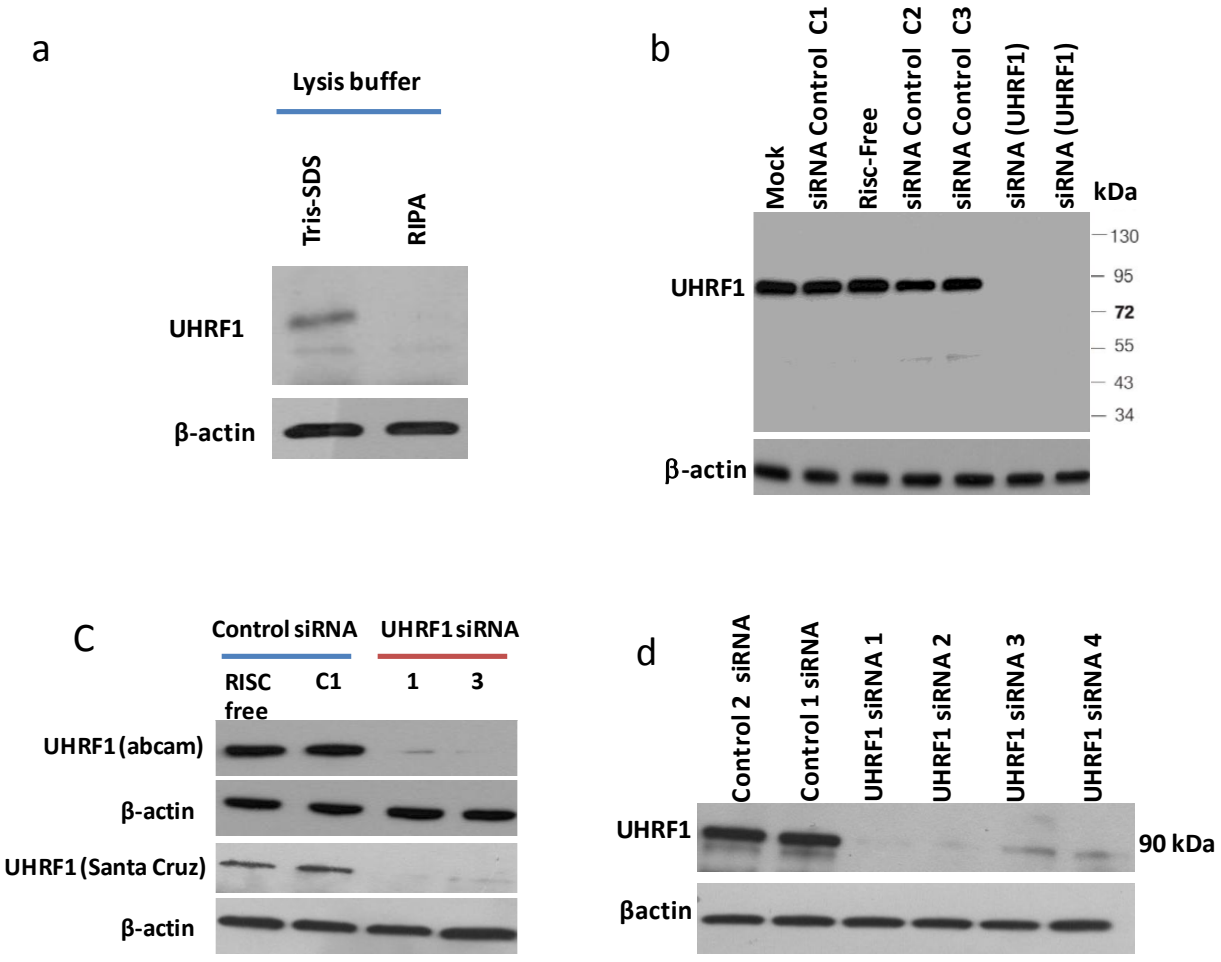

Figure 4-1. UHRF1 antibody validation (a) UHRF1 detection using the Abcam antibody in Panc-1 cells using Tris-SDS or RIPA lysis buffer. (b) MiaPaca-2 cells following transfection with control siRNAs (C1, C2, C3), Risc-Free or 30 nM UHRF1-targeting siRNAs (1 and 3) for 72 h (n=3). (c) Western blot analysis for UHRF1, using Abcam and Santa Cruz antibodies, following treatment

of MiaPaca-2 cells with Risc-Free, control siRNA or 30 nM UHRF1-targeting siRNAs 1 and 3 for 72 h (n=3). (d) Western blot of UHRF1 following UHRF1 depletion using 4 different UHRF1-targeting siRNA, 30 nM of each siRNA was used for 72 h (n=2). β-actin was examined in figure 1a, b and c to verify equal loading of samples.

4.1.3 Validation of UHRF1 antibodies in IHC experiments:

Thirty-two pancreatic cancer cases provided by the Liverpool CRUK tissue bank were examined for UHRF1 expression using the two antibodies (Abcam and Santa Cruz). As shown in Figure 4-2 a, both antibodies detected nuclear UHRF1 expression as indicated by positive staining. Interestingly, staining in the cytoplasmic compartment was also detected using the Abcam antibody. Complete absence or very low levels of cytoplasmic UHRF1 was detected with the Santa cruz antiboy. The percentages of positive nuclei detected by each antibody was highly correlated (Rho=0.89, $p<0.001$) providing strong evidence of specificity for nuclear UHRF1 (Figure 4-2 b). Our study therefore focused on nuclear UHRF1 expression.

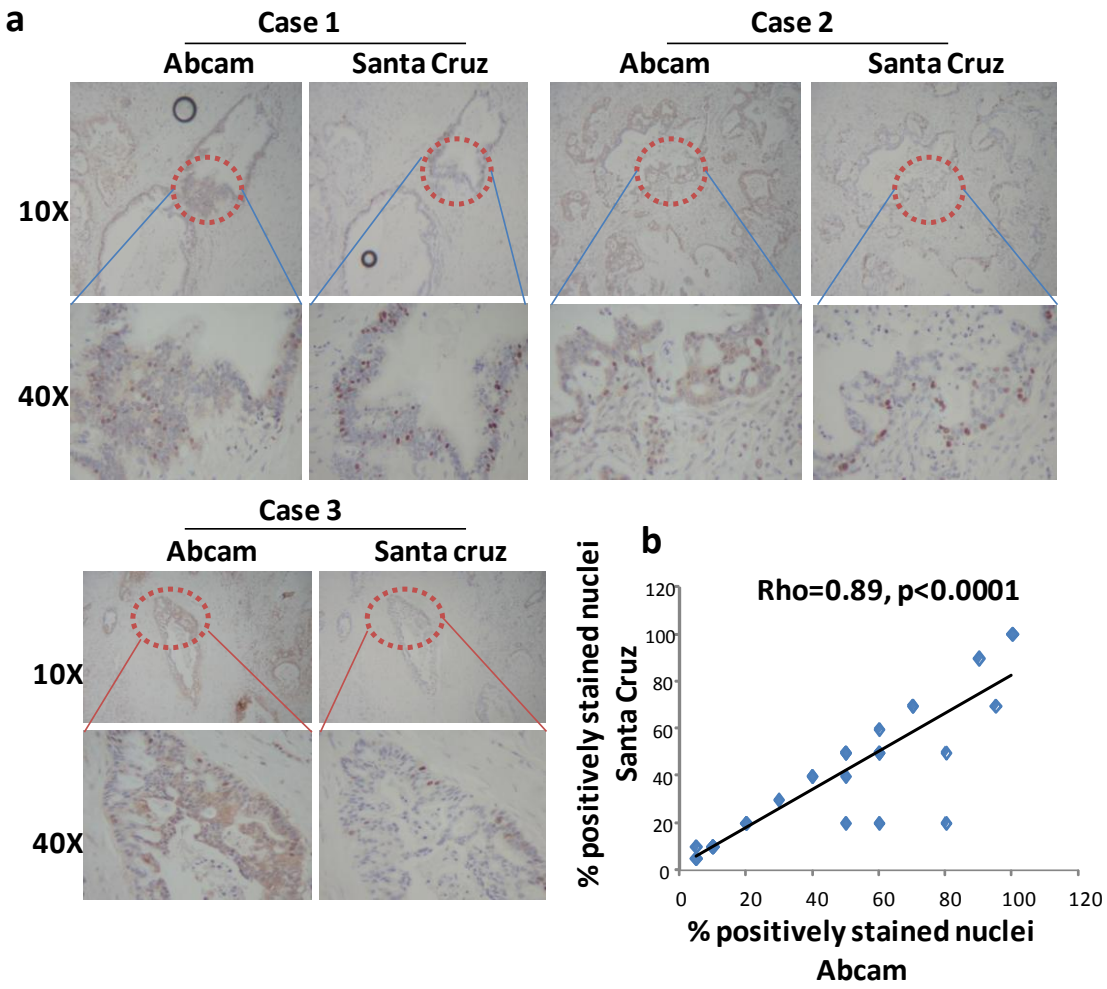

Figure 4-2. Comparison of Abcam and Santa Cruz UHRF1 antibodies. (a) Immunohistochemical staining of UHRF1 in 3 independent pancreatic cancer cases. (b) UHRF1 positive nuclei stained with Abcam or Santa Cruz antibodies were highly correlated in 32 cases.

4.1.4 UHRF1 protein expression in pancreatic cancer cell lines:

Pancreatic cancer cell lines, including, MiaPaca-2, CFpac-1, Panc-1, Suit-2 and BxPc-3 were examined for UHRF1 protein expression by western blotting analysis. As shown in Figure 4-3, the level of UHRF1 expression was variable between the examined cell lines with high levels observed in MiaPaca-2 and BxPc-3 cell lines and lower levels observed in CFpac-1 and Panc-1 cells.

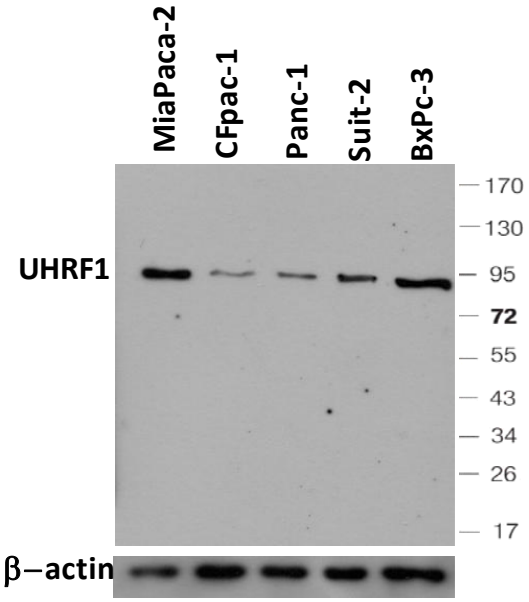

Figure 4-3. Western blot analysis of UHRF1 expression in a panel of pancreatic cancer cell lines. Whole cell lysate from pancreatic cancer cell, MiaPaca-2 shows the highest expression of UHRF1 while CFpac-1 is the lowest (n=5).

4.1.5 Evaluation of UHRF1 protein expression in 132 cases of pancreatic cancer:

Immunohistochemical analysis of a pancreatic cancer tissue micro-array (Figure 4-4 a) containing 132 cases containing matched duplicate non-malignant and malignant cores revealed variable nuclear UHRF1 staining, with 18 patient tumours scored 0 (negative), 36 scored 1 (weak), 48 scored 2 (moderate) and 30 scored 3 (strong). The scores were based on the nuclear intensity of UHRF1 protein staining (Figure 4-4 b).

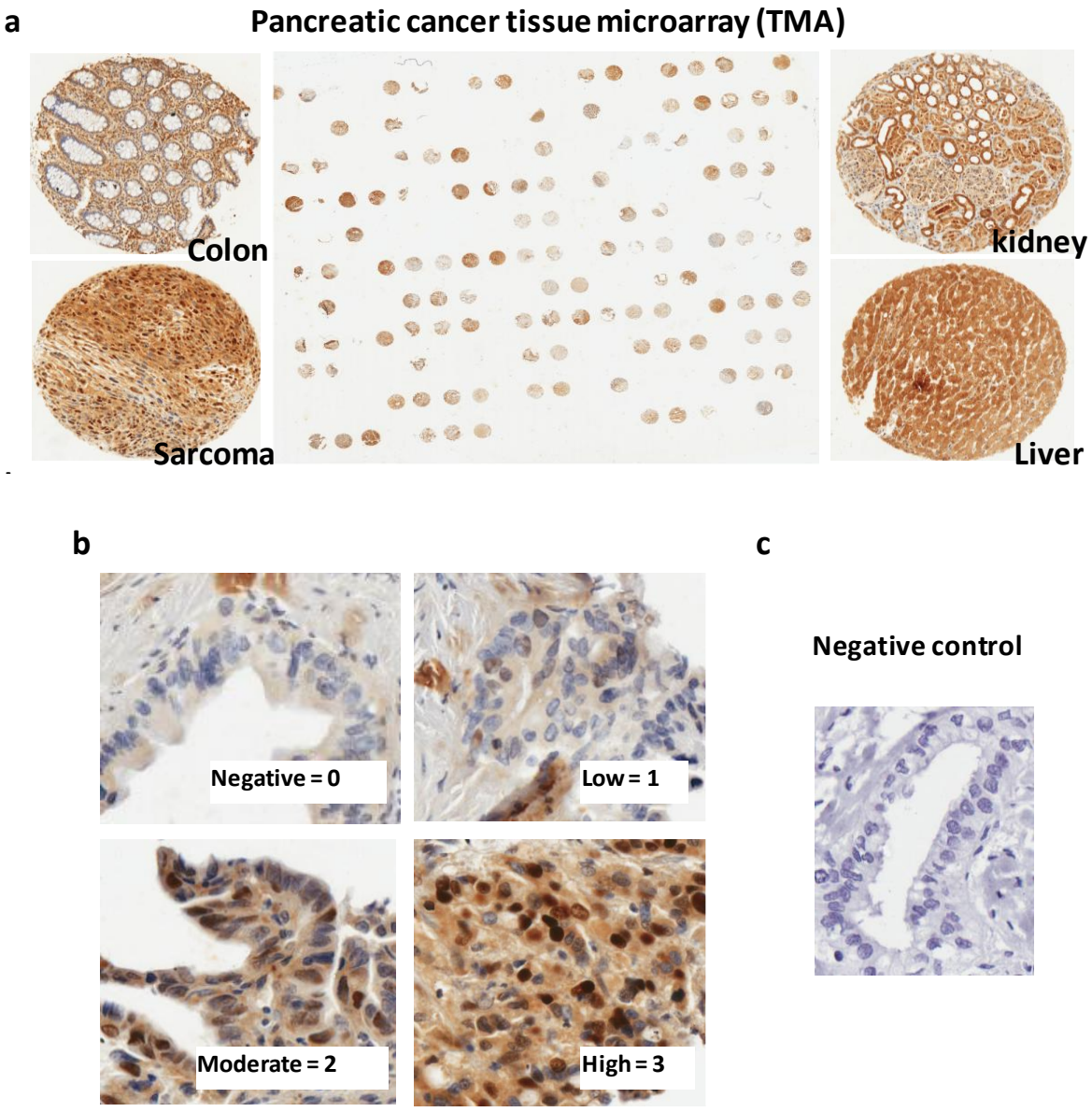

Figure 4-4. Immunohistochemcial analysis of a pancreatic cancer tissue micro-array for the detection of UHRF1. (a) TMA slide, the order of the cases in each slide was labeled and cores of colon, sarcoma, kidney and liver tissues were used for orientation. (b) UHRF1 expression levels in pancreatic cancer tissue scored from 0 to 3 according to the intensity of nuclear UHRF1 staining. (c) Secondary antibody alone was used as a negative control.

Of note, PanIN lesions were stained for UHRF1 at variable levels. In general for the cases where matched tumours and PanIN were available (n=9), the extent of nuclear UHRF1 staining was usually greater in the cancer compared to PanIN (Figure 4-5).

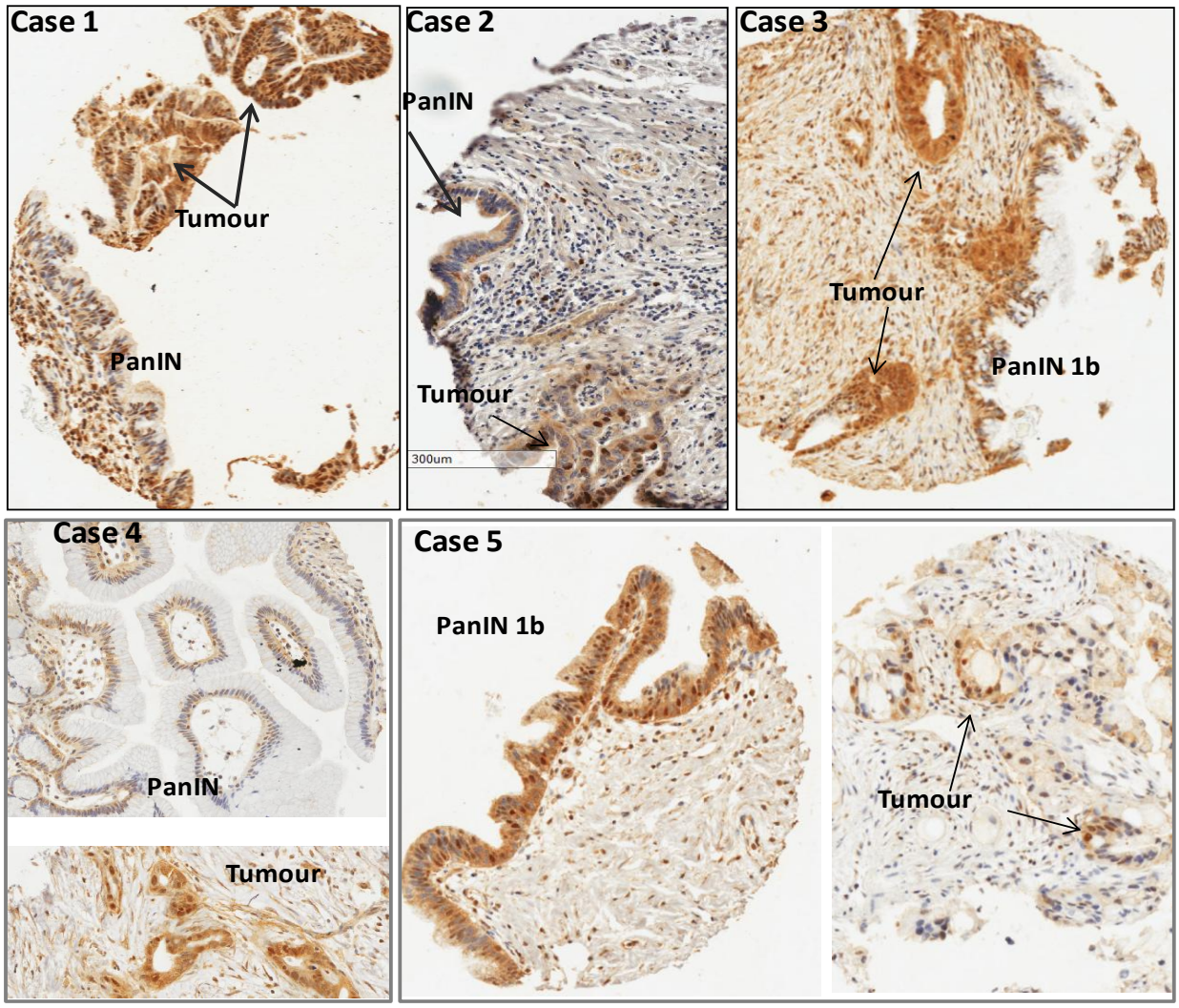

Figure 4-5. Immunohistochemical analysis of UHRF1 in matched PanIN and tumor. Cases 1 – 4 show higher nuclear UHRF1 staining in tumours compared to PanINs. Case 5 shows higher staining in the PanINs compared to tumours. Generally 9 cases were matched and 8/9 showed higher tumour staining compared to PanINs.

Twenty five benign ducts were scored for nuclear UHRF1. Of these, 20 cases (80 %) were negative and the remaining 5 cases were positive for nuclear UHRF1 staining (Figure 4-6).

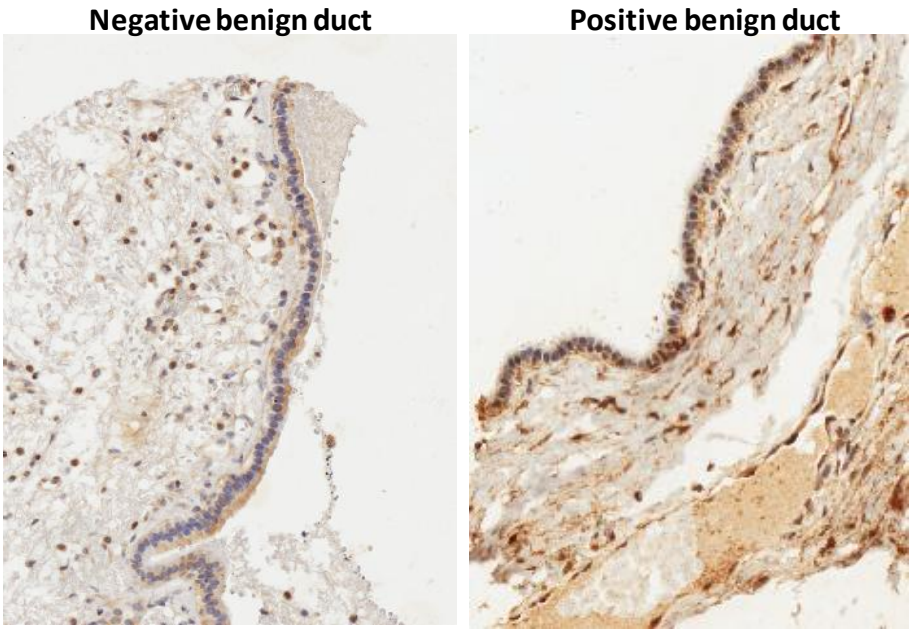

Figure 4-6. Immunohistochemical staining of UHRF1 in pancreatic benign ducts. A total number of 25 benign ducts were stained and scored as either negative or positive. The majority, 80% (20/25), were negative and 20% (5/25) were positive.

Of note, UHRF1 expressed at high levels in inflammatory cells in the stroma (Figure 4-7), case 1 and case 2 showing expression of UHRF1 in tissue section of a patient with pancreatic cancer and pancreatitis. UHRF1 expressed in the stroma in approximately 90 % of the positive tumour cases. This interesting observation needs further analysis and investigations.

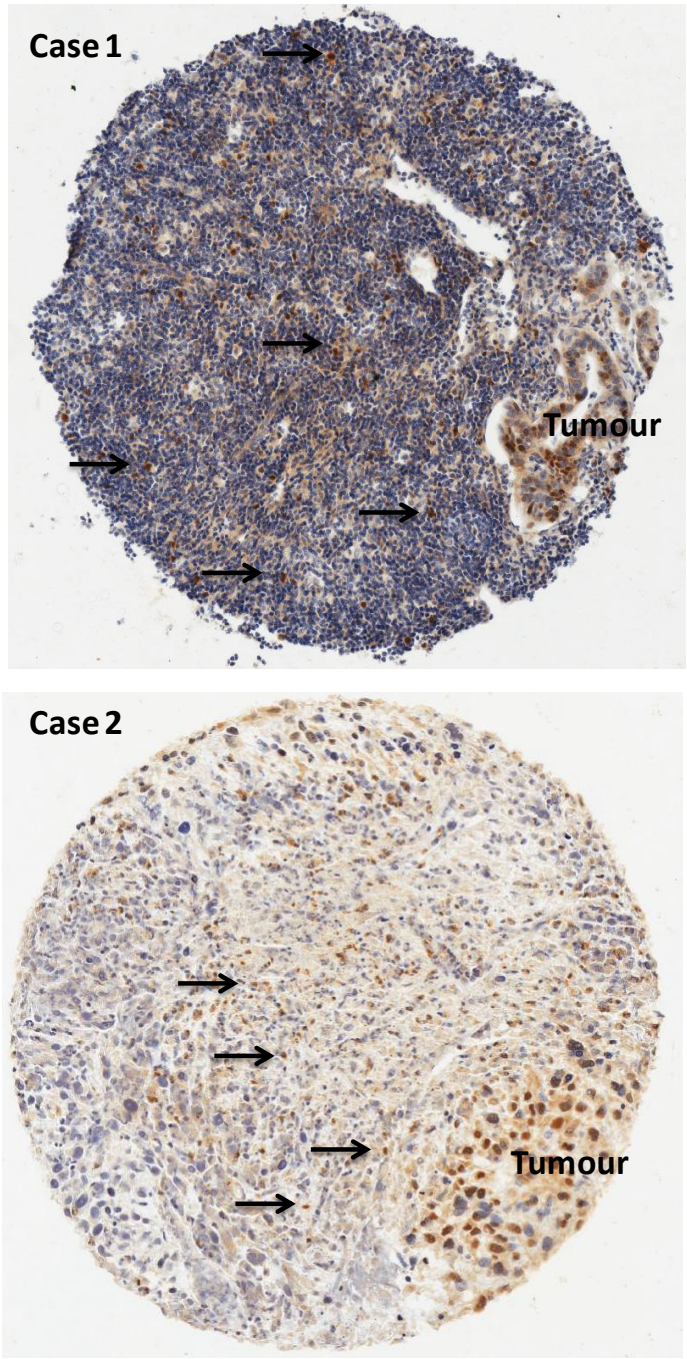

Figure 4-7: Pancreatic cancer sections with positive UHRF1 staining in the stroma. IHC of pancreatic cancer sections stained for UHRF1, the brown staining indicating UHRF1 expression, the blue staining Haematoxylin (nuclei dye). The black arrows point towards UHRF1-positive inflammatory cells.

4.1.6 Statistical analysis of immunohistochemically stained TMAs for nuclear UHRF1:

For analysis, nuclear UHRF1 levels were categorized into two groups according to UHRF1 presence in tissue sections. The first grouping was referred to as negative (score 0) and the second grouping was referred to as positive (score of 1, 2, 3). UHRF1 presence was not associated with age (< or > 60 years Fisher's Exact p=0.35), gender (Fisher's Exact p=0.61), lymph node status (Fisher's Exact p=0.99), grade (poor, moderate, well; Chi Square p=0.09) or outcome (Kaplan Meier test, Logrank p=0.98). However, positive expression of UHRF1 was associated with larger tumour sizes (> 20 or ≤ 20 mm diameter; Fisher's Exact p=0.02) as summarised in Table 8.

Patient's parameter	P value
Age (> 60)	Fisher's Exact p=0.35
Gender	Fisher's Exact p=0.61
Lymph node status	Fisher's Exact p=0.99
Grade (poor, moderate, well)	Chi Square p=0.09
Survival	Kaplan Meier test, Logrank p=0.98
Tumour sizes (> 20 or ≤ 20 mm diameter)	Fisher's Exact **p=0.02**

Table 8: Statistical analysis of the nuclear UHRF1 (negative or positive) to patient's parameters. UHRF1 staining negative (scored 0) in 18/132 cases while the positive cases (scored: 1,2,3) were the majority 86 %.

Another analysis was used to group cases that either lack UHRF1 expression or show weak staining of UHRF1 nuclear indicating low expression in one group (scores 0 or 1), where the medium-high (scores 2 or 3) expression of UHRF1 cases were grouped together indicating high

expression. UHRF1 expression was not associated with age (< or > 60 years Fisher's Exact p=0.18), gender (Fisher's Exact p=0.37) or lymph node status (Fisher's Exact p= > 0.99). On the other hand, UHRF1 expression was correlated with tumour grade (poor, moderate, well; Chi Square p=0.04), outcome showed a trend toward poor survival with UHRF1 high cases (Figure 4-8) (Kaplan Meier analysis, Log-rank p=0.07) and high UHRF1 almost had a significant correlation with larger tumour sizes (> 20 or ≤ 20 mm diameter; Mann Whitney U, p=0.051). The statistical analysis of these groups are summarised in Table 9.

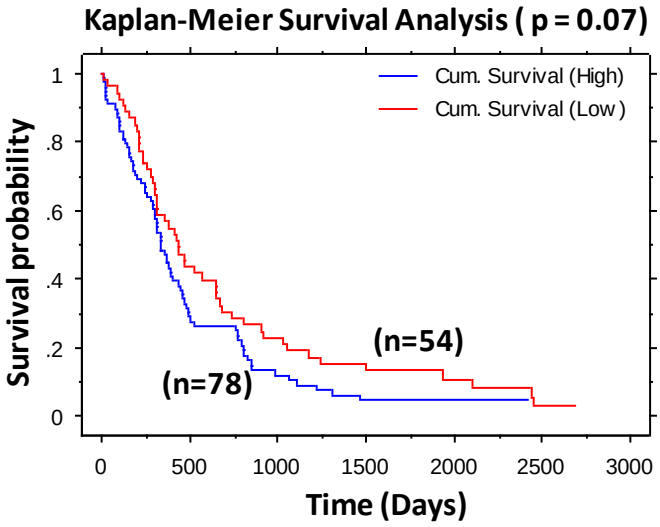

Figure 4-8. Correlation of nuclear UHRF1 expression to patient's survival. Kaplan Meier analysis for 132 pancreatic cancer cases indicating that patients with higher UHRF1 expression have poor survival.

Data		n=132 (%)	Nuclear UHRF1 expression		P
			Low (scored 0/1) (n=54) (%)	High (scored 2/3) (n=78) (%)	
Gender	**Male**	75	28	47	0.37
	Female	57	26	31	
Tumour size	**> 20**	104	39	65	**0.051**
	≤20	28	15	13	
Tumour grade	**Well**	19	6	13	**0.04**
	Moderate	71	36	35	
	Poor	42	12	30	
Age	**>60**	107	44	66	0.18
	≤60	25	14	12	
Lymph node	**Yes**	106	43	66	> 0.99
	No	20	8	12	
Survival		132	54	78	**0.07**

Table 9. Correlation of nuclear UHRF1 expression (low or high) to patient's clinical data. UHRF1 levels were grouped as low (scored 0/1) and high (scored 2/3).

4.1.7 Summary and discussion of UHRF1 protein expression in pancreatic cancer cell lines and in pancreatic cancer tissue

Little is known about UHRF1 expression in pancreatic cancer. No descriptive or functional studies of UHRF1 in this cancer type have been published. Therefore, UHRF1 expression in pancreatic tumors and pancreatic cancer cell lines was investigated here. We observed variable nuclear UHRF1 staining in 132 pancreatic cancer tissues (negative, low, moderate and high), although the majority were positive (86 %). That was also observed in a panel of four pancreatic cancer cell lines including MiaPaca-2, CFpac-1, Panc-1 and Suit-2. MiaPaca-2 showed the highest

UHRF1 protein expression while CFpac-1 showed the lowest. In tissue sections in the matched tumours and PanIN (n=9), the extent of nuclear UHRF1 staining was usually greater in the tumour compared to PanIN, whilst the benign ducts were mostly negative for nuclear UHRF1 staining (80 %). In patient sections, negative UHRF1 expression was statistically correlated with tumour size P=0.02.

In this study, all four pancreatic cancer cells stained positive for UHRF1, with different expression levels. The lack of normal pancreatic cells limits our interpretation of UHRF1 expression in pancreatic cancer cell lines. Also in tissue sections, normal pancreatic cancer specimens were very small in number and that limits our comparison with the tumour sections. This is because the normal tissue sections loaded in the TMA were taken from the same pancreatic cancer patients from normal lesions surrounding the tumour and in most cases it shows early stages of tumour development.

In pancreatic cancer tissue sections, we evaluated UHRF1 expression using two different UHRF1 antibodies. The percentages of positive nuclei detected by both antibodies were highly correlated, providing strong evidence of specificity for nuclear UHRF1. The Santa Cruz antibody was less sensitive for cytoplasmic UHRF1 in pancreatic cancer tissue. Both antibodies are mouse monoclonal, but the abcam antibody is raised against amino acids 694-794 of human UHRF1, which is at the C-terminal of the protein, while the Santa Cruz antibody is raised against amino acids 199-298 of human UHRF1 at the N-terminal of the protein. Our knockdown data support the validity of the cytoplasmic staining since depletion of UHRF1 led to loss of cytoplasmic as well nuclear staining. Cytoplasmic expression in tumour cells and stromal expression in the

inflammatory cells of UHRF1 has not been reported previously. This is an important observation that merits additional study in the future.

In our pancreatic cancer tissue sections, we observed that the presence of UHRF1 was associated with larger tumour sizes. This observation did not however translate into a change in the outcome for those patients. Although UHRF1 has been associated with poor outcome in a variety of tumours [57, 60, 62], in our study no such association was established.

4.2 Examination of the functional role of UHRF1 in pancreatic cancer cells:

4.2.1 UHRF1 is required for optimal growth of pancreatic cancer cells:

The positive association between UHRF1 expression and tumour size as indicated in the previous section 4.1.5.1 suggests that UHRF1 may contribute to pancreatic tumour growth. To examine the validity of this hypothesis we attempted to examine the direct effect of depletion of UHRF1 protein on pancreatic cancer cell growth (Figure 4-9).

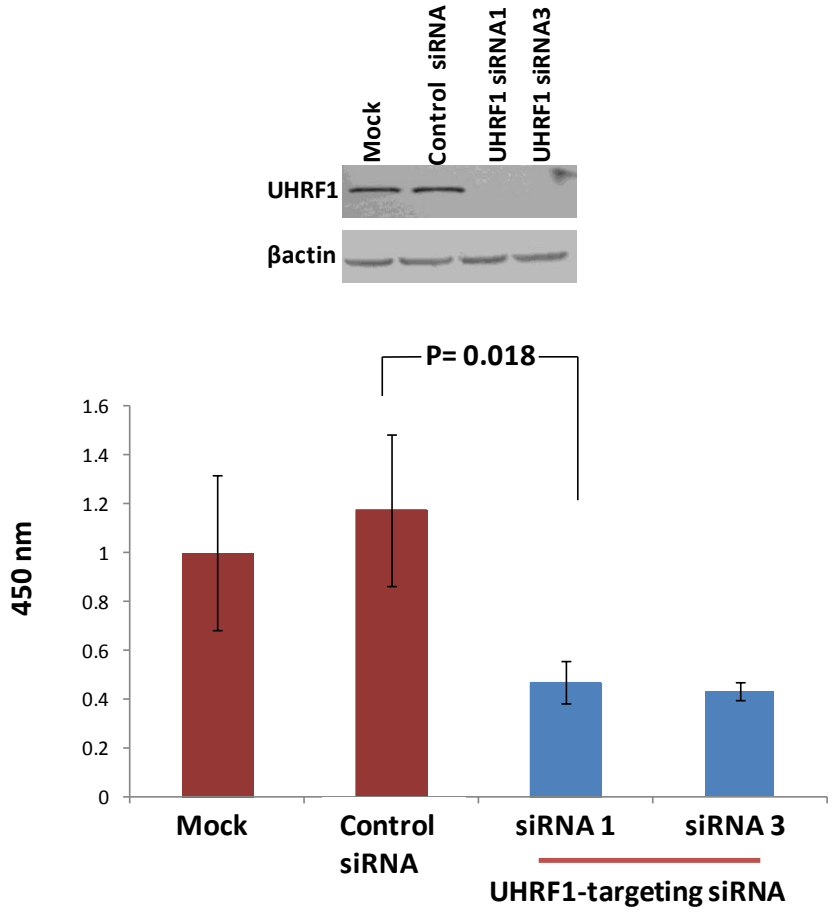

Figure 4-9 . UHRF1 depletion reduced cell proliferation. The MiaPaca-2 cells were either transfected with 30 nM UHRF1-targeting siRNA (siRNA1 or siRNA3) or transected with control siRNA (C1 siRNA) or left untreated as a control cells (MocK), cell viability was then assessed by MTS assay 72h post transfection. Results are a mean of triplicate samples ±SD.

Therefore, the pancreatic cancer cell lines MiaPaca-2, Panc1 and CFpac1 cells were transfected with UHRF1 siRNA or off-target control siRNA for 72 h, as shown in Figure 4-10, siRNA-mediated down-regulation of UHRF1 expression resulted in clearly diminished cell numbers compared with off-target siRNA treatment, as evidenced by phase contrast microscopy and by immunocytochemistry.

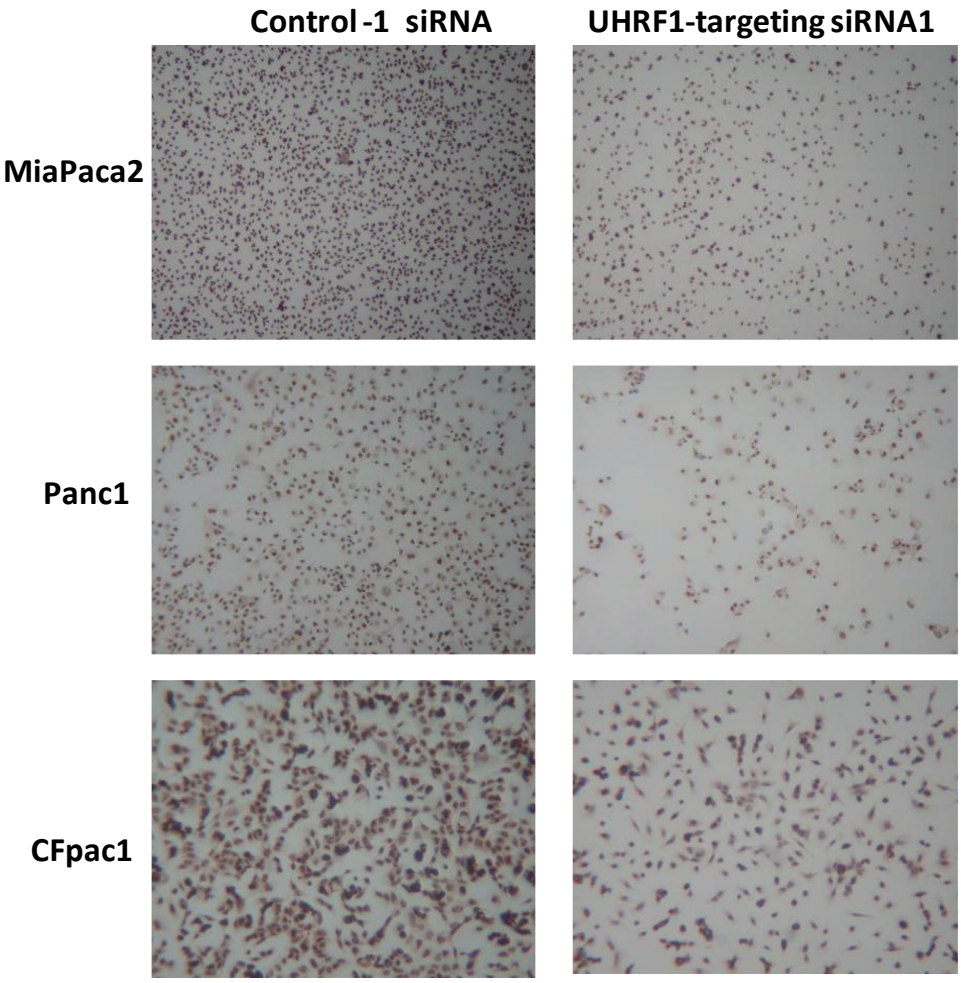

Figure 4-10: Immunocytochemistry of pancreatic cancer cells. Indicated cells were analysed 72 h post treatment with control siRNA or 30 nM UHRF1-targeting siRNA. UHRF1 depletion was associated with pancreatic cancer cell growth.

4.2.2 Phenotypic characteristics of pancreatic cancer cells following UHRF1 depletion:

Given that UHRF1 depletion resulted in diminished cell number (Figure 4-10), we attempted to examine phenotypic characteristics of pancreatic cancer cells following the depletion of UHRF1 expression. MiaPaca-2 cells were transfected with UHRF1-targeting siRNA or an off-target siRNA control. As shown in Figure 4-11, UHRF1 depletion resulted in characteristic phenotypic changes, where the cells are smaller in size and more rounded in shape compared to control cells. This observation was made following every UHRF1 knockdown in all pancreatic cancer cell lines used in my thesis, MiaPaca-2, Panc-1, CFpac-1 and Suit-2.

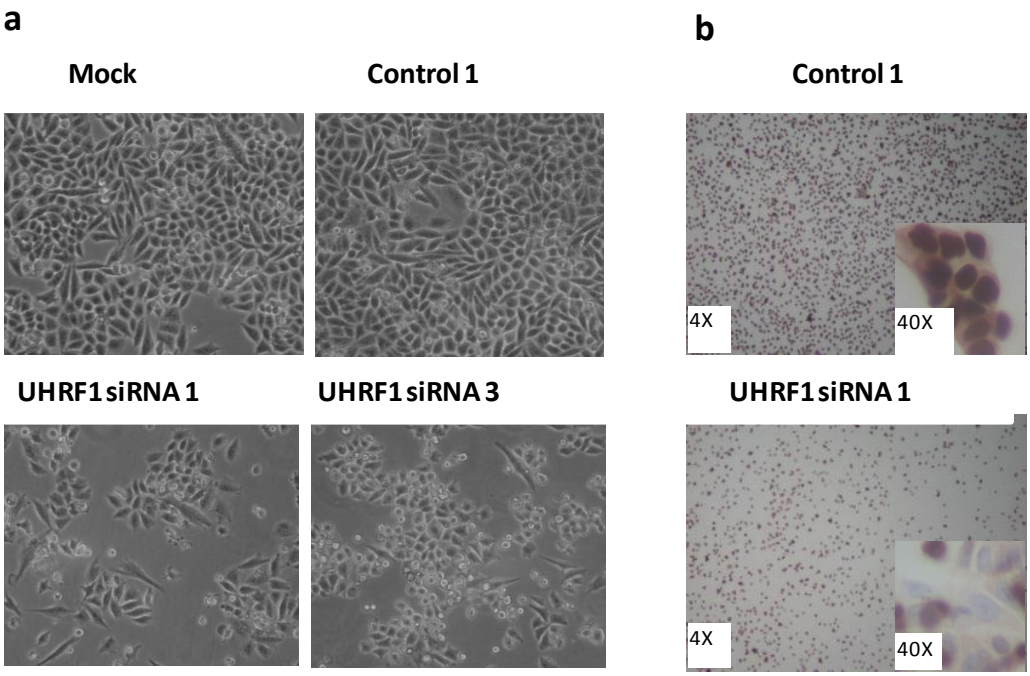

Figure 4-11: UHRF1 is required for pancreatic cancer cell growth. (a) Light microscopy image of MiaPaca-2 cells treated with lipofectamine alone (Mock) or with control- or UHRF1-targeting siRNAs. (b) Immunocytochemistry (ICC) for UHRF1 expression in MiaPaca-2 cells transfected with control- or UHRF1-targeting siRNA.

4.2.3 UHRF1 cellular localization, as observed by immunofluorescence analysis:

Our finding of cytoplasmic UHRF1 expression in paraffin embedded pancreatic cancer tissues using the abcam antibody (Figure 4-4) was somewhat surprising. Moreover, our ICC analysis of cultured pancreatic cancer cells (Figure 4-11) also revealed cytoplasmic staining although nuclear expression was more prominent. Therefore, we further investigated UHRF1 expression within cells in culture using the technique of immunofluorescence staining. In Panc-1 cells, we observed (n=2), as well as in MiaPaca-2 (n=1) and Suit-2 (n=1), both cytoplasmic and nuclear UHRF1 expression as demonstrated in Figure 4-12, although cytoplasmic expression was lower in level compared to nuclear UHRF1 expression. Treatment with UHRF1-targeting siRNA decreased both cytoplasmic and nuclear UHRF1, indicating that the cytoplasmic staining observed is also likely to be specific.

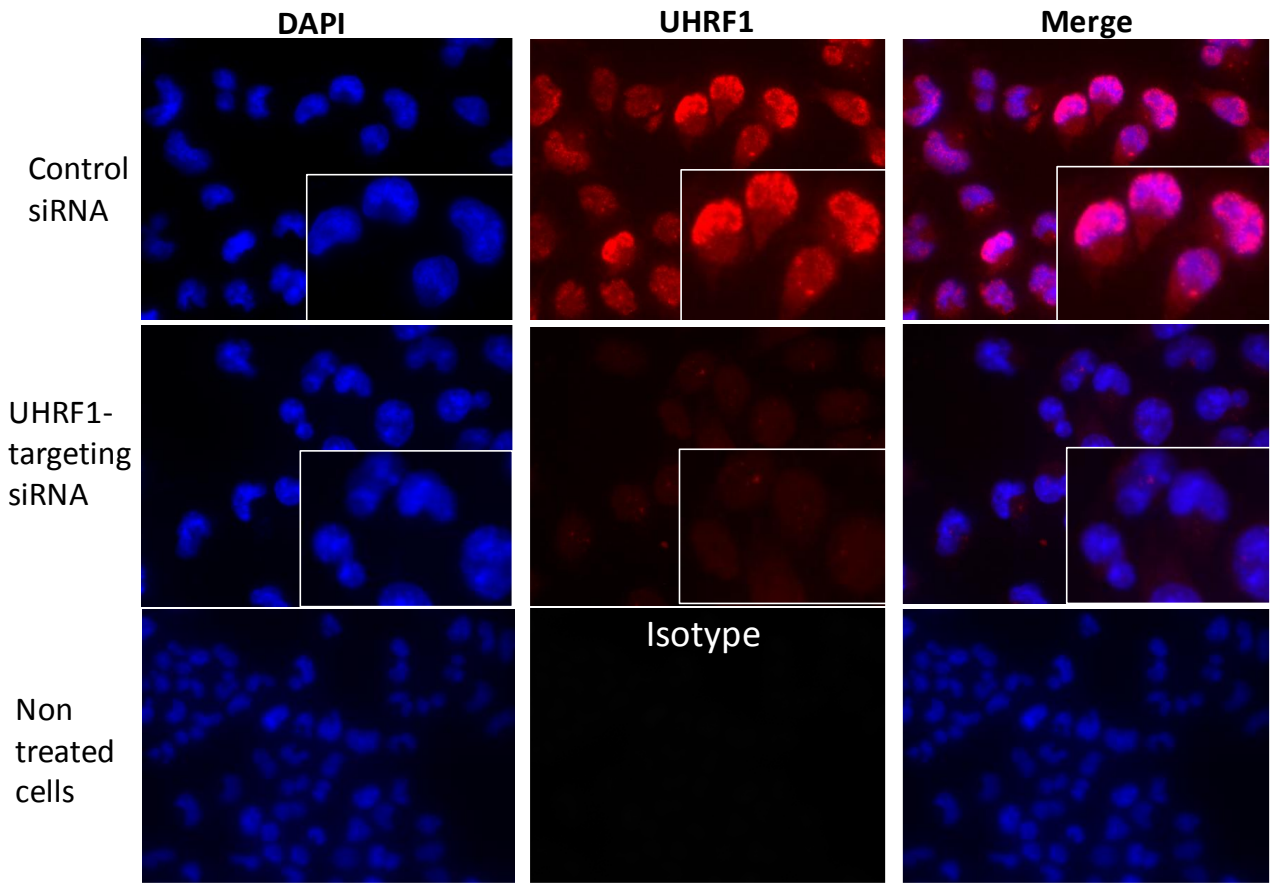

Figure 4-12. Immunofluorescence staining for UHRF1 in Panc-1 cells. Microscopic examination of Panc-1 cells stained for UHRF1. The blue staining indicates DAPI, the red staining is UHRF1, and the pink represents the merged colours. The non-treated cells were stained with the secondary antibody only as a negative control.

4.3 UHRF1 expression levels vary according to the stages of the cell cycle:

4.3.1 UHRF1 expression at the microscopic level:

Detailed microscopic examination of ICC-stained CFpac-1 cells revealed variation in the level of UHRF1 protein expression within different cells from the same population, indeed within the same microscopic field (Figure 4-13). Moreover, UHRF1 chromatin binding was also noted as indicated by an arrow in Figure 4-13. This observation was made with other cell lines including CFpac-1, MaiPaca-2 and Suit-2.

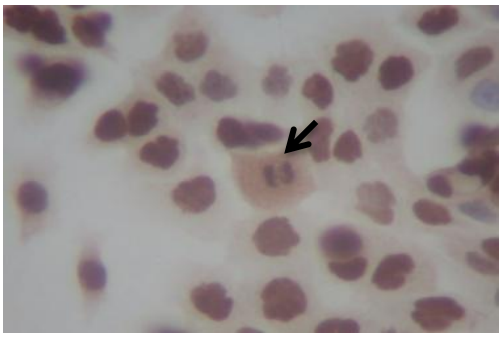

Figure 4-13. Microscopic examination of UHRF1 expression in CFpac-1 cells. Different levels of UHRF1 protein expression is shown, as is UHRF1 chromatin binding (indicated with an arrow).

4.3.2 UHRF1 expression is cell-cycle stage dependent:

Given that previous results (Figure 4-13) obtained from microscopic examination of UHRF1 expression revealed variable levels of expression between cells, we attempted to determine whether these changes in UHRF1 expression reflected different stages of the cell cycle. Therefore, the pancreatic cancer cell line CFpac-1 was subjected to a double thymidine block to

arrest cells at G1/S of the cell cycle and the level of UHRF1 protein was measured at specified times following release from the thymidine block. FACS analysis was used to confirm the double thymidine block as well as monitor cell cycle phases after release from the block. UHRF1 expression was assessed by western blot analysis. The expression levels of cyclin E, cyclin A and cyclin B were also examined to confirm different stages of the cell cycle as an internal marker for the cell cycle phases (n=1). As shown in Figure 4-14, UHRF1 protein levels were high in cells accumulated in S phase (0 h post release), were relatively low as cells proceeded through G1/S (2 h and 4 h post release), peaked at 7 h post release as cells reached G2/M and dropped significantly at 9 h, as cells exited mitosis (n=1). This observation was also made in MiaPaca-2 cell (n=1) as following release from double thymidine block UHRF1 expressed at variable levels at different time points.

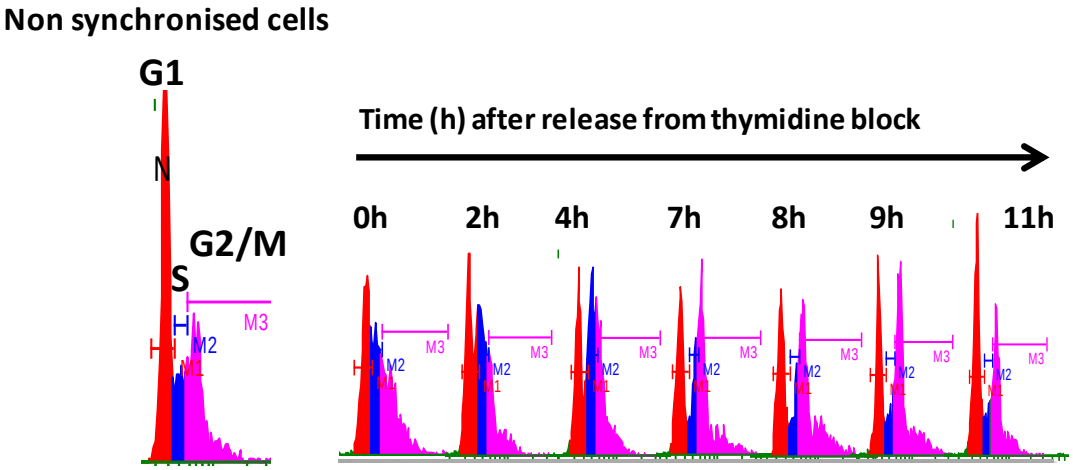

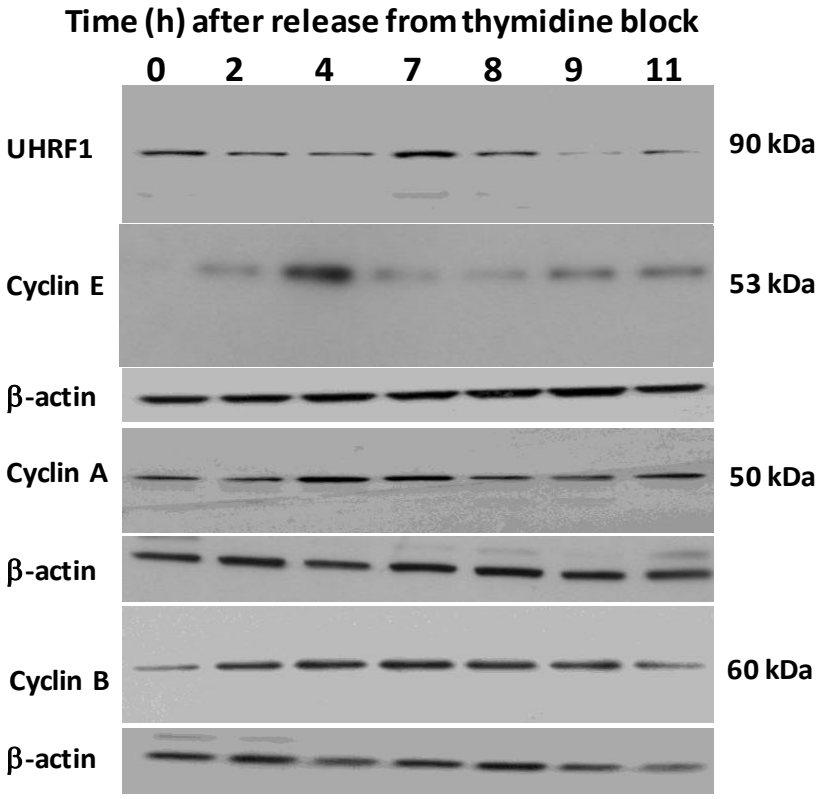

Figure 4-14: Variable UHRF1 expression at different time points during the cell cycle. FACS analysis (peaks are labeled with color code, red: G1, blue: S and pink: G2/M) and cyclin E, A and B measurement by western blotting of CFpac-1 cells/extracts sampled at the indicated time points following release from a double thymidine (G1/S) block. Data are representative of n=2.

4.3.3 UHRF1 depletion arrests the cell cycle in G2/M:

To determine whether the peak in UHRF1 at G2/M was functionally important, FACS analysis was conducted 72 h post UHRF1-targeting siRNA transfection. Our data suggested an increase in the proportion of cells in G2/M. This observation was made in at least 3 independent runs using MiaPaca-2 cells. We also noted an increase in the sub-G1 population, pointing towards an increase in apoptosis (Figure 4-15).

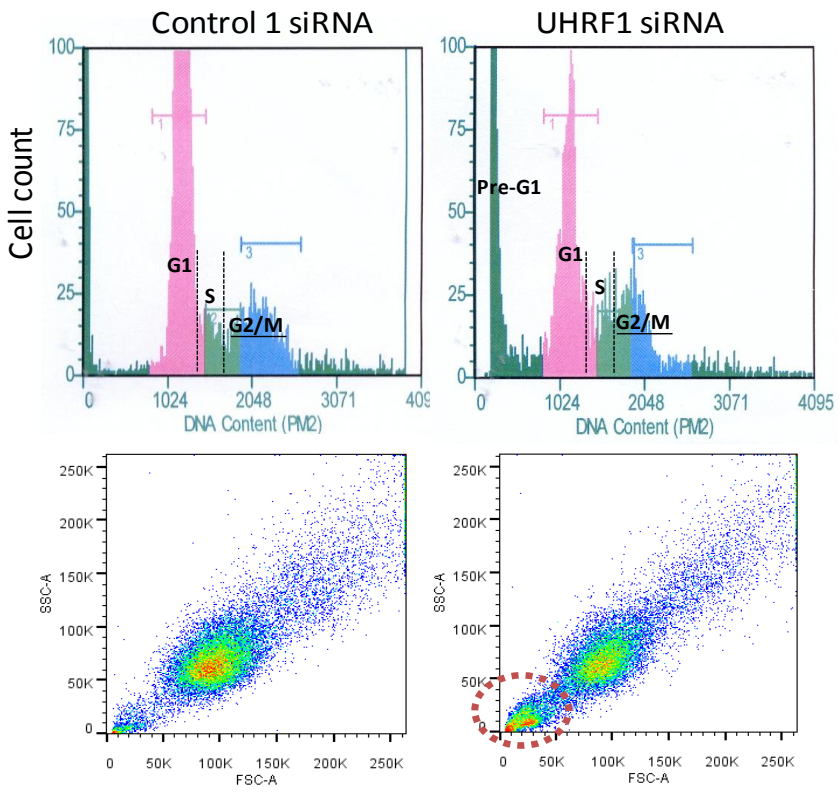

Figure 4-15. FACS analysis of MiaPaca-2 cells following UHRF1 depletion. The top graphs show FACS analysis of PI stained cells (peaks are labeled with color code, red: G1, blue: S and pink: G2/M) for cells treated with control siRNA and 30 nM UHRF1-targeting siRNA for 72 h. An additional peak in the UHRF1 depleted cells was detected; in the figure it is green and labeled pre-G1, indicating dead cells. The lower graphs show SSC/FSC plots for PI stained cells treated with control siRNA and 30 nM UHRF1-targeting siRNA for 72 h. In the UHRF1 depleted cells, a bigger population of dead cells was detected (in the red circle) (n=4).

To examine if the alteration in G2/M and the sub-G1 population was specific to MiaPaca-2 cells, we extended the study to additional pancreatic cancer cells, including CFpac-1, Panc-1 and Suit-2. We observed an increase in the G2/M cell count in each of these cell lines and an accumulation in the sub-G1 population in MiaPaca-2, CFpac-1 and Suit-2 cells following UHRF1 knockdown. An increase in polyploidy cells was also observed in Panc-1 and Suit-2 cells (Figure 4-16).

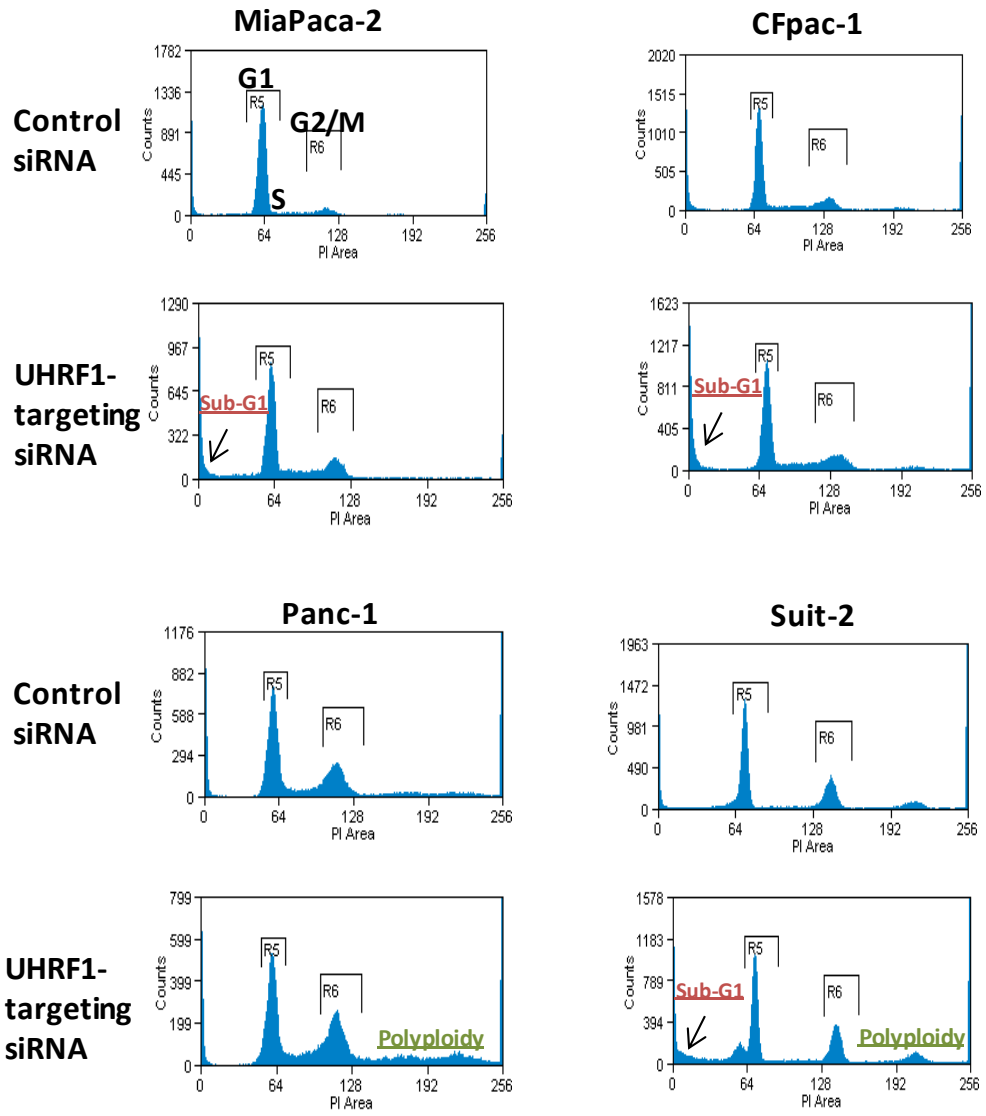

Figure 4-16. FACS analysis of pancreatic cancer cells transfected with UHRF1-targeting siRNA. Cells were treated with control siRNA or 30 nM UHRF1 targeting siRNA for 72 h and stained with PI. R5: cells in G1 phase and R6: cells in G2/M phase. A general increase in cell accumulation in G2/M phase was observed in UHRF1 depleted cells compared to control siRNA. In MiaPaca-2, CFpac-1 and Suit-2 a sub-G1 peak was observed. In Suit-2 and Panc-1 an increase in polyploidy cells was observed (n=3).

For further confirmation of G2/M cell arrest following UHRF1 knockdown, Suit-2 cells were treated with UHRF1-targeting siRNA, non-targeting siRNA or mock transfected or left untreated and synchronised at 2 different points of the cell cycle, G1/S using a double thymidine

treatment and G2/M using thymidine/nocodazole treatment (n=2). The cells were treated with thymidine for 19 h followed by UHRF1-targeting siRNA transfection then subjected to a second block by treatment with either nocodazole or thymidine at a time point of 3 h and 9 h respectively, and cells were maintained for 48 h from the time of transfection. UHRF1 depletion was confirmed by western blot analysis (Figure 4-17 a). Cell cycle arrest was confirmed by FACS analysis (Figure 4-17 b and c). Consistent with our observation that UHRF1 protein expression peaked at G2/M phase of the cell cycle (Figure 4-14), cells treated with thymidine/nocodazol, which blocks the cells at G2/M (lane 2, Figure 4-17 a) exhibited higher UHRF1 expression than cells blocked in G1/S (lane 1, Figure 4-17 a). In Figure 4-17 b cells were examined 24 h following release from G1/S. UHRF1-depleted cells showed fewer cells in G1 (200 ± 20 cells), compared to control cells in G1 (300 – 400 cells), suggesting fewer UHRF1-depleted cells have completed a cell cycle and returned to G1. This may be due to a delay in either S phase and/or in G2/M when UHRF1 is depleted. In Figure 4-17 c there was no significant differences in cell count between control cells and UHRF1 depleted cells.

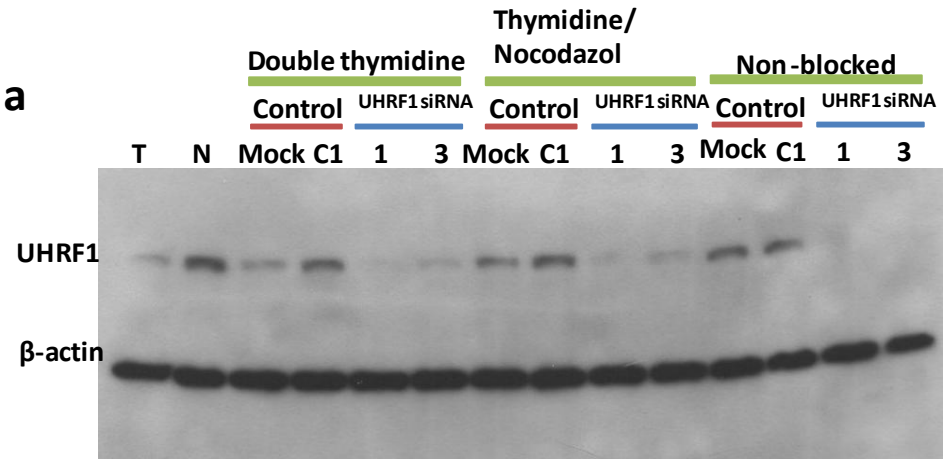

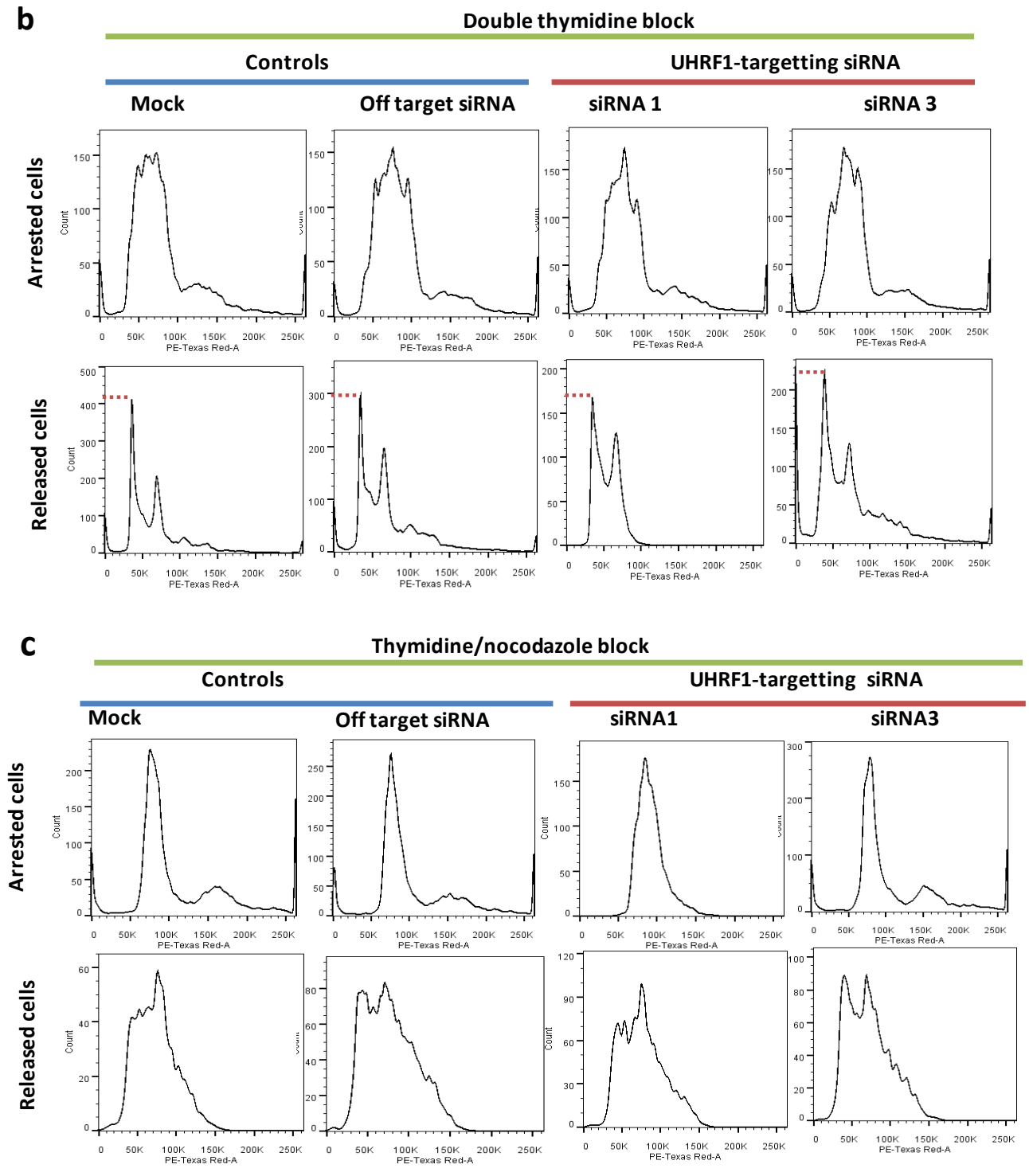

Figure 4-17. Synchronized Suit-2 cells at 2 different points of the cell cycle using double thymidine and thymidine/nocodazole treatment. (a) Western blots showing successful UHRF1 depletion in the treated Suit-2 cells, (T: double thymidine block only, N: thymidine/nocodazole block). β-actin was used as a loading control. (b) FACS analysis for cells treated with double

thymidine and either control siRNA or 30 nM UHRF1-targeting siRNA for 48 h. The upper panel shows arrested cells, just prior to release from the block, the lower panel shows cells 24 h post release and 48 h post transfection with siRNA. The red dot lines showing more cells in G1 in the control set compared to UHRF1 depleted cells. (c) FACS analysis for cells treated with thymidine/nocodazole and either control siRNA or 30 nM UHRF1-targeting siRNA for 48 h. The upper panel shows arrested cells, just prior to release from the block, the lower panel shows cells 24 h post release and 48 h post transfection with siRNA.

4.3.4 UHRF1 depletion induces apoptosis in pancreatic cancer cells:

The sub-G1 population observed in UHRF1-depleted cells (Figure 4-16) pointed towards apoptosis. To examine directly the effect of UHRF1 depletion on apoptosis, the pancreatic cancer cell line Suit-2 was transfected with UHRF1-targeting siRNA, control siRNA and 72 h later, subjected to annexin V/PI analysis by FACS. As shown in Figure 4-18, UHRF1 depletion results in increased Annexin V/PI staining in cells transfected with UHRF1-targeting siRNA compared to control cells (Figure 4-18 a). This observation was also made in CFpac-1 cells. This finding was further confirmed for Suit-2 cells by higher levels of Caspase 3/7 activity following UHRF1 depletion. The activity of the caspases was higher in UHRF1-depleted cells compared to control cells ($p= 0.033$) (Figure 4-18b). Moreover, the higher caspase 3/7 activity was confirmed by the increased cleavage of the pro-caspase 3 protein, as evaluated by western blot analysis of caspase 3 after UHRF1 depletion (Figure 4-18 c). Further evidence of apoptosis induction following UHRF1 depletion included cyclin E cleavage (Figure 4-18 d) and down-regulation of cyclin A and cyclin B (Figure 4-18 e).

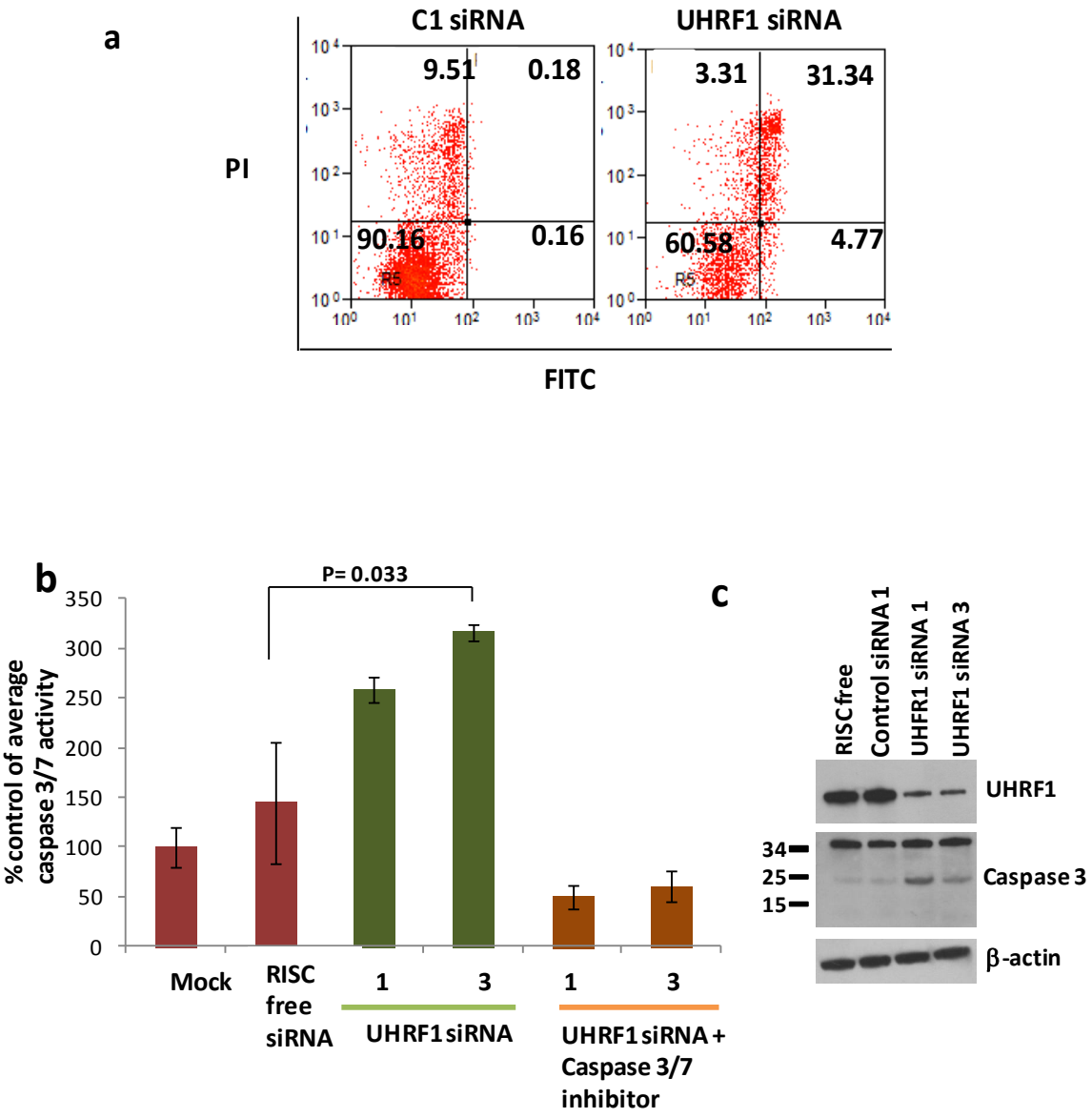
a
C1 siRNA
UHRF1 siRNA
PI
FITC
9.51
0.18
90.16
0.16
3.31
31.34
60.58
4.77
R5
b
P= 0.033
% control of average caspase 3/7 activity
Mock
RISC free siRNA
1
3
UHRF1 siRNA
UHRF1 siRNA + Caspase 3/7 inhibitor
c
RISC free
Control siRNA 1
UHFR1 siRNA 1
UHRF1 siRNA 3
UHRF1
Caspase 3
β-actin
34
25
15

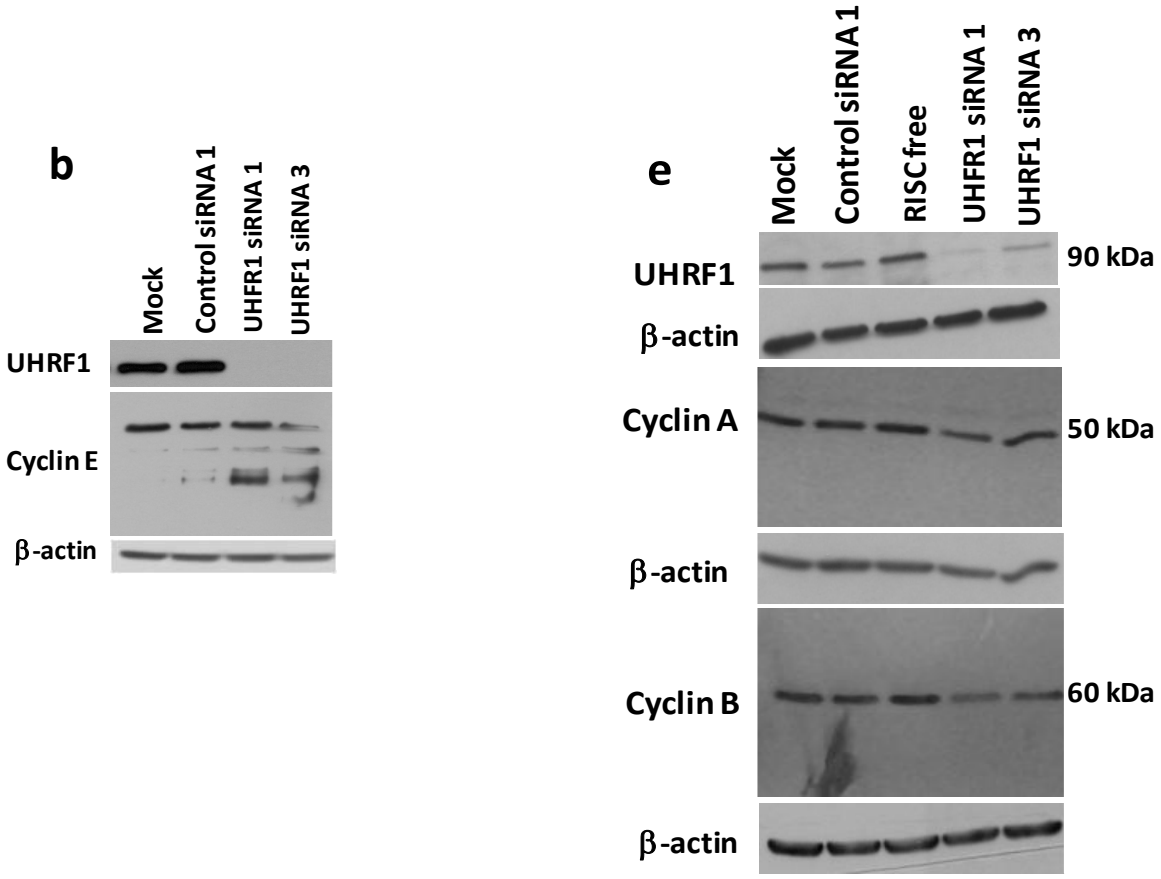

Figure 4-18. UHRF1 depletion induces apoptosis. (a) Annexin V/PI staining for Suit-2 cells treated with control siRNA or 30 nM UHRF1-targeting siRNA for 72 h (n=2) the numbers in each square indicating % of cells. (b) Caspase 3/7 activity in Suit-2 cells following indicated treatments in triplicate. The caspase 3/7 inhibitor used is 30 μM ZVAD (c) Western blot of Suit-2 cell extract showing increased levels of cleaved caspase 3 following UHRF1 depletion (n=3). (d) Western blots showing cyclin E cleavage. (e) Down-regulation of cyclin A and cyclin B following UHRF1 depletion. Data are representative of at least 3 independent experiments and β-actin was used as a loading control.

4.3.5 Summary and discussion of results following examination of the functional role of UHRF1 in pancreatic cancer cells:

In this study we examined the role of UHRF1 in cell cycle regulation in detail. Using pancreatic cell synchronisation experiments, we demonstrated variable UHRF1 protein expression at different time points in the cell cycle and noted a peak in UHRF1 levels at G2/M of the cell

cycle. This is in contrast to the work of *Hervouet et al*., [81] who showed UHRF1 expression levels in glioma cells to be constant in all phases of the cell cycle. UHRF1 knockdown from pancreatic cancer cells was accompanied by an accumulation of cells in G2/M. Consistent with our findings, *Tien et al*., [79] also reported cell cycle arrest in G2/M-phase of cancer cells following depletion of UHRF1 and described concomitant activation of the DNA damage response pathway. In this study, we showed that depletion of UHRF1 in pancreatic cancer cells led to a visible loss in cell number, consistent with reports in non-small cell lung cancer [64], colorectal cancer [61], and prostate cancer [62]. The growth-inhibitory effect of UHRF1 on the pancreatic cancer cell lines tested in this study suggests that UHRF1 is a potentially important target for cancer drugs, as noted in other reports [38, 40]. Besides UHRF1's role in cell cycle regulation, UHRF1 contributes to the maintenance of DNA methylation by recruiting DNMT1 to hemi-methylated DNA. UHRF1 is an established epigenetic regulator contributing to maintenance of DNA methylation [158] and the modification of histones [159].

4.4 DNA methylation status in pancreatic cancer:

UHRF1 is an established epigenetic regulator contributing to maintenance of DNA methylation [158]; it is a key protein in the mechanism which is responsible for recruiting DNMT1 to the hemi-methylated DNA. DNA global hypomethylation is a common epigenetic process in cancer [105], as is the silencing of TSGs by the hypermethylation of their promoters. In pancreatic cancer *CDKN2A* [92], *RASSF1* [93] are frequently hypermethylated. In this study we examined whether loss of UHRF1 protein levels would affect the global DNA methylation level and the methylation levels of the frequently methylated TSGs in pancreatic cancer cells.

4.4.1 Global methylation status in pancreatic cancer cells:

In order to examine the effect of UHRF1 protein on the global methylation status in pancreatic cancer cells, we first attempted to examine the basal methylation levels of *LINE-1* and *Alu-V* elements in pancreatic cancer cell lines by pyrosequencing. We identified the methylation status of both *LINE-1* and *ALu-V* in 3 different cell lines (MiaPaca-2, CFpac-1 and Suit-2). The mean level of *LINE-1* methylation was the highest in MiaPaca-2 cells with a methylation index of 70.9 % ± 0.34 compared with 58.6 % ± 0.34 and 57.4 % ± 1.2 of CFpac1 and Suit 2 respectively (Figure 4-19). These results represent the methylation index of 3 independent experiments.

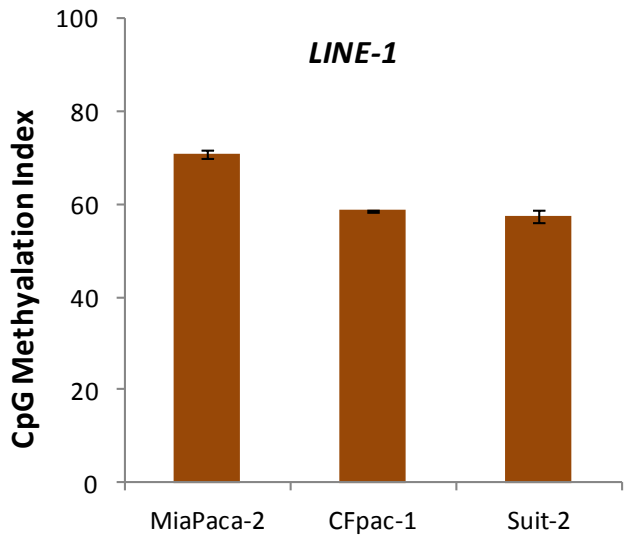

Figure 4-19. The basal DNA methylation status of *LINE-1* promoter in pancreatic cancer cells. The basal methylation levels of LINE-1 was the highest in MiaPaca-2 cells.

The methylation index of *Alu-V* elements was also estimated via 3 independent runs in MiaPaca-2 (46 % ±2.2) and estimated via 2 independent runs in CFpac-1 (40 % ± 1.4) and Suit-2 (41.5% ± 1.4) (Figure 4-20).

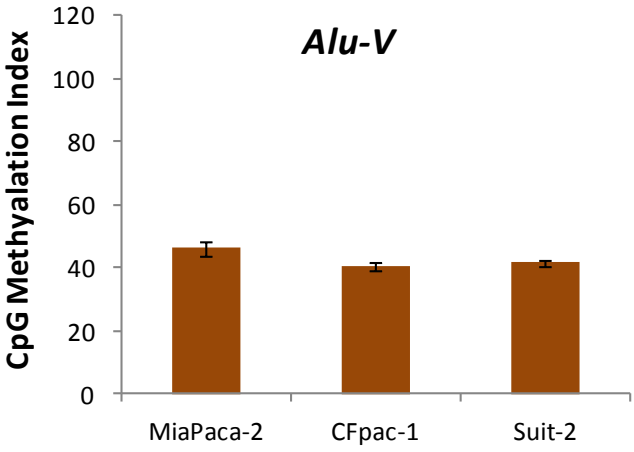

Figure 4-20. The basal DNA methylation status of Alu-V elements in pancreatic cancer cells. The average of methylation measured by pyrosequencing.

4.4.2 Confirmation of de-methylation of *LINE-1* elements in pancreatic cancer by 5-aza-deoxycytidine:

MiaPaca-2 and Suit 2 cells were treated with the de-methylation drug 5-aza-deoxycytidine for 48 h and then the methylation status of *LINE-1* was examined. A statistically significant difference with an approximate 50 % reduction in *LINE-1* methylation was observed in the examined cell lines (Figure 4-21).

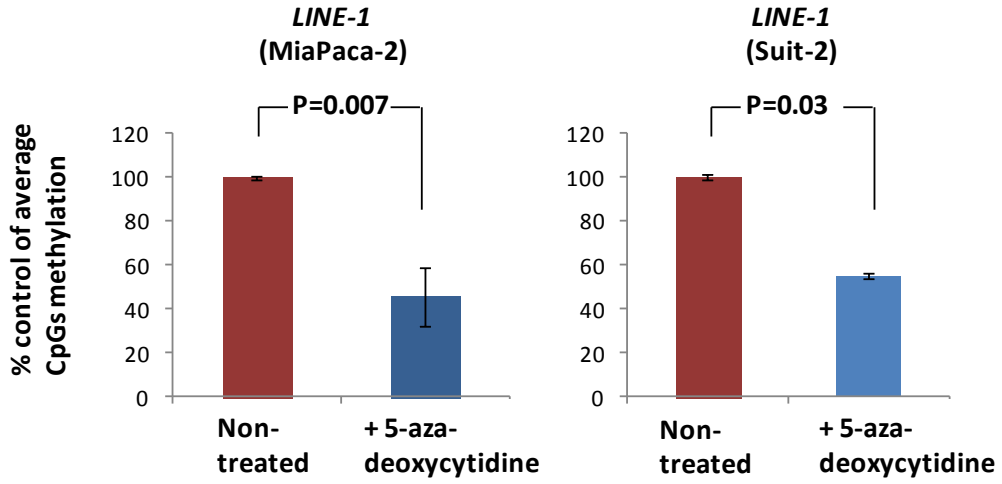

Figure 4-21. The DNA methylation levels of the *LINE-1* promoter in cells treated with 5-aza-deoxycytidine. Methylation was estimated in MiaPaca-2 (n=3) and Suit-2 (n=2).

4.4.3 UHRF1 expression and global methylation in pancreatic cancer cells:

As UHRF1 contributes to the maintenance of DNA methylation, we next examined whether loss of UHRF1 protein levels would have an impact on global DNA methylation in pancreatic cancer cells. Therefore, we measured differences in the methylation index of *LINE-1* and *ALu-V* elements using pyrosequencing following UHRF1 down regulation. In MiaPaca-2, CFpac-1 and Suit-2 the methylation levels of the *LINE-1* promoter were decreased in cells transfected with

30 nM UHRF1-targeting siRNA for 72 h compared to mock or control transfected cells, by 14 % ± 1.9, 13 % ± 1.6 and 16 % ± 1.7 respectively (Figure 4-22 a). These data were calculated from 6 independent runs in MiaPaca-2 cells and the observation was made in 3 independent runs in CFpac-1 and Suit-2 cells. Alu-V methylation levels were reduced following UHRF1 depletion by 13.3 % ± 1 in MiaPaca-2 (n=3) and in Suit-2 by 15% (Figure 4-22 b). UHRF1 depletion was confirmed by western blot prior to DNA extraction and pyrosequencing.

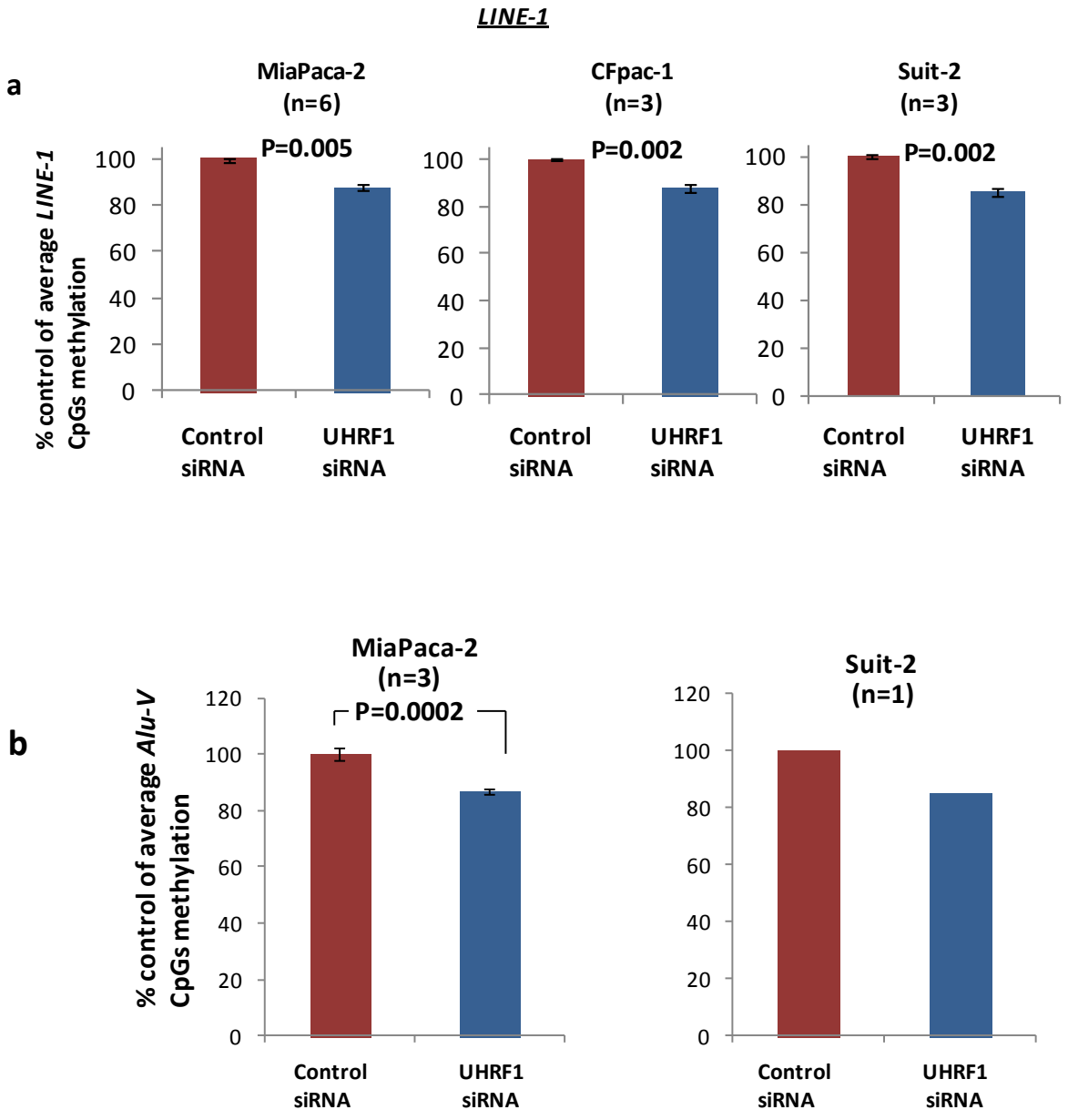

Figure 4-22. DNA methylation levels in *LINE-1* and *Alu-V* elements following UHRF1 depletion. (a) *LINE*-1 in MiaPaca-2 (n=6), CFpac-2 (n=3) and in Suit-2 (n=3). (b) *Alu*-V in MiaPaca-2 (n=3) and Suit-2 (n=1). The data are presenting UHRF1 depeltion with UHRF1-targeting siRNA3 and the same results were obtained (with UHRF1-targeting siRNA1) as each run was performed with 2 different siRNA controls and 2 different UHRF1-targeting siRNAs.

4.4.4 Evaluation of global DNA methylation following UHRF1 depletion combined with 5-aza-deoxycytidine treatment:

As shown in Figure 4-22, UHRF1 depletion reduced the global DNA methylation level in pancreatic cancer cells. We next examined whether a combination of UHRF1 knockdown and 5-aza-deoxycytidine treatment would cause an even greater decrease in the global DNA methylation in pancreatic cancer than any single treatment. UHRF1 protein was down-regulated in Miapaca-2 cells by siRNA-mediated depletion followed by 5-aza-deoxycytidine treatment and measurement of *LINE-1* methylation levels. The experiment was designed to include control cells (including non-treated cells and cells treated with non-targeting siRNA), cells treated with UHRF1-targeting siRNA only (the effect was previously evaluated (n=6) as shown in Figure 4-22 a), cells treated with 5-aza-deoxycytidine only (the effect was previously evaluated (n=3) as shown in Figure 4-21) and cells treated with a combination of UHRF1-targeting siRNA and 5-aza-deoxycytidine. The control cells with either condition, non-treated or with non-targeting siRNA treatment showed equal methylation level of *LINE-1*, for this reason

we indicated one control in Figure 4-23 b. Treated cells showed changes to their appearance in culture (Figure 4-23 a). In cells treated with 30 nM UHRF1-targeting siRNA for 72 h, a reduction in DNA methylation levels of 14 % was observed, while cells treated with 100 nM of 5-aza-deoxycytidine for 48 h exhibited a reduction in methylation levels of 48 %, the combined treatment caused the greatest reduction in methylation levels (63 %) (Figure 4-23 b).

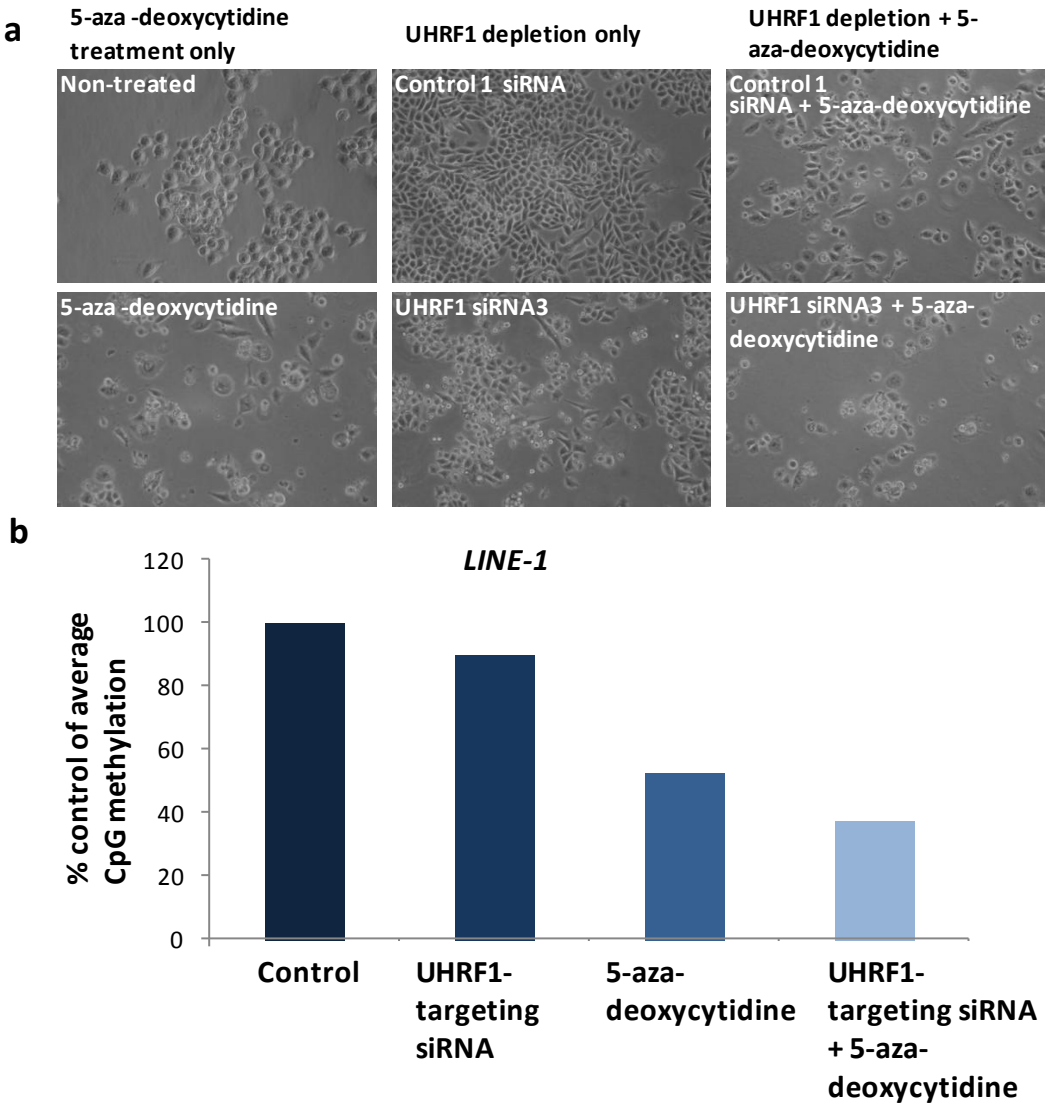

Figure 4-23. UHRF1 depletion combined with 5-aza-deoxycytidine treatment effect on the global methylation level. (a) Microscopic examination of MiaPaca-2 cells treated with 5-aza-

deoxycytidine, UHRF1-targeting siRNA and cells treated with both UHRF1-targeting siRNA and 5-aza-deoxycytidine. (b) DNA methylation status in each treated cells.

4.4.5 Recovery of UHRF1 following depletion restores global DNA methylation:

Having observed that UHRF1 depletion decreases global DNA methylation, we next asked whether restoration of UHRF1 after knockdown was accompanied by a corresponding restoration of global DNA methylation. To achieve this, MiaPaca-2 cells were incubated with UHRF1-targeting siRNA for 72 hours and UHRF1 levels and *LINE-1* promoter methylation status measured on the next day and each subsequent day for a total of seven days. We observed that the cellular morphology started to recover on day 4 following the UHRF1 knockdown (Figure 4-24 a). UHRF1 protein was also detected by western blot analysis on day 5 after depletion (Figure 4-24 b), and was fully restored by day 6. The time course observation was made in 2 different cell lines, MiaPaca-2 and Suit-2 (n=3). Global DNA methylation was reduced following UHRF1 depletion, as shown previously in Figure 4-22 and continue to decrease with a maximum reduction in day 4, then returned to control levels at day 5 (Figure 4-24 c). The methylation levels following 5-aza-deoxycytidine treatment alone did not recover in the examined period of 5 days (Figure 4-24 d). Pointing towards that the influence of the DNA methylation level was due to change in UHRF1 expression level.

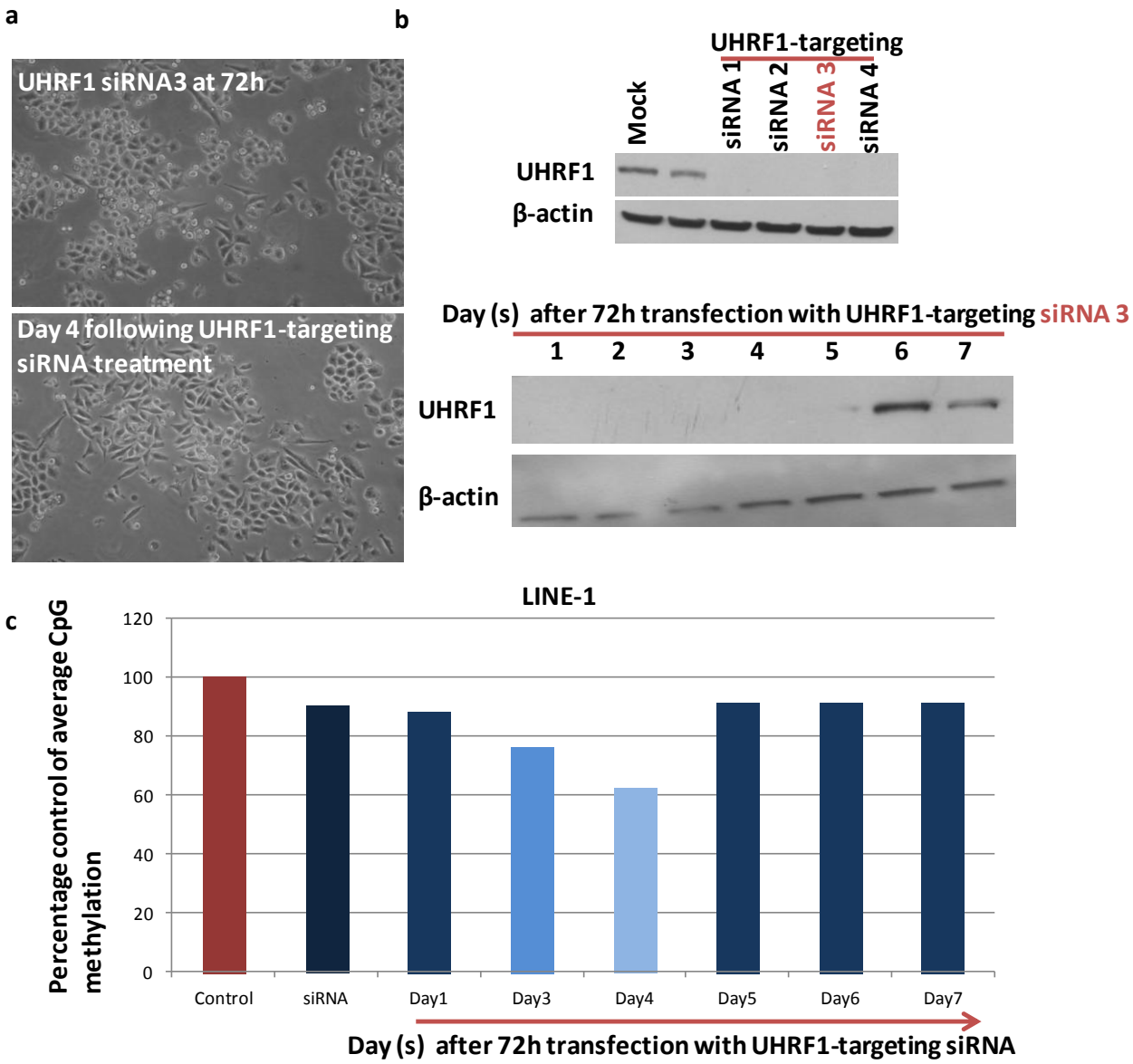
a
UHRF1 siRNA3 at 72h
Day 4 following UHRF1-targeting siRNA treatment
b
UHRF1-targeting
Mock
siRNA 1
siRNA 2
siRNA 3
siRNA 4
UHRF1
β-actin
Day (s) after 72h transfection with UHRF1-targeting siRNA 3
1 2 3 4 5 6 7
UHRF1
β-actin
c
LINE-1
Percentage control of average CpG methylation
120
100
80
60
40
20
0
Control
siRNA
Day1
Day3
Day4
Day5
Day6
Day7
Day (s) after 72h transfection with UHRF1-targeting siRNA

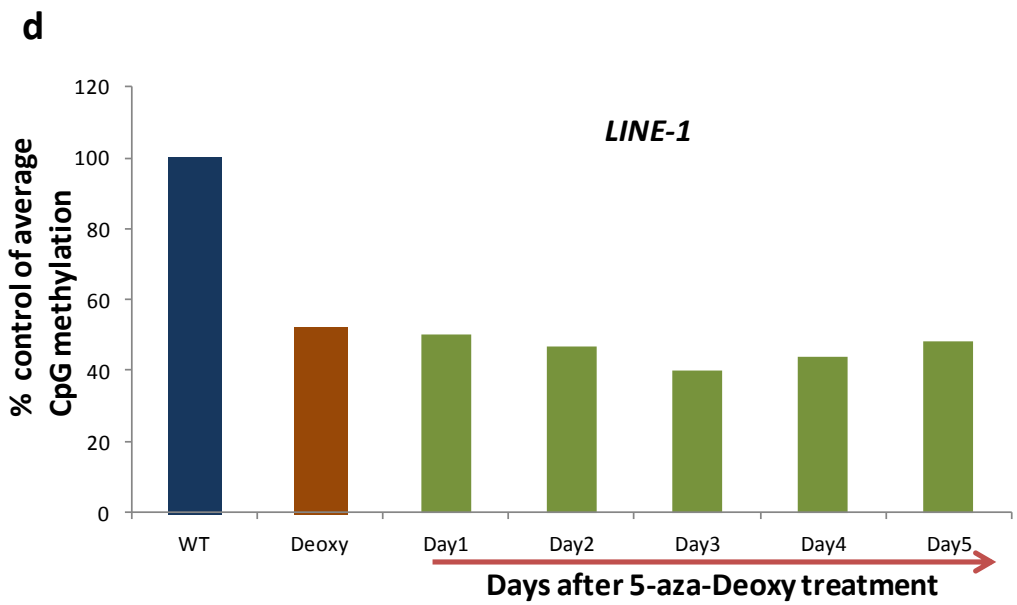

Figure 4-24. UHRF1 influences global DNA methylation. (a) Microscopic examination of MiaPaca-2 cells transfected with UHRF1-targeting siRNA for 72 h and 4 days post-knockdown. (b) Western blot analysis examining the time course of UHRF1 expression in the days following UHRF1 knockdown. β-actin was used as a loading control. (c) and (d) *LINE-1* methylation status following UHRF1 siRNA (c) and 5-aza-deoxycytidine treatment (d).

4.4.6 The methylation status of tumour suppressor genes in pancreatic cancer cells:

The relationship between UHRF1 expression and the hypermethylation of frequently methylated *CDKN2A* [29] and *RASSF1* [93] tumour suppressor genes in pancreatic cancer was examined.

We analysed the basal methylation levels of the *CDKN2A* promoter in CFpac-1 (where the gene is wildtype; the gene is fully deleted in MiaPaca-2, and mutated in Suit-2 cells), and the *RASSF1* promoter in MiaPaca-2, CFpac-1 and Suit-2 by Pyrosequencing. The mean methylation index of the *CDKN2A* promoter in CFpac-1 was found to be 93 % ± 2. While the mean basal methylation level of *RASSF1* in MiaPaca-2 was very high with a value of 94.5 % ± 1.2, the methylation index

in CFpac-1 was 17.7 % ± 2.6 and in Suit-2 was 37.4 % ± 3.3 (Figure 4-25). These data were calculated as the mean value of 3 independent runs.

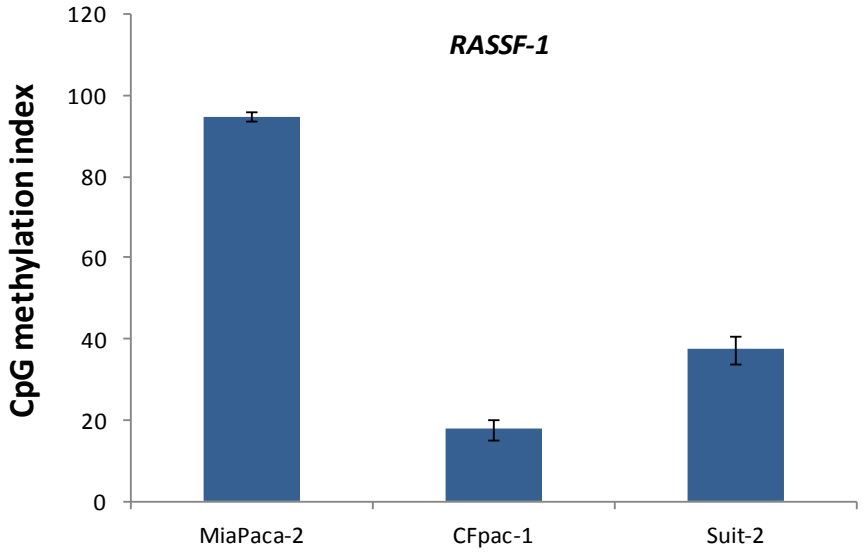

Figure 4-25. The DNA methylation levels of *RASSF1* promoter in pancreatic cancer cells. The average methylation was calculated from 3 independent runs by pyrosequencing.

4.4.7 The relationship between UHRF1 expression and *RASSF1* promoter methylation in pancreatic cancer cells:

In MiaPaca-2, CFpac-1 and Suit-2 cells, UHRF1 depletion resulted in decreases in *RASSF1* promoter methylation of 5 % ± 0.4, 81 % ± 3.3 and 17.4 % ± 0.9 respectively (Figure 4-26). These data were calculated from 5 independent runs in MiaPaca-2 and 4 independent runs in CFpac-1 and Suit-2. UHRF1 depletion was confirmed by western blot prior to DNA extraction and pyrosequencing.

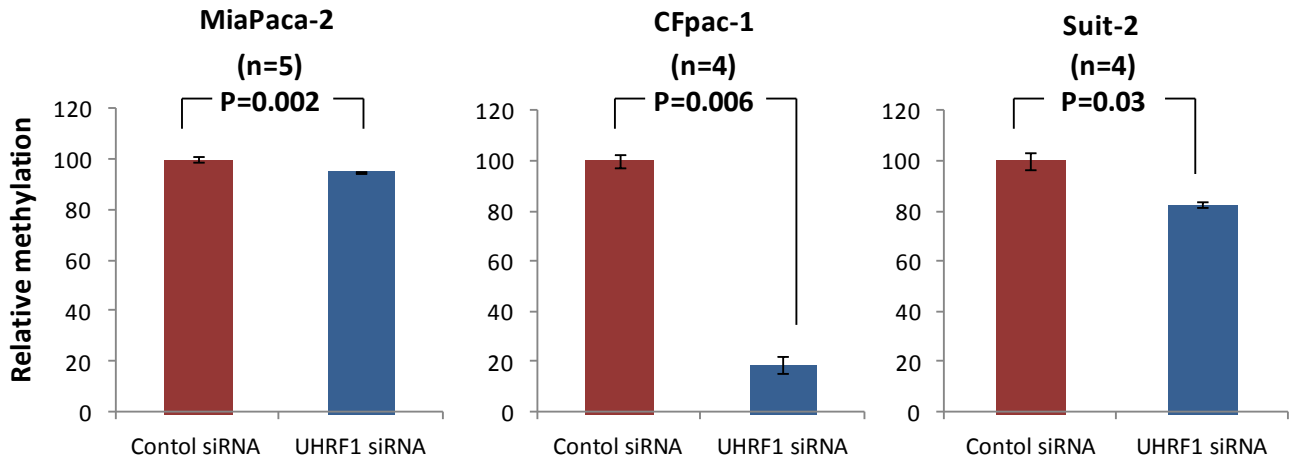

Figure 4-26. DNA methylation levels of the *RASSF1* gene promoter. UHRF1 depletion resulted in reduced methylation levels of the *RASSF1* gene promoter.

4.4.8 The relationship between UHRF1 depletion and *CDKN2A* promoter methylation and expression in CFpac-1 cells:

The high basal level (93 % ± 6) of *CDKN2A* promoter methylation in CFpac-1 cells was reduced by 21 % ± 6 following UHRF1 knockdown (Figure 4-27 a and b). These data were calculated from 3 independent runs and each run was performed with 2 different control siRNAs and 2 different UHRF1-targeting siRNAs. UHRF1 depletion was confirmed by western blot prior to DNA extraction and pyrosequencing.

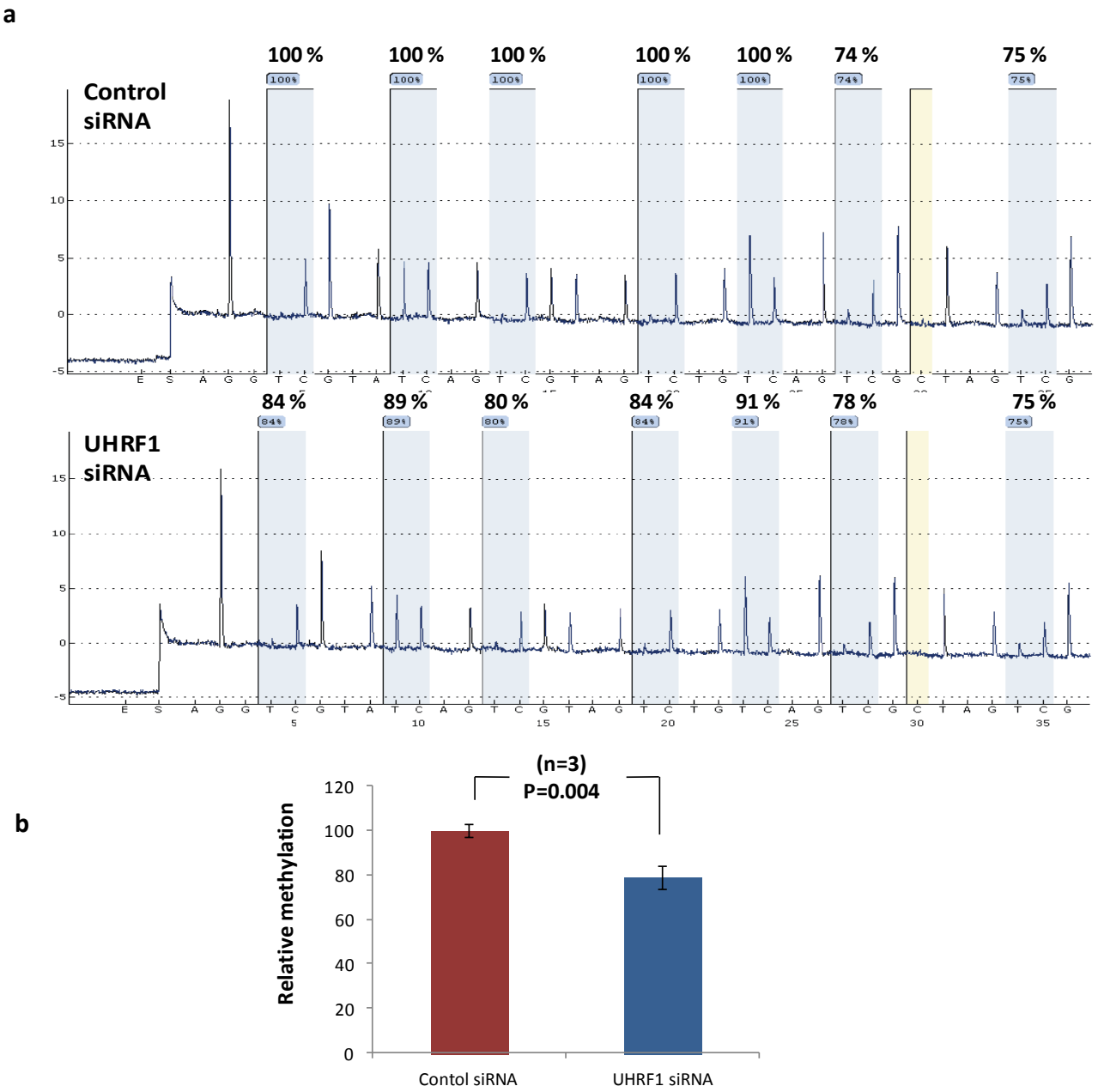

Figure 4-27. DNA methylation status of *CDKN2A* promoter following UHRF1 depletion. (a) Pyrogram of the *CDKN2A* promoter in CFpac-1 cells transfected with control- or 30 nM UHRF1-targetting siRNAs for 72 h (n=3). The basal methylation index for *CDKN2A* was 93 %. In the Pyrogram the blue columns indicated the CpGs location and the blue boxes on top of it indicated the % of methylation measured at each CpG, the yellow column is the internal quality control location, the sequence at the X-axis is the dispensation order and the Y-axis is the light intensity measured for each base (b) Mean of triplicate DNA methylation measurements of the *CDKN2A* promoter following treatment with control- or UHRF1-targetting siRNAs.

In order to study the relation between UHRF1 and *CDKN2A* in more depth, we examined the expression of the protein product of the *CDKN2A* gene, P16 following UHRF1 depletion in pancreatic cancer cells. UHRF1 depletion alone was not sufficient to cause measurable accumulation of P16 protein (Figure 4-28 a). On the other hand, treatment of the cells with the demethylation drug 5-aza-deoxycytidine resulted in detectable P16 (Figure 4-28 b). This observation was made in at least 4 independent experiments. Moreover, combining UHRF1 knockdown with 5-aza-deoxycytidine treatment resulted in higher levels of P16 protein compared to control siRNA-treated cells (Figure 4-28 c).

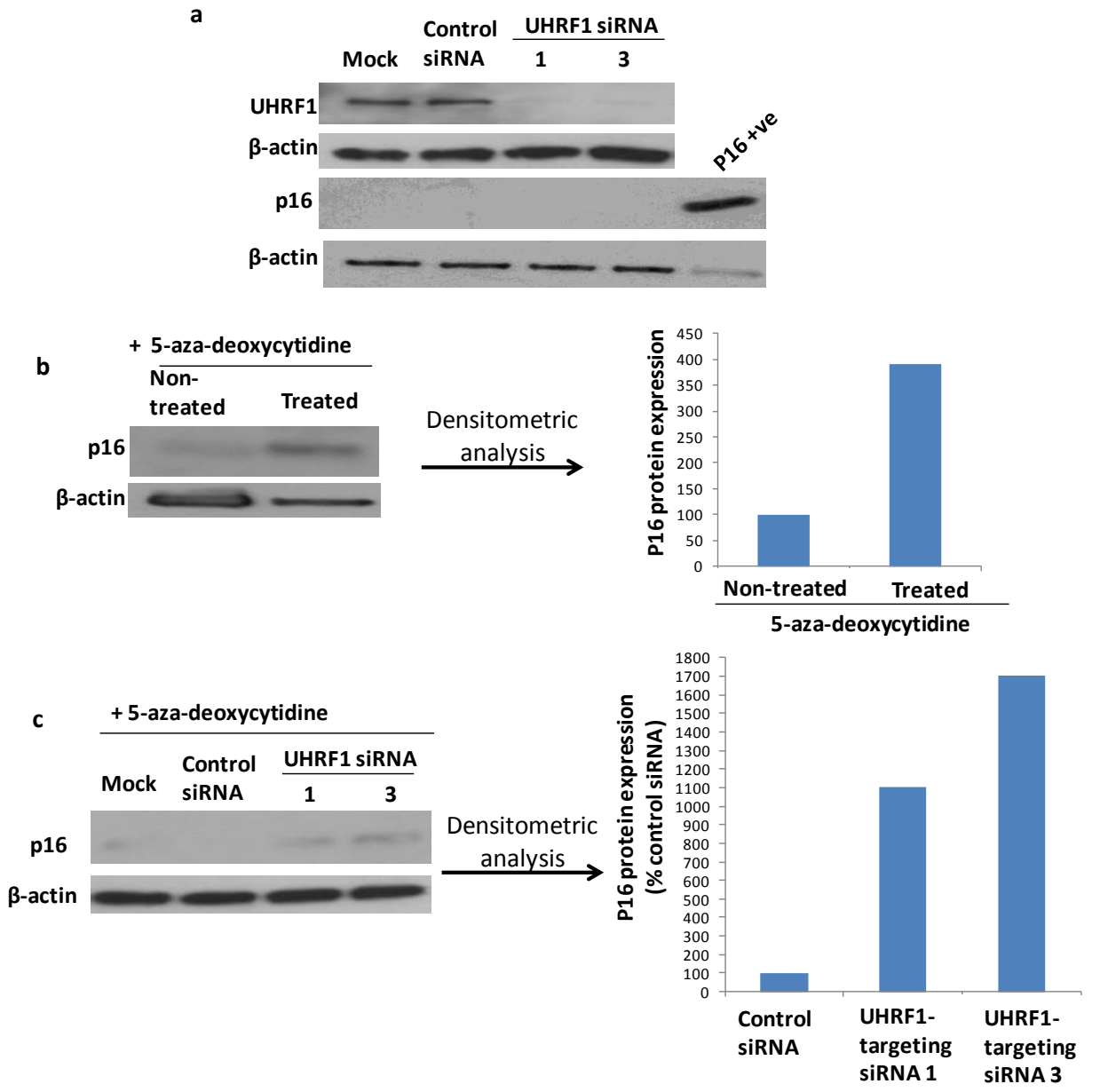

Figure 4-28. UHRF1 and P16 expression in CFpac-1 cells. (a) Western blot for P16 detection in CFpac1 cells following treatment with lipofectamine alone (Mock) or with control- or 30 nM UHRF1-targetting siRNAs for 72 h. (b) Western blot analysis and its densitometric analysis for cells treated with 100 µM 5-aza-deoxycytidine for 48 h (c) or treated with 100 µM 5-aza-deoxycytidine for 48 h combined with UHRF1 depletion for 72 h. Western data are representative of three independent replicates. β-actin was used as a loading control. The P16 positive control used is lysate from human embryonic kidney HEK 293 cells.

4.4.9 Summary and discussion of UHRF1 role in regulation of methylation status in pancreatic cancer cells:

Generally in the panel of pancreatic cancer cells lines (MiaPaca-2, CFpac-1, Panc-1 and Suit-2), cells with high UHRF1 protein expression showed a higher level of DNA methylation.

Therefore, we measured differences in the methylation index of *LINE-1* promoter and *ALu-V* elements using pyrosequencing following UHRF1 knockdown. The methylation levels of *LINE-1* promoter were sizably reduced in pancreatic cancer cells following depletion of UHRF1 protein, in agreement with a previous report [158]. Moreover, we noted that UHRF1 expression levels reflected the basal DNA global methylation of *LINE-1* and *Alu-V* elements; the pancreatic cancer cell lines with the highest UHRF1 levels had the highest global methylation levels. Furthermore, time course analysis of transient UHRF1 depletion and recovery of UHRF1 protein suggested a strong correlation between UHRF1 expression and global DNA methylation. In addition, the effect of UHRF1 depletion on *LINE-1* promoter methylation was additive to the effect of the de-methylation agent 5-aza-deoxycytidine treatment. In lung cancer, UHRF1 upregulation was significantly correlated with DNA hypermethylation [64], but global DNA hypomethylation of *LINE-1* and *Alu-V* elements has also been demonstrated in response to UHRF1 overexpression [160]. As a focus for future work, it remains to be seen what effect UHRF1 over-expression can have on the global DNA methylation status in pancreatic cancer cells.

In addition to effects on global methylation, we also observed effects on TSG promoter methylation. We showed that the *CDKN2A* promoter, which is hypermethylated in CFpac-1 pancreatic cells [92] and in colorectal cancer cells [61] had reduced promoter methylation

following UHRF1 knockdown. However, the loss in *CDKN2A* promoter methylation caused by UHRF1 depletion was not sufficient to result in detectable expression of the $p16^{INK4a}$ protein. In contrast, UHRF1 depletion from colorectal cancer cells was sufficient to result in detectable $p16^{INK4a}$ protein [61]. However, we were able to detect $p16^{INK4a}$ protein when we combined UHRF1 depletion with de-methylation treatment using 5-aza-deoxycytidine. From our observations, UHRF1 depletion assisted 5-aza-deoxycytidine in activating *CDKN2A* gene expression and restoration of $p16^{INK4a}$ protein expression in pancreatic cancer cells; we suggest UHRF1 as a potentially interesting target for cancer therapy to assist reactivation of TSGs that have been silenced by promoter hypermethylation.

Future work should study the correlation between UHRF1 and the methylation status of genes of interest in DNA extracted from patients' tissue with pancreatic cancer tumours and normal pancreas.

4.5 UHRF1 regulates *KEAP1* promoter methylation and activates the KEAP1/NRF2 pathway:

It has been previously reported by this laboratory that 70 % of PDAC lack KEAP1 expression [128]. Therefore we attempted to investigate whether the *KEAP1* gene promoter is silenced through methylation in pancreatic cancer cells, as has been previously reported for other cancers [151-154], and whether UHRF1 contributed to this process.

4.5.1 Examining KEAP1 protein expression levels in pancreatic cancer cells:

Several pancreatic cancer cell lines, including, MiaPaca-2, CFpac-1, Panc-1 and Suit-2 were examined for KEAP1 protein expression by western blotting analysis. As shown in Figure 4-29, the level of KEAP1 expression was variable between the examined cell lines with high protein expression observed in MiaPaca-2 cells, and lower expression of KEAP1 detected in CFpac-1, Panc-1 cells and Suit-2 cells. The western blot analysis of KEAP1 expression showed 2 bands (Figure 4-29 a), the top band was at the expected molecular weight of KEAP1 (70 kDa) and at the level of the positive control. The positive control is human embryonic kidney HEK 293 cells transfected with Keap1-V5. To investigate the specificity of KEAP1 antibody, we treated the cells with KEAP1-targeting siRNA. Following KEAP1 knockdown, the protein levels in the lower band with molecular weight at 55 kDa, was not changed, while the top band at the expected molecular weight of KEAP1 was depleted in the cells treated with KEAP1-targeting siRNA (Figure 4-29 b). This observation was made in MiaPaca-2 (n=3), Suit-2 (n=3) and CFpac-1 (n=3). As evaluation of KEAP1 protein detection, we used 2 different lysis buffers for sample preparation. KEAP1 protein was detectable in samples prepared with Tris-SDS only, while samples prepared

with RIPA buffer showed only the expression of the lower non-specific band as shown in Figure 4-29 c.

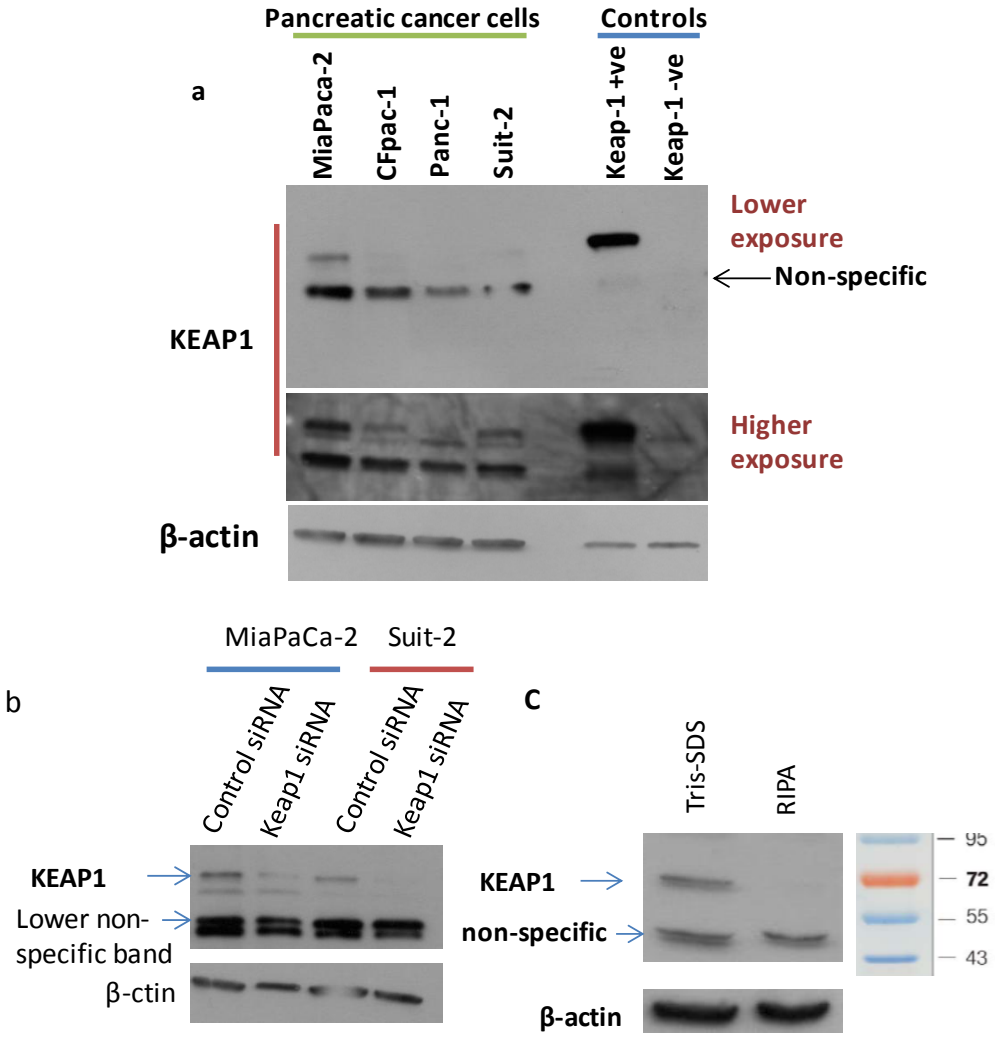

Figure 4-29. KEAP1 protein expression in a panel of pancreatic cancer cell lines. (a) The basal expression levels of KEAP1 protein. The positive control is human embryonic kidney HEK 293 cells transfected with KEAP1-V5, the negative control is mock transfected HEK 293 cells. (b) KEAP1 expression following KEAP1 depletion in MiaPaca-2 and Suit-2 cells. (c) Western blot for KEAP1 protein detection in Suit-2 using 2 different lysis buffers (Tris-SDS and RIPA). β-actin was used as a loading control.

4.5.2 The DNA methylation status of the *KEAP1* promoter in pancreatic cancer cell lines:

Next, we used pyrosequencing to quantify the level of the methylation of the promoters of *KEAP1* in four cell lines (MiaPaca-2, CFpac-1, Panc-1 and Suit-2). Transcription of the *KEAP*1 gene is controlled by 2 transcription start sites (TSS), thus we examined the methylation status in the regions upstream of each TSS which is 435 bp away from each point. The region upstream of TSS1 was referred to as *KEAP1*a and the region upstream of TSS2 was referred to as *KEAP1b* (Figure 4-30).

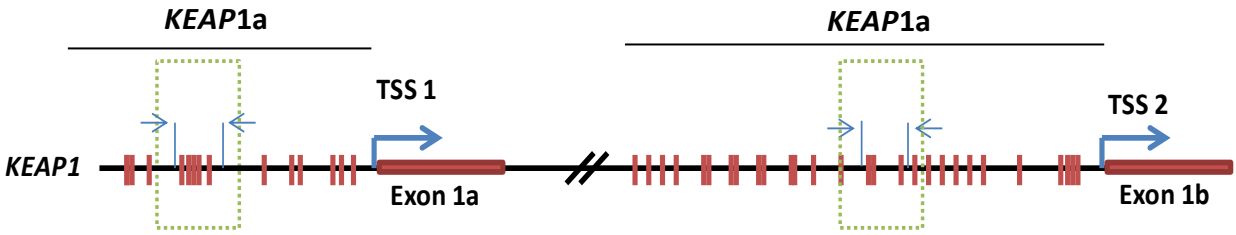

Figure 4-30. Schematic representation of the *KEAP*1 promoter region. The diagram shows the *KEAP*1 promoters including *KEAP1*a and *KEAP1*b regions. The red vertical lines are showing locations of the CpGs in the promoter regions. TSS: transcriptional start site. The green dot boxes indicated the amplified sequence of each promoter sites that we included in our study.

Three of the four cell lines examined showed methylation of the *KEAP1a* promoter. MiaPaca-2 cells exhibited a high basal level of *KEAP1a* promoter methylation (68 %) compared to Suit2 (27 %) and CFpac-1 (15 %). Methylation of the examined region of the *KEAP1a* promoter was not detected in Panc-1 cells (Figure 4-31). The methylation levels of another region of *KEAP1* promoter, referred to as the *KEAP1*b promoter. The *KEAP1*b promoter was not methylated in all the examined cell lines.

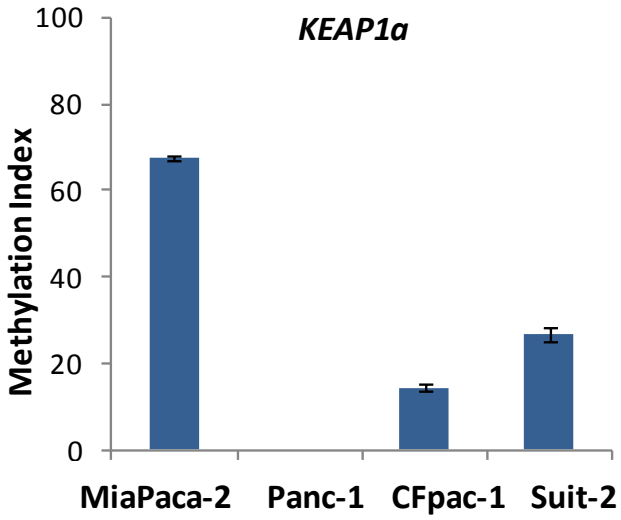

Figure 4-31. The basal methylation levels of *KEAP1* promoters in pancreatic cancer cells. The methylation levels of *KEAP1*a promoter detected in different pancreatic cancer cell lines by pyrosequencing (n=3).

4.5.3 Depletion of UHRF1 is associated with loss of *KEAP1* promoter methylation and up-regulation of Keap1 protein:

In order to examine the relationship between de-methylation of the *KEAP1* promoters and Keap1 protein levels, we depleted UHRF1, and extracted DNA and protein for analysis. Following DNA extraction and bisulphite treatment, we amplified a region of the *KEAP1*a promoter by PCR (Figure 4-32).

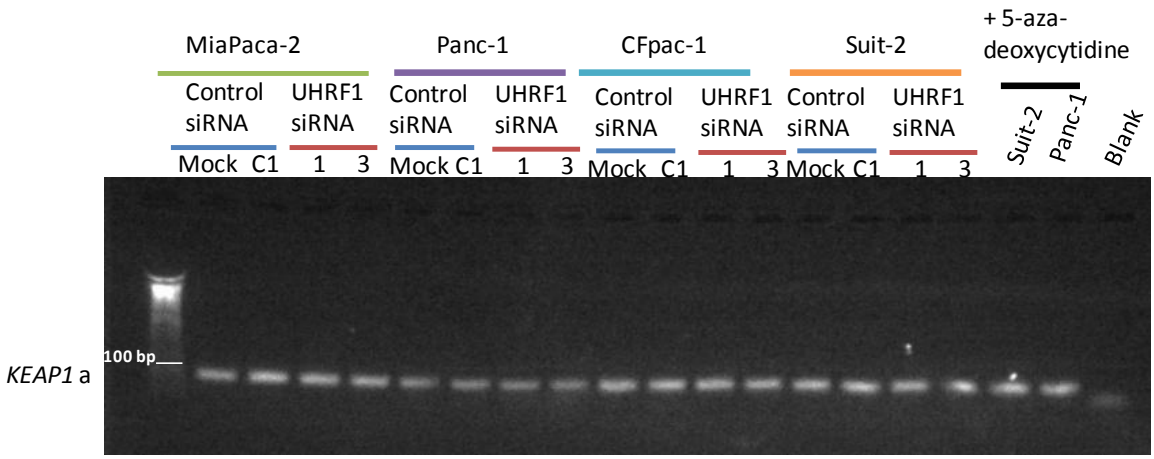

Figure 4-32. PCR products for a region of the *KEAP1*a promoter. The PCR products for the *KEAP1*a promoter, following UHRF1 knockdown or control, were separated on a 2 % agarose gel.

Pyrosequencing data indicated that depletion of UHRF1 resulted in a loss of *KEAP1*a promoter methylation in MiaPaca-2, Suit-2 and CFpac-1 cells of 6 %, 42 % and 9 % respectively (Figure 4-33).

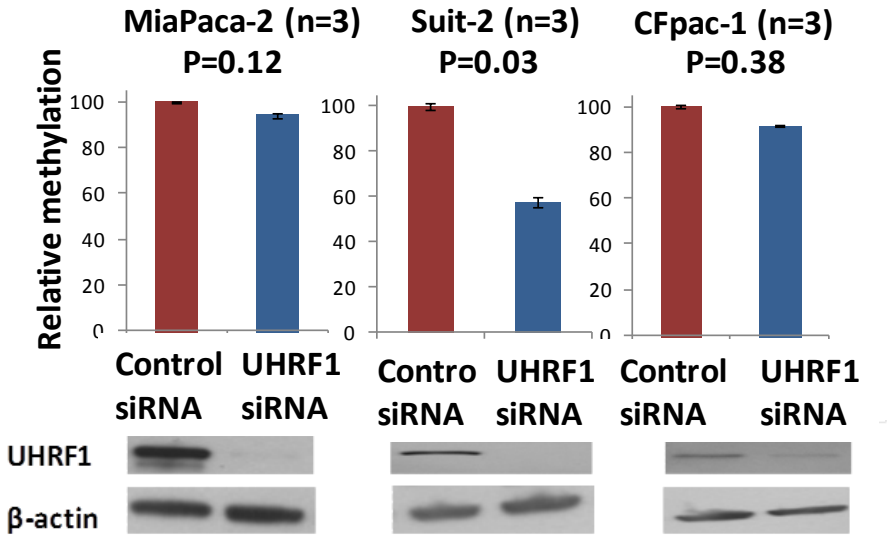

Figure 4-33. UHRF1 depletion reduces the methylation level of KEAP1 promoter in pancreatic cancer cells. Mean of triplicate DNA methylation measurements of KEAP1a promoter methylation in MiaPaca-2, Suit-2 and CFpac-1 cells following transfection with control- or UHRF1-targetting siRNAs. The data are presenting UHRF1-targeting siRNA3 effect; the same

results were obtained with UHRF1-targeting siRNA1 as each run included 2 different control siRNAs and 2 different UHRF1-targeting siRNA.

In order to study the relationship between UHRF1 and *KEAP1*a in depth, we examined the expression of KEAP1 protein following UHRF1 depletion in pancreatic cancer cells including Mia-Paca-2, CFpac-1 and Suit-2. UHRF1 depletion was accompanied by a gain in KEAP1 protein level in Sui-2 cells as shown in Figure 4-34 a, the same observation was made in MiaPaca-2 and CFpac-1 cells. KEAP1 up-regulation was also examined at 3 time points of UHRF1 depletion in Suit-2 cells (n=2). We observed significant correlation between UHRF1 loss and KEAP1 up-regulation at 24, 48 and 72 h (Figure 4-34 b). This observation was also made in CFpac-1 and MiaPaca-2 cells (n=2). From these results, UHRF1 depletion affects the expression level of KEAP1 as an early event at 24 h following knockdown. Further analysis based on this observation (by another PhD student) showed an increase in KEAP1 mRNA at 24 h following UHRF1 depletion.

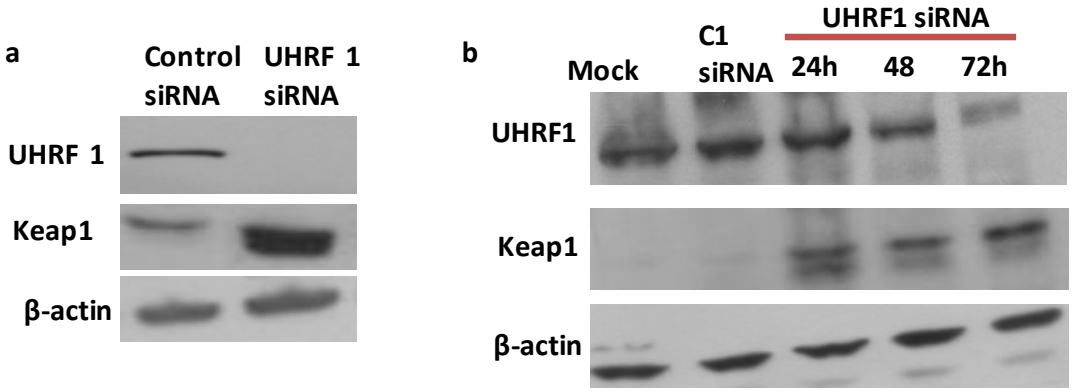

Figure 4-34. Depletion of UHRF1 in Suit-2 is associated with up-regulation of KEAP1 protein in Suit-2 cells. (a) and (b) showing western blot analysis examining UHRF1 and KEAP1 protein expression following UHRF1 depletion. β-actin was used as a loading control.

We next examined whether altering the methylation of the *KEAP1*a promoter in a different manner could also affect KEAP1 protein levels. We found that treating Suit-2 cells with the de-methylation drug 5-aza-deoxycytidine (100 µM) resulted in a reduction in *KEAP1*a promoter methylation by 80 % (Figure 4-35 a) and corresponding up-regulation of KEAP1 protein levels (Figure 4-35 b).

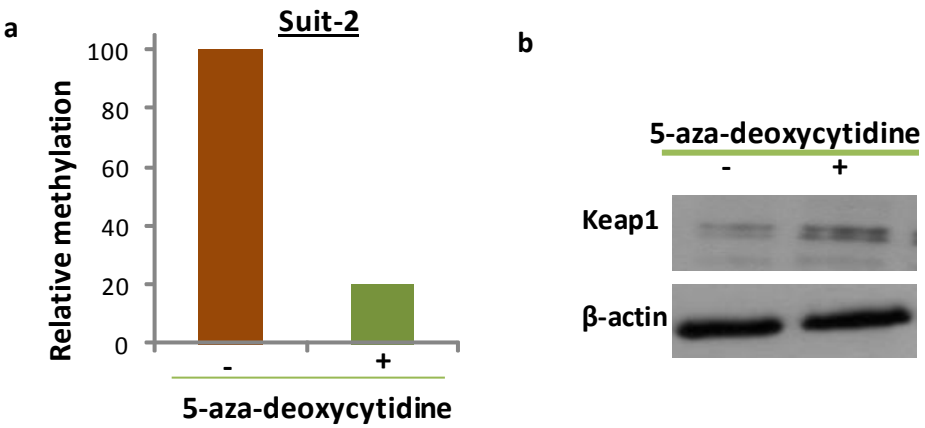

Figure 4-35. DNA methylation controls KEAP1 expression. (a). The methylation level of KEAP1 promoter measured by pyrosequencing in Suit2 cells treated with 5-aza-deoxycytidine. (b) Western blot analysis showing up-regulation of KEAP1 following treatment in a. β-actin was used as a loading control (n=1).

To determine whether the increased KEAP1 protein was functionally relevant, Nrf2 protein levels were measured. The gain in KEAP1 protein following UHRF1 depletion was concomitant with a loss in NRF2 protein level. Moreover, a decrease in the level of NRF2 downstream protein Heme Oxygenase 1 (HO-1), was also observed following UHFR-1 knockdown (Figure 4-36 a). Densitometric measurements showed that the gain of KEAP1 paralleled the reduction in NRF2 and HO-1 (Figure 4-36b).

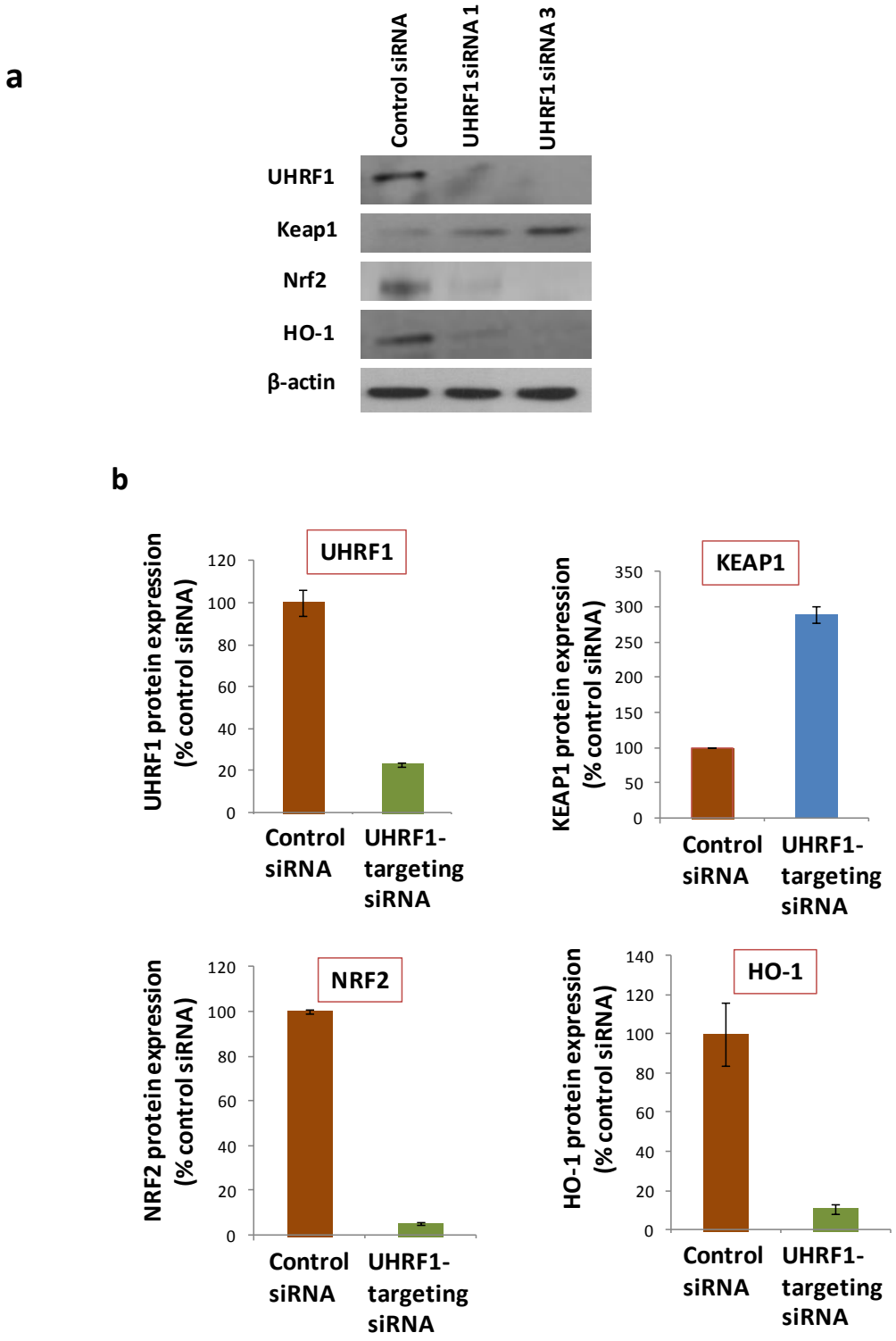

Figure 4-36. Immunoblot detection of UHRF1, KEAP1, NRF2 and HO-1 in MiaPaca-2. (a). Western blot analysis following UHRF1 depletion, showing gain in KEAP1 protein (n=8), down-regulation of NRF2 (n=5) and HO-1 (n=4), β-actin was used as a loading control. (b) Densitometric analysis for the blots in (a).

Additional NRF2 downstream proteins were examined following UHRF1 depletion, namely Glutamate-cysteine ligase catalytic subunit (GCLC) and cytochrome P450 2A6 (CYP2A6). UHRF1 depletion resulted in down-regulation of GCLC (Figure 4-37 a) and CYP2A6 (Figure 4-37 b).

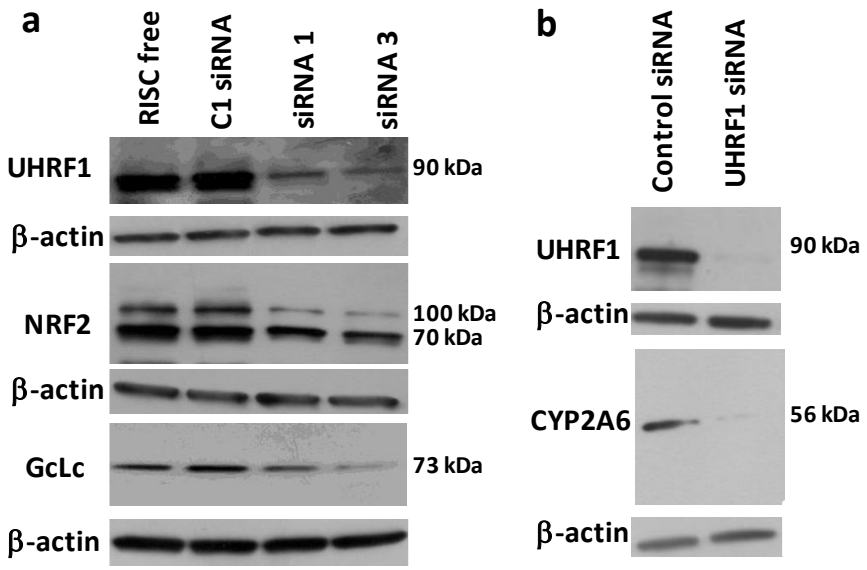

Figure 4-37. Western blot analysis following UHRF1 depletion. (a) Down-regulation of NRF2 and GCLC (n=3), (b) Down-regulation of CYP2A6 (n=3). β-actin was used as a loading control.

Furthermore, preliminary analysis (n=2) showed that the mRNA levels of *NRF2* and its downstream gene *GCLC* genes were decreased as well as the mRNA level of the *KEAP1* gene following UHRF1 depletion for 72 h in Suit-2 cells (Figure 4-38). Further analysis based on this observation (by another PhD student) showed an increase in *KEAP1* mRNA at 24 h followed by reduction at 48 and 72 h after UHRF1 depletion.

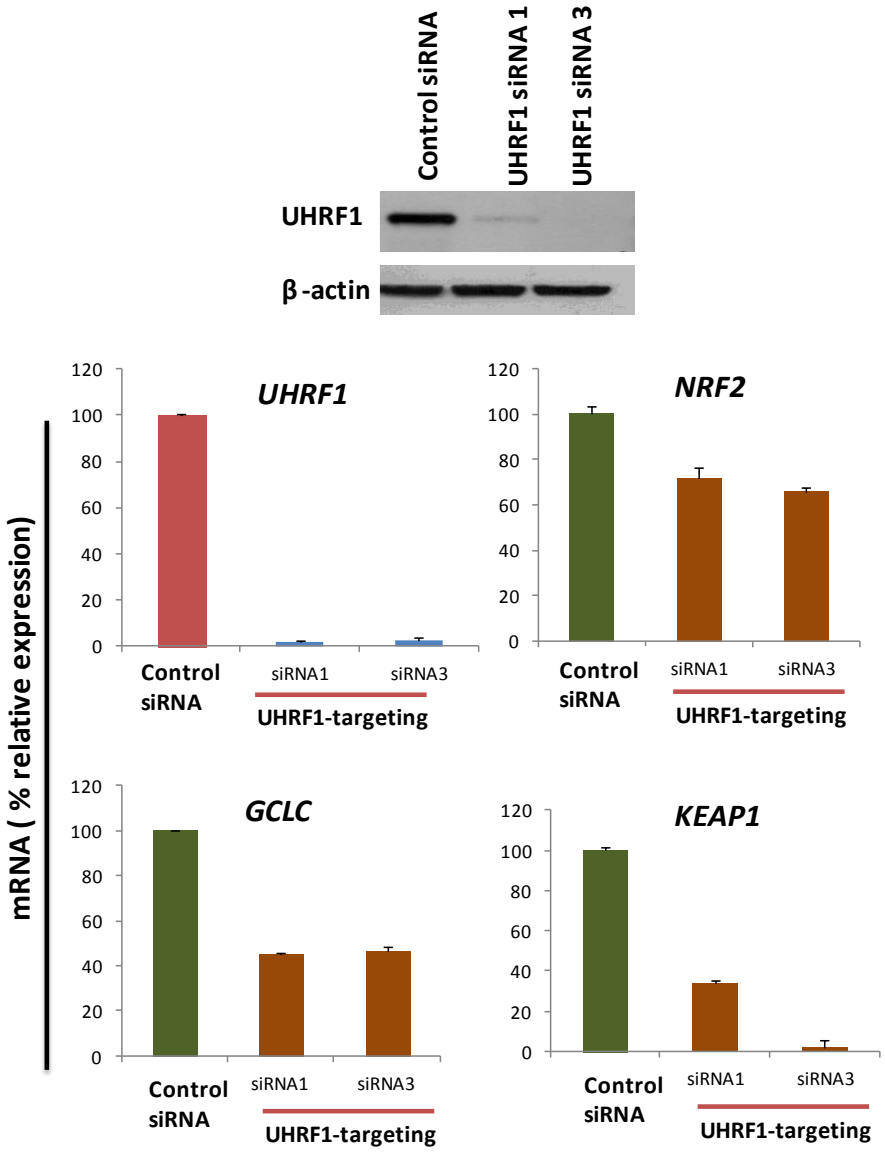

Figure 4-38. UHRF1 depletion by siRNA for 72 h decreased the mRNA level of the *KEAP1, NRF2* and *GCLC* genes in Suit-2 cells (n=2). Mean of triplicate mRNA measurements following treatment with control- or UHRF1-targetting siRNAs. GAPDH was used a housekeeping gene.

4.5.4 K-RAS depletion down-regulates UHRF1 protein expression level:

K-RAS activation is the most common genetic change in pancreatic cancer [29]. In pancreatic cancer cells, K-RAS depletion causes a decrease in NNF2 mRNA levels and increases reactive oxygen species (ROS) which would promote tumourgenesis [118]. We examined the effect of UHRF1 depletion on K-RAS, which lies upstream of NRF2 [118]. The expression level of K-RAS was unaffected by UHRF1 depletion (Figure 4-39). This observation was made in Suit-2 and MiaPaca-2 (n=2).

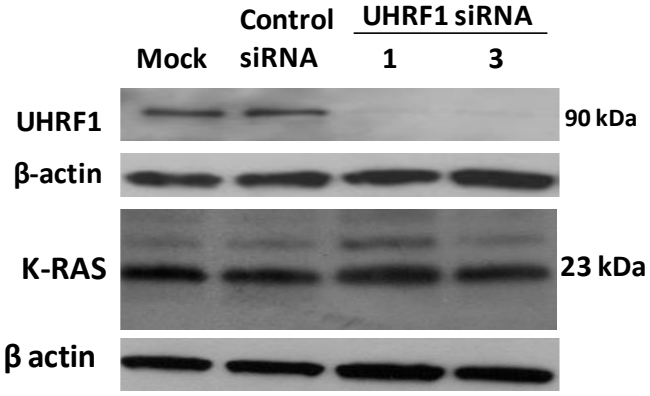

Figure 4-39. K-RAS expression was unaffected by UHRF1 depletion in Suit-2 cells. Western blot analysis of UHRF1 and K-RAS following UHRF1 depletion by 30 nM UHRF1-targeting siRNA for 72 h (n=2). β-actin was used as a loading control.

We further examined the effect of UHRF1 expression following K-RAS depletion in Suit-2 cells. We found that siRNA-mediated K-RAS knockdown resulted in UHRF1 down-regulation (Figure 4-40). The K-RAS knockdown lysates used in Figure 4-40 were kindly provided by another PhD student in our laboratory (Mr Robert Ferguson).

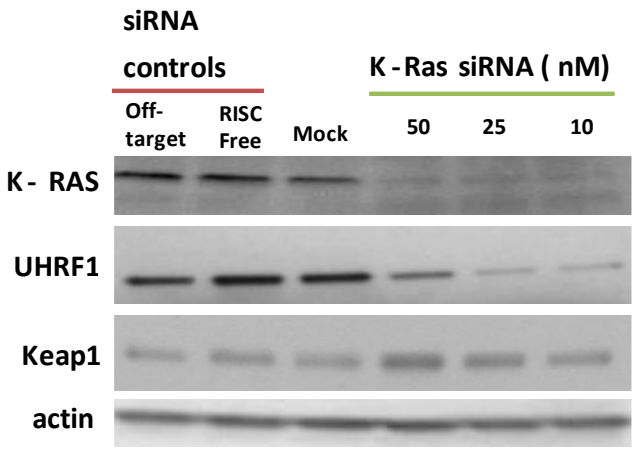

Figure 4-40. K-RAS depletion is associated with UHRF1 down regulation in Suit-2 cells. β-actin was used as a loading control.

4.5.5 UHRF1 expression in pancreatic tumours is associated with low KEAP1 levels:

Based on the observed inverse relationship between UHRF1 and KEAP1 levels in pancreatic cell lines, we sought to determine if this was relevant in patient tumour samples. KEAP1 expression was evaluated by IHC for 124 patients in this study, (57/124 patients were previously stained by Dr. Taoufik Nedjadi in our laboratory). We stained pancreatic cancer tissue micro-array for KEAP1 and scored the cases as either positive or negative, based on the presence of either cytoplasmic or extracellular membrane expression of KEAP1 in the tumour cells (Figure 4-41).

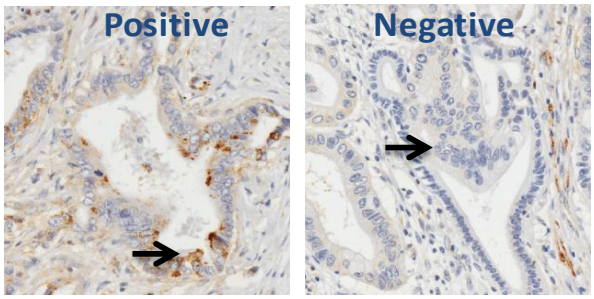

Figure 4-41. IHC for KEAP1 in pancreatic cancer tissue. (a) Positive cytoplasmic KEAP1 expression. (b) Negative KEAP1 expression in the ducts as indicated by the arrows.

Of the 124 patients, UHRF1 scores were attributed as follows: 17 scored 0 (negative), 32 scored 1 (weak), 46 scored 2 (moderate) and 29 scored 3 (strong). For patients with the highest UHRF1 levels (score 3), the majority (86 %; 25/29) were negative for KEAP1 expression. By contrast, for patients lacking UHRF1 expression (score 0), the majority (10/17) expressed KEAP1, with only 41 % lacking KEAP1 expression. The percentages lacking KEAP1 in the weak and moderate UHRF1 expressers were 72 % and 78 % respectively (Figure 4-42). Thus the inverse association between UHRF1 level and KEAP1 observed in cell lines was upheld in PDAC tissue (Fisher's Exact p=0.002).

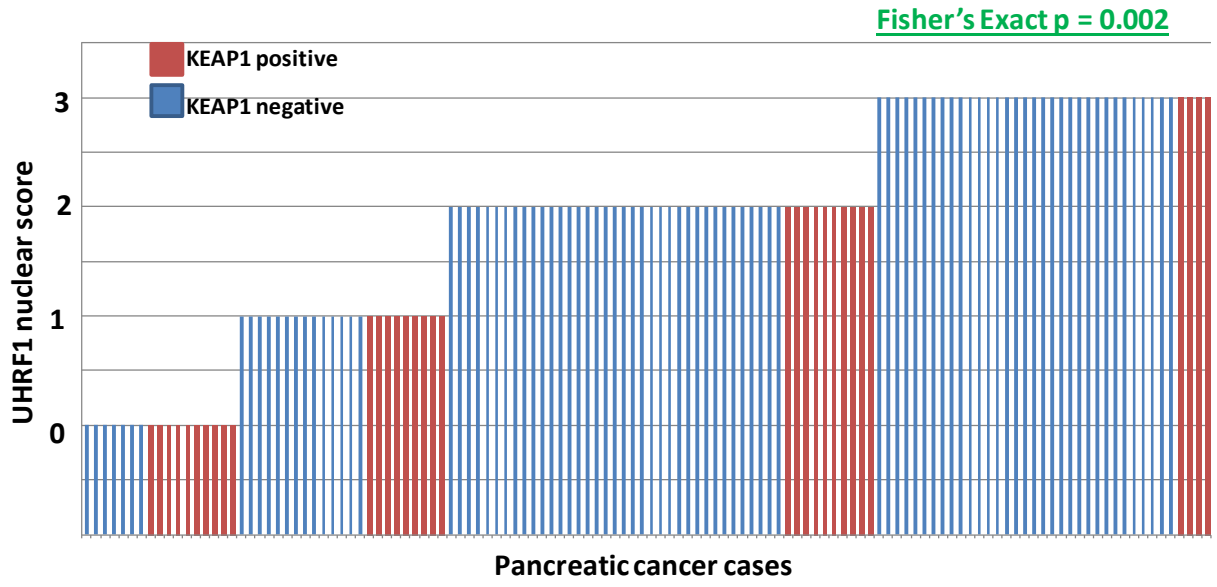

Figure 4-42. UHRF1 expression in pancreatic tumours is associated with low KEAP1 levels. The scores attributed for nuclear UHRF1 expression are plotted, grouped according to score, and KEAP1 status (white bar = negative; black bar = positive) indicated.

4.5.6 UHRF1 expression levels are increased by sulforaphane treatment in pancreatic cancer cells:

To gain insight into the physiological role of UHRF1 in the KEAP1/NRF2 pathway, we examined the effect of sulforaphane on NRF2 and KEAP1 expression levels. Sulforaphane is known to act as an activator of NRF2. We observed an increase in an NRF2 expression in cells treated with 5 µM sulforaphane for 12 h, and KEAP1 expression was not affected (Figure 4-43 a and b).

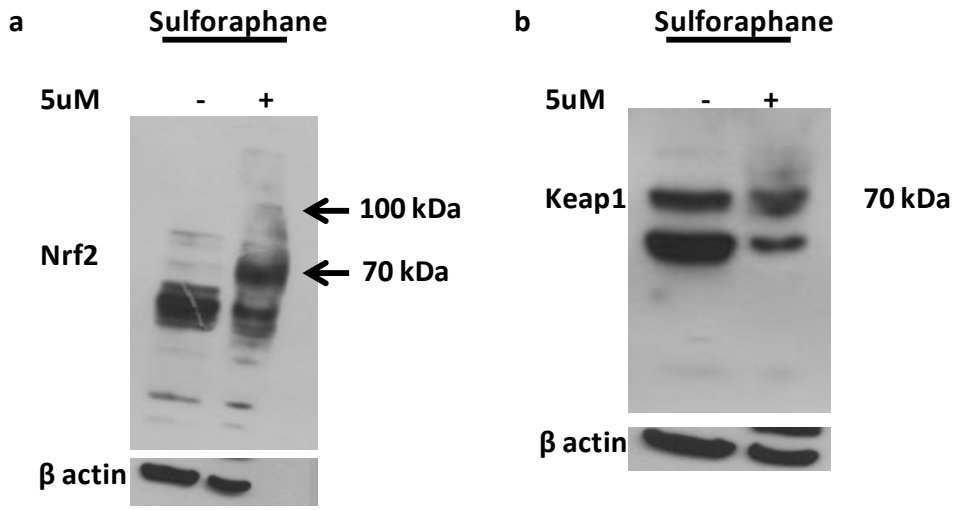

Figure 4-43. Western blot analysis for Suit-2 cells treated with sulforaphane. (a) NRF2 expression and (b) KEAP1 expression. (n=2).

We sought to combine sulforaphane treatment with UHRF1 depletion using UHRF1-targeting siRNA, but first we asked a question of what effect sulforaphane has on UHRF1 expression. To answer this question we treated pancreatic cancer cells with 5 µM sulforaphane for 12 h. We found a significant gain in UHRF1 levels following treatment (Figure 4-44 a). This observation was made in Suit-2 and MiaPaca-2 cells (n=2). To confirm our observation we studied the effect of sulforaphane on UHRF1 expression in a dose-dependent manner. Interestingly we have

observed increased levels of UHRF1 as the dose of sulforaphane increased (Figure 4-44 b) in Suit-2 cells (n=1).

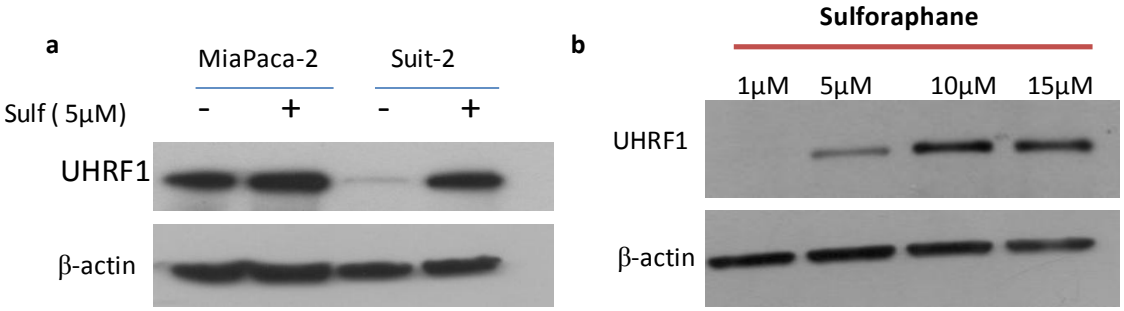

Figure 4-44. Immunoblot detection of UHRF1 in cells treated with sulforaphane. (a) MiaPaca-2 and Suit-2 cells were treated with 5 μM sulforaphane for 12 h (n=2). (b) UHRF1 expression following dose dependent treatment with sulforaphane in Suit-2 cells (n=1). β-actin was used as a loading control.

Based on this observation, sulforaphane has the opposite effect on UHRF1 expression to UHRF1 siRNA. Combining the treatments might not have an effect on the expression of UHRF1 or NRF2. To examine the effect of this combined treatment, a preliminary study (n=1) was done using Suit-2 cells treated with 5 μM sulforaphane for 12 h following UHRF1 depletion for 72 h. The results of this experiment were not conclusive, as the levels of KEAP1 or NRF2 were not changed following transfecton with UHRF1-targeting siRNA1, while changes were noted when the cells were transfected with UHRF1-targeting siRNA3 (Figure 4-45). Of note, the effect of sulforaphane was normalised with UHRF1 depletion as the observations in Figure 4-43 and Figure 4-45 were examined at the same time.

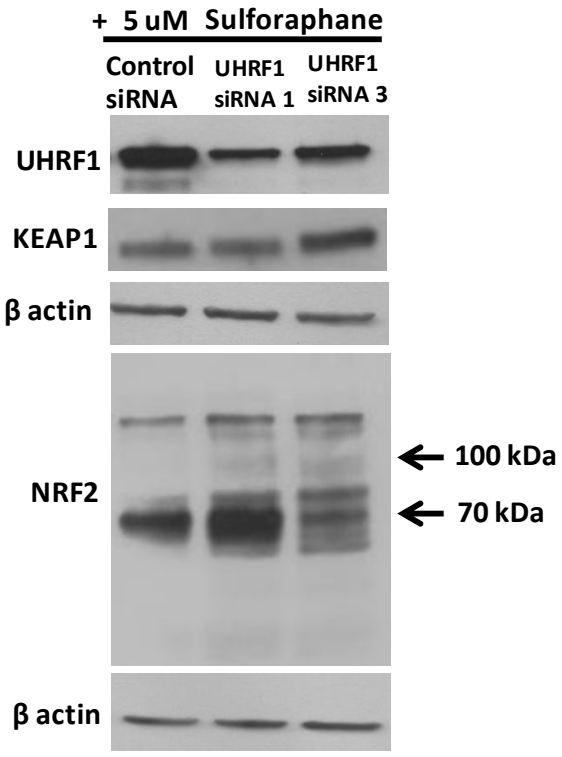

Figure 4-45. Western blot analysis of UHRF1, NRF2 and Keap1 in Suit-2 cells treated with sulforaphane and UHRF1-targeting siRNA. (n=1). β-actin was used as a loading control.

4.5.7 KEAP1 depletion reverses the effect of UHRF1 depletion on cell proliferation:

In a preliminary analysis (n=2), we attempted to examine the cell proliferation in cells treated with combined depletion of UHRF1 and KEAP1 using MiaPaca-2 cells. UHRF1 depletion alone caused a reduction in cell growth by 60 % (Figure 4-46); this observation was previously shown in Figure 4-9 while KEAP1 depletion alone resulted in an increase proliferation by approximately 60 % (Figure 4-46). The double knockdown of UHRF1 and KEAP1 for 72 h resulted in increased proliferation by approximately 40 % (Figure 4-46). This observation was made using 3 different siRNA combinations. The knockdowns were confirmed by western blot analysis prior to MTS analysis.

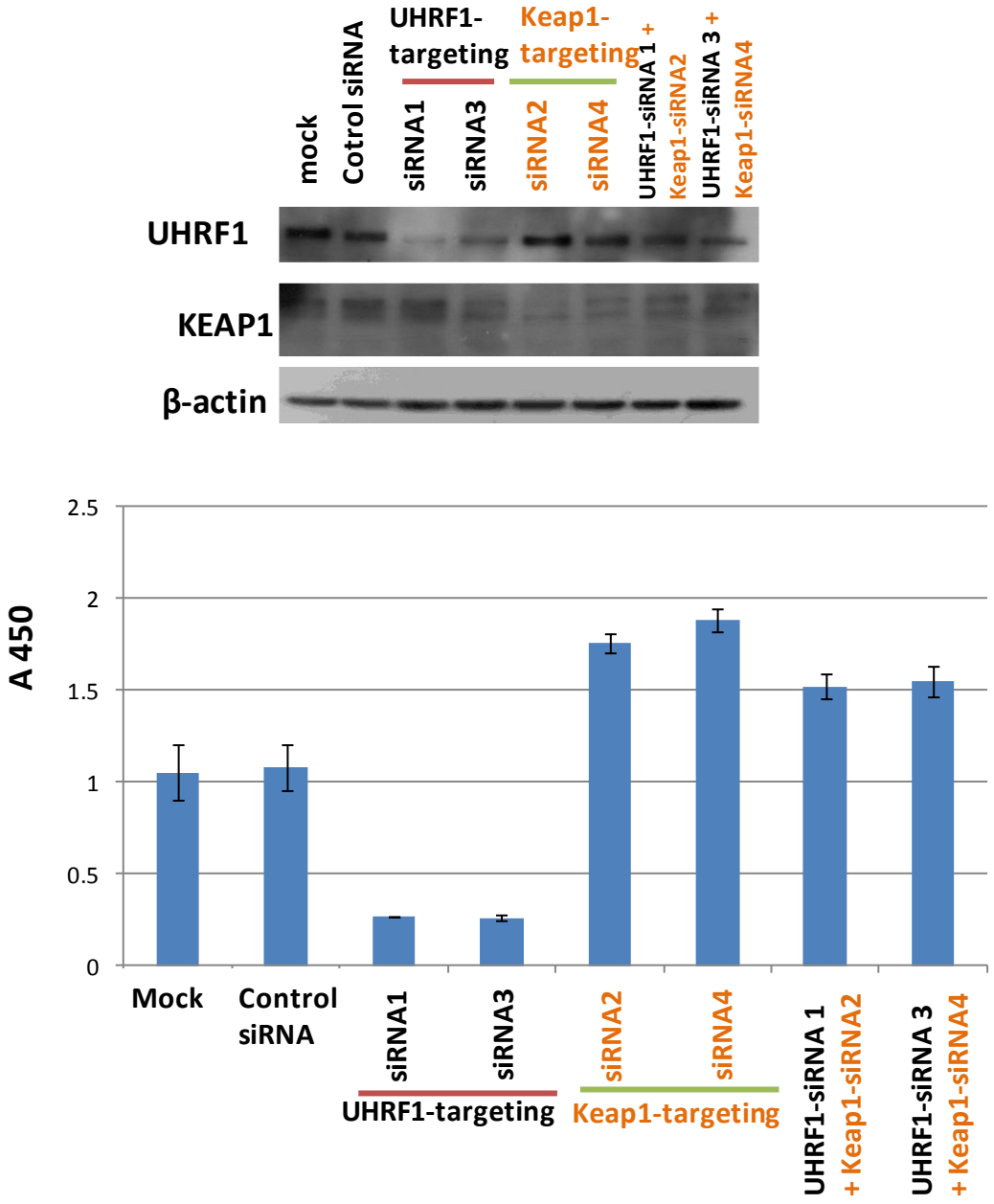

Figure 4-46. MTS analysis of Miapaca-2 cells following combined KEAP1 and UHRF1 depletion. Cells were treated with either non-targeting or 30 nM targeting siRNA (UHRF1 or KEAP1 or combined) cell viability was then assessed by MTS assay 72h post transfection. Results are a mean of triplicate samples ±SD. The western blot analysis for UHRF1 and KEAP1 confirmed successful knockdown.

4.5.8 Changing cellular location of KEAP1 following UHRF1 knockdown:

In order to examine UHRF1 and KEAP1 protein expression levels and cellular localization in pancreatic cancer, we stained fixed cells and probed with anti-KEAP1 antibodies. As previously shown, MiaPaca-2, CFpac-1, Panc-1 and Suit-2 cells show nuclear expression of UHRF1 (Figure 4-10) The expression of KEAP1 is perinuclear and also cytoplasmic in these cells apart from Suit-2 cells, which interestingly show nuclear expression of KEAP1 in most cases (Figure 4-47 a, b and c). When MiaPaca-2 and Suit2 cells were treated with UHRF1-targeting-siRNA, KEAP1 protein appeared to translocate from the cytoplasm to the plasma membrane (Figure 4-47 a). This was less apparent in Suit-2 cells. In Figure 4-47 b Panc-1 cells were weakly stained for KEAP1, but some cells show higher expression. CFpac-1 cells showed weak staining for KEAP1 and cells in mitosis showed elevated expression of KEAP1 (indicated by arrow in Figure 4-47 c).

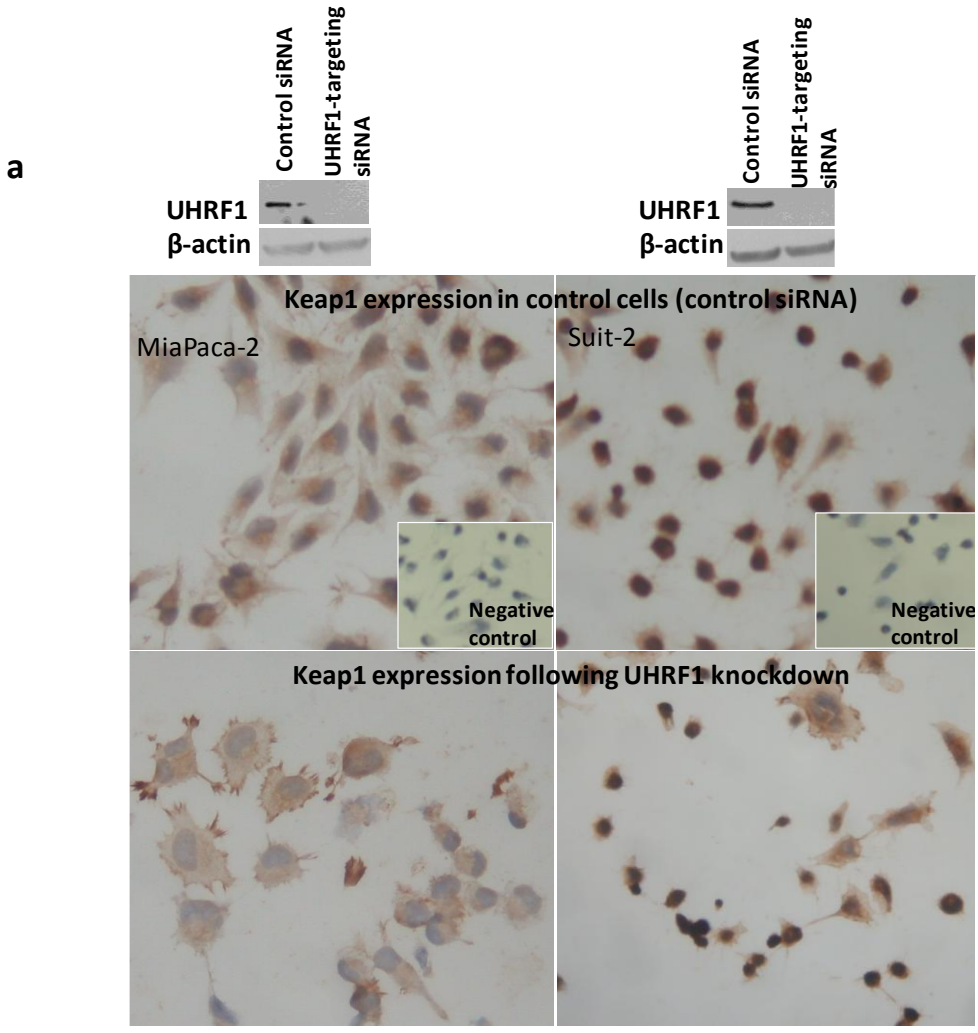
a
Control siRNA
UHRF1-targeting siRNA
UHRF1
β-actin
Control siRNA
UHRF1-targeting siRNA
UHRF1
β-actin
Keap1 expression in control cells (control siRNA)
MiaPaca-2
Suit-2
Negative control
Negative control
Keap1 expression following UHRF1 knockdown

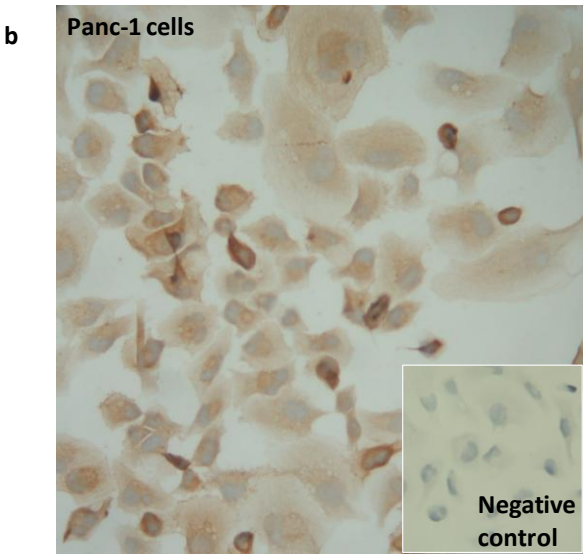
b
Panc-1 cells
Negative control

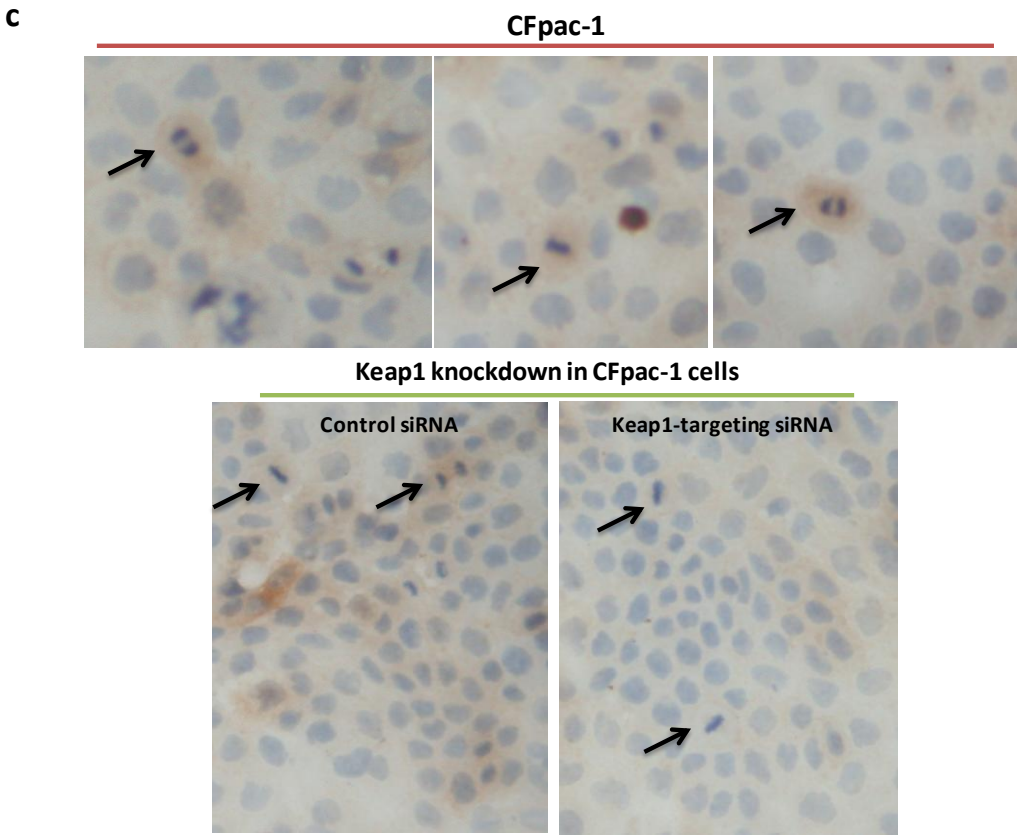

Figure 4-47. ICC of pancreatic cancer cells stained for KEAP1. (a) MiapPaca-2 and Suit-2 cells treated with UHRF1-targetting siRNA or control siRNA, stained for KEAP1. (n=2) (b) Non treated Panc-1 cells stained for KEAP1. (c) CFpac-1 cells stained for KEAP1 following KEAP1 knockdown.

4.5.9 Summary and discussion of UHRF1 role in *KEAP1* promoter methylation regulation and activation of the KEAP1/NRF2 pathway:

This is the first study showing that *KEAP*1 promoter is methylated in pancreatic cancer cells and that UHRF1 plays a role in controlling this process. Strong evidence has been presented that KEAP1 expression is controlled by its promoter methylation, as the protein level was increased following treatment with the demethylation agent 5-aza-deoxycytidine. UHRF1 knockdown resulted in loss in *KEAP1* promoter methylation and a measurable increase in KEAP1 protein expression in pancreatic cancer cells. Although UHRF1 depletion resulted in a small decrease in

methylation level in some cell lines, namely MiaPaca-2 and CFpac-1, it had a greater effect at the protein level.

Furthermore, the inverse relationship between UHRF1 and KEAP1 levels observed in cell lines was maintained in pancreatic cancer tissue samples, substantiating the notion that UHRF1 contributes to the control of KEAP1 expression in pancreatic cancer.

In our study we showed that Panc-1 cells have very low KEAP1 protein expression, although this disagrees with the report of Lister *et al*. [128]. In response to UHRF1 depletion and KEAP1 upregulation, we observed loss of NRF2 and NRF2-downstream proteins. Thus a model emerges in which UHFR1 expression maintains *KEAP1* promoter methylation and hence low KEAP1 levels, which in turn allows NRF2 levels to remain elevated and corresponding NRF2 downstream proteins to be expressed. However, UHRF1 levels alone were not sufficient to explain all KEAP1 expression patterns. This is exemplified by the fact that a small proportion of high UHRF1 expressers (14 %) nonetheless express KEAP1, while 41 % of patients lacking UHRF1 also lacked KEAP1. Thus additional control mechanisms are clearly in place governing the KEAP1/NRF2 pathway in pancreatic cancer. The study of the methylation status of the *KEAP1* promoter was limited to pancreatic cancer cell lines. In the future, an expanded study to examine *KEAP1* promoter methylation in DNA extracted from pancreatic cancer tissues is needed to cover the methylation status of *KEAP1* promoter in this cancer type.

NRF2 is an important protein for cell protection, in normal cells sulforaphane is known to increase its level and activity. In the case of cancer, a continuous induction of NRF2 by using sulforaphane is not recommended during treatment as it increases the cell protection against chemotherapy [161]. In our preliminary data, the effect of sulforaphane might be mediated by

UHRF1, as the former lost its effect on NRF2 when combined with UHRF1 depletion. More investigations regarding this interesting observation are needed to clarify mechanisms.

The preliminary observation of a possible translocation of KEAP1, from the cytoplasm to the plasma membrane, in response to UHRF1 knockdown in pancreatic cancer cells is interesting and requires further validation.

KEAP1 depletion, in agreement with our preliminary observation, and NRF2 activation have been reported to promote proliferation of pancreatic cancer cells and resistance to chemo- and radiotherapy [128]. NRF2 promotes proliferation and cell growth in other cancers such as prostate cancer [155]. Moreover, activating the NRF2 antioxidant program allows cancer cells to suppress reactive oxygen species (ROS) [118]. It will be interesting to determine whether UHRF1 fits into this scheme. In a genetic model of pancreatic cancer, targeting of the NRF2 pathway impaired K-RAS (G12D)-induced proliferation and tumourigenesis in vivo [118]. Given that NRF2 is possibly regulated by KEAP1-independent mechanisms [119], and our data demonstrate a decrease in NRF2 mRNA levels in UHRF1 depleted cells, it is possible that UHRF1 plays a role in directly regulating NRF2. This would be a focus for future work; it would be interesting to examine the effect of UHRF1 depletion or overexpression on NRF2 expression in cells negative for KEAP1.

It has been reported that K-RAS regulates NRF2 expression levels in pancreatic cancer cell lines, by decreasing the mRNA levels of NRF2 following K-RAS depletion [118]. In our study we showed that K-RAS depletion from pancreatic cancer cells downregulates UHRF1 expression levels and upregulates KEAP1 expression. Moreover, UHRF1 depletion from pancreatic cancer cells has no effect on K-RAS expression levels. Additionally, in preliminary analysis, we observed

that UHRF1 depletion slightly decreased NRF2 mRNA levels in pancreatic cancer cells. Taken together, it suggests that K-RAS may act upstream of UHRF1. Accordingly, it is possible that UHRF1 mediates the action of K-RAS on NRF2, although this hypothesis requires testing in future experiments.

Our preliminary analysis of the mRNA levels of KEAP1 indicated that they were upregulated 24 h post-UHRF1 knockdown, and decreased at 48 h and 72 h following UHRF1 depletion. This suggests that KEAP1 protein upregulation is an early event following UHRF1 knockdown. We observed elevated KEAP1 protein levels at 72 h post UHRF1 knockdown. Further analysis, such as the measurement of KEAP1 protein half-life, is required to understand why KEAP1 protein levels are high when mRNA levels are low.

Chapter 5:

Discussion and future work

5 Discussion:

UHRF1 is an established epigenetic regulator contributing to maintenance of DNA methylation [158] and the modification of histones [159]. In this study, we documented UHRF1 expression in pancreatic cancer cell lines and pancreatic tumour specimens, in contrast to its infrequent expression in benign epithelial ducts. Interestingly, where matched PanINs and tumours were available, most cases had stronger UHRF1 expression in tumour cells than in PanINs suggesting that UHRF1 protein levels increase during the process of tumourigenesis. UHRF1 may therefore facilitate pancreatic cancer cell growth. We observed that depletion of UHRF1 in pancreatic cancer cells led to a visible loss in cell number, consistent with reports in non-small cell lung cancer [64], colorectal cancer [61], and prostate cancer [62]. Our cell synchronisation experiments pointed towards a peak in UHRF1 levels at G2/M of the cell cycle. Consistent with our findings, Tien *et al*. [79] also reported cell cycle arrest in the G2/M-phase of cancer cells following depletion of UHRF1 and described concomitant activation of the DNA damage response pathway. This is in contrast to the work of Hervouet *et al*. [81] who showed UHRF1 expression levels to be constant in all phases of the cell cycle.

Of note, in our pancreatic cancer tissue sections, we observed that the presence of UHRF1 was associated with larger tumour size. This observation did not however translate into a change in the outcome for those patients. Although UHRF1 has been associated with poor outcome in a variety of tumours [57, 60, 62], in our study no significant association was established. Consistent with its role in epigenetic gene silencing, depletion of UHRF1 was accompanied by loss of global LINE1 promoter methylation and tumour-specific *CDKN2A* and *RASSF1* promoter methylation. Moreover, we showed for the first time that the *KEAP1* promoter is methylated in

pancreatic cancer cells and that UHRF1 plays a role in controlling this process. The loss in KEAP1 promoter methylation led to a measurable increase in KEAP1 protein, a phenomenon that was not observed with $p16^{INK4a}$, where UHRF1 depletion alone was not sufficient to result in detectable $p16^{INK4a}$ protein. Furthermore, the inverse relationship between UHRF1 and KEAP1 levels observed in cell lines was maintained in tissue samples, substantiating the notion that UHRF1 contributes to the control of KEAP1 expression in pancreatic cancer.

In response to UHRF1 depletion and KEAP1 upregulation, we reported loss of NRF2 and NRF2-downstream proteins due to Keap1 regulation. Thus UHFR1 expression maintains KEAP1 promoter methylation levels, which in turn allows NRF2 levels to remain elevated and corresponding NRF2 downstream proteins to be expressed. Here we reported for the first time an additional control mechanism for KEAP1/NRF2 pathway in pancreatic cancer (Figure 5-1).

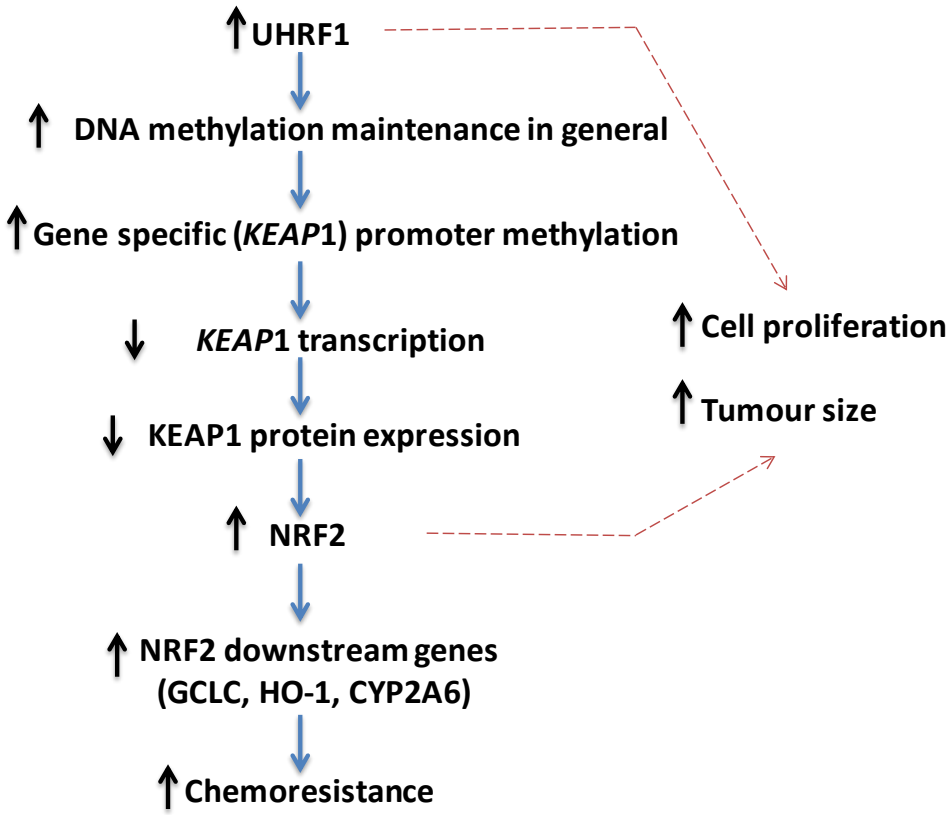

Figure 5-1. Summary of the effect of UHRF1 depletion on the KEAP1/NRF2 pathway and its potential impact in pancreatic cancer.

In pancreatic cancer, NRF2 has been reported to promote proliferation of pancreatic cancer cells and resistance to chemo- and radiotherapy [128] and the same observation was made in prostate cancer [155]. Activating the NRF2 antioxidant program in pancreatic cancer cells of genetically modified mice, also increases cells proliferation and reduces the suppression of the reactive oxygen species (ROS) [118]. In the future, it will be interesting to determine whether UHRF1 fits into this scheme. NRF2 regulates the inflammatory response and the expression of NRF2-dependent genes involved in this process. In a model of acute inflammation, the recruitment of macrophages was delayed in Nrf2-deficient mice [162]. It will be interesting to determine wither UHRF1 is involved in the inflammatory response, as we have shown the

presence of inflammatory cells in high UHRF1 expressing pancreatic cancer tissue sections. Pancreatic cancer is highly resistant to chemotherapy [20] and several clinical trials are ongoing to improve its treatment [10]. Our data suggests that UHRF1 is a potentially important target for pancreatic cancer drugs, due to its multiple effects on pancreatic cancer cells; the growth-inhibitory effect of UHRF1 depletion on pancreatic cancer cell lines as well as the effect in restoring the expression of TSGs that are commonly silenced by their promoter methylation (with a greater effect noted when UHRF1 siRNA was combined with the DNMT1 inhibitor 5-aza-deoxycytidine. Restoring the function of TSGs using epigenetic drugs has shown promise for cancer therapy [163-165]. Our novel discovery (upregulation of KEAP1 and downregulation of NRF2 by targeting UHRF1 by siRNA in pancreatic cancer cells) makes UHRF1 an interesting drug target in pancreatic cancer. It has been reported that targeting NRF2 by siRNA causes a decrease in proliferation and an increase in cell resistance to certain drugs [128, 166]. Targeting NRF2 alone resulted in a decrease in chemo-resistance to cancer therapy, but this could be a double-edged sword due to its ability to protect against cancer initiating insults in normal cells [167, 168]. Our results show the dual effect of UHRF1 depletion on the KEAP1/NRF2 pathway. This is an important finding, especially as UHRF1 depletion appears to inhibiting NRF2 through regulating *KEAP1* promoter methylation; this might be an advantage in pancreatic cancer treatment, by sensitizing the cells to chemotherapy [166].

In summary, in this first detailed study of UHRF1 in pancreatic cancer, we provide evidence for a role of UHRF1 in pancreatic cancer cell proliferation, and promoter methylation. Finally we have uncovered a novel role for UHRF1 in controlling the levels of KEAP1 gene expression and

shown that this relationship affects the KEAP1/NRF2 cellular stress pathway, which is known to play a role in cancer cell proliferation and chemoresistance.

6 Future work:

In our study we used pancreatic cancer cell lines and pancreatic cancer tissues for detection of UHRF1 protein expression. We reported both UHRF1 expression in the nucleus and interestingly in the cytoplasm. The cytoplasmic expression of UHRF1 has not previously been reported and it will be important to investigate in the future.

In this study, we evaluated the effect of UHRF1 on DNA methylation status. Our observations showed that depletion of UHRF1 resulted in reduced DNA methylation levels when DNA was extracted from pancreatic cancer cell lines. In the future, it will be interesting to expand the study and examine the DNA methylation levels and the effect of UHRF1 on global DNA methylation (LINE1 and Alu-V) as well as on specific genes (*KEAP1, CDKN2A and RASSF1*) in DNA extracts from patients specimens in order to support our observations.

This study has shown for the first time that the *KEAP1* gene promoter is methylated in pancreatic cancer cell lines. Evidence of *KEAP1* gene promoter methylation from primary tissue samples should be sought. Our novel results showed involvement of UHRF1 in regulating the KEAP1/NRF2 pathway in pancreatic cancer, as depletion of UHRF1 resulted in KEAP1 upregulation in pancreatic cancer cells and tissue samples, thus down-regulating NRF2 and its downstream genes. The possibility of a feedback loop with KEAP1 or NRF2 regulating UHRF1 expression was not completely investigated in this study; evaluating the effect of KEAP1 or NRF2 depletion on UHRF1 expression in pancreatic cancer cell is required in the future.

It is possible that UHRF1 plays a direct role regulating NRF2 and its downstream effects. It would be interesting to examine the effects of UHRF1 depletion on NRF2 in pancreatic cancer cells that lack KEAP1 expression. Our preliminary observation of KEAP1 cellular translocation in response to UHRF1 knockdown in pancreatic cancer cells is also interesting and requires further validation in future studies.

We showed that UHRF1 plays an important role in cell proliferation; UHRF1 and NRF2 depletion both resulted in reduced cellular proliferation. NRF2 is also known to increase cell resistance to chemotherapy. It would be interesting to determine whether UHRF1 promotes cell proliferation and resistance to chemo- and radiotherapy in pancreatic cancer in NRF2-deficient cells. Finally, it will also be important to evaluate the correlation of UHRF1 and NRF2 in inflammatory cells, as our observations showed increased levels of UHRF1 in inflammatory cells within pancreatic tissue samples.

Generally our results in this thesis are based on UHRF1 depletion in pancreatic cancer cells. Thus, the effect of UHRF1 overexpression on cell proliferation, DNA methylation status and the KEAP1/NRF2 pathway is an important focal point for our future work.

Appendices

7 Appendices:

7.1 Appendix 1: Database of pancreatic cancer patients used in this study.

Case	SURVIVAL (Days)	Censored	Age	Tumor size	Size (mm)	Tumor Grade	Gender	Lymph nodes	Keap1	Nuclear UHRF1
1	990	uncensored	< 60	NA	> 20	Moderate	Male	yes	Negative	3
2	23	uncensored	> 60	20	< 20	Well	Male	No	Negative	3
3	646	uncensored	> 60	20	< 20	Moderate	Female	No	Negative	0
4	357	uncensored	> 60	20	< 20	Poor	Male	yes	Negative	2
5	297	uncensored	> 60	30	> 20	Moderate	Male	yes	Negative	2
6	122	uncensored	< 60	28	> 20	Moderate	Male	yes	Negative	2
7	1171	uncensored	< 60	19	< 20	Poor	Male	yes	Negative	0
8	923	uncensored	> 60	20	< 20	Well	Female	No	Positive	0
9	2108	uncensored	> 60	20	< 20	Moderate	Male	No	Negative	1
10	2452	uncensored	> 60	19	< 20	Moderate	Female	No	Negative	1
11	356	uncensored	> 60	3	< 20	Moderate	Female	yes	Negative	1
12	279	uncensored	< 60	25	> 20	Moderate	Male	yes	Positive	1
13	98	uncensored	> 60	38	> 20	Moderate	Female	yes	Positive	2
14	127	uncensored	< 60	50	> 20	Moderate	Female	yes	NA	0
15	792	uncensored	> 60	19	< 20	Moderate	Male	yes	Negative	2
16	525	uncensored	< 60	25	> 20	Moderate	Male	yes	Negative	0
17	315	uncensored	> 60	35	> 20	Well	Male	NA	Negative	2
18	9	uncensored	> 60	NA	> 20	Poor	Female	yes	Positive	2
19	1239	uncensored	> 60	40	> 20	Moderate	Female	yes	Positive	0
20	288	uncensored	< 60	15	< 20	Moderate	Female	yes	Positive	0
21	247	uncensored	> 60	22	> 20	Poor	Male	yes	Negative	3
22	1308	uncensored	> 60	30	> 20	Moderate	Male	No	Positive	2
23	138	uncensored	> 60	40	> 20	Moderate	Female	No	Negative	1
24	489	uncensored	< 60	65	> 20	Moderate	Female	No	Negative	3
25	338	uncensored	> 60	70	> 20	Well	Female	No	Positive	2
26	756	uncensored	> 60	50	> 20	Moderate	Male	NA	Negative	3
27	153	uncensored	< 60	26	> 20	Poor	Male	yes	Negative	1
28	463	uncensored	> 60	30	> 20	Poor	Male	yes	Positive	2
29	1114	uncensored	< 60	25	> 20	Poor	Male	yes	Negative	2
30	1463	uncensored	> 60	35	> 20	Moderate	Female	yes	Positive	3
31	2442	uncensored	< 60	25	> 20	Well	Male	yes	Negative	1
32	367	uncensored	> 60	12	< 20	Poor	Female	No	Negative	2
33	27	uncensored	> 60	70	> 20	Poor	Male	yes	Negative	3
34	505	uncensored	> 60	30	> 20	Poor	Male	yes	Negative	2
35	31	uncensored	> 60	37	> 20	Moderate	Female	yes	Positive	0

36	438	uncensored	> 60	17	< 20	Moderate	Male	No	Negative	0
37	444	uncensored	> 60	50	> 20	Poor	Male	yes	Negative	2
38	240	uncensored	> 60	35	> 20	Moderate	Female	yes	Negative	1
39	390	uncensored	< 60	25	> 20	Moderate	Male	yes	Negative	3
40	2698	Censored	< 60		> 20	Moderate	Female	yes	Negative	1
41	158	uncensored	> 60	30	> 20	Poor	Female	yes	Negative	3
42	853	uncensored	> 60	35	> 20	Moderate	Male	yes	Negative	3
43	156	uncensored	< 60	40	> 20	Poor	Male	yes	Negative	3
44	194	uncensored	> 60	30	> 20	Poor	Male	yes	Positive	3
45	480	uncensored	> 60	20	< 20	Moderate	Male	yes	Negative	3
46	647	uncensored	< 60	20	< 20	Moderate	Male	yes	Negative	1
47	314	uncensored	> 60	70	> 20	Poor	Female	yes	Negative	0
48	1704	Censored	> 60	15	< 20	Poor	Male	No	Positive	3
49	433	uncensored	> 60	21	> 20	Well	Female	yes	Negative	3
50	825	uncensored	> 60	25	> 20	Poor	Female	yes	Negative	3
51	688	uncensored	> 60	20	< 20	Well	Female	yes	Positive	1
52	1495	uncensored	< 60	9	< 20	Moderate	Male	yes	Negative	1
53	317	uncensored	> 60	35	> 20	Well	Male	No	Negative	2
54	25	uncensored	> 60	38	> 20	Moderate	Male	yes	Negative	3
55	471	uncensored	< 60	30	> 20	Moderate	Male	yes	Positive	1
56	280	uncensored	> 60	NA	> 20	Poor	Female	yes	Negative	2
57	209	uncensored	> 60	20	< 20	Poor	Male	yes	Positive	0
58	175	uncensored	> 60	20	< 20	Poor	Male	yes	Negative	2
59	167	uncensored	< 60	65	> 20	Poor	Male	yes	Positive	2
60	217	uncensored	< 60	22	> 20	Moderate	Male	yes	Positive	0
61	1057	uncensored	< 60	8	< 20	Well	Female	yes	Positive	1
62	150	uncensored	> 60	30	> 20	Moderate	Male	yes	Negative	3
63	810	uncensored	> 60	25	> 20	Moderate	Female	yes	Negative	1
64	651	uncensored	> 60	45	> 20	Poor	Female	yes	Positive	1
65	88	uncensored	> 60	60	> 20	Moderate	Male	yes	Negative	3
66	734	uncensored	> 60	NA	> 20	Poor	Male	No	Negative	1
67	337	uncensored	> 60	25	> 20	Moderate	Female	yes	Negative	3
68	98	uncensored	> 60	37	> 20	Moderate	Female	yes	Negative	2
69	242	uncensored	> 60	30	> 20	Moderate	Male	yes	Negative	3
70	196	uncensored	> 60	NA	> 20	Moderate	Male	yes	Negative	0
71	768	uncensored	> 60	50	> 20	Moderate	Male	yes	Negative	3
72	432	uncensored	> 60	20	< 20	Moderate	Female	yes	Positive	0
73	492	uncensored	> 60	30	> 20	Poor	Female	yes	Positive	2
74	222	uncensored	> 60	30	> 20	Moderate	Female	yes	Positive	3
75	187	uncensored	> 60	30	> 20	Moderate	Male	yes	Positive	1
76	18	uncensored	> 60	40	> 20	Moderate	Male	yes	Negative	2

77	340	uncensored	> 60	35	> 20	Moderate	Male	No	Negative	2
78	423	uncensored	> 60	33	> 20	Moderate	Male	yes	Negative	1
79	176	uncensored	> 60	45	> 20	Moderate	Male	yes	Negative	2
80	291	uncensored	> 60	20	< 20	Moderate	Female	yes	Negative	2
81	1934	uncensored	> 60	45	> 20	Moderate	Female	yes	Positive	1
82	1034	uncensored	> 60	35	> 20	Moderate	Female	yes	Positive	1
83	382	uncensored	> 60	25	> 20	Well	Male	yes	Negative	3
84	674	uncensored	> 60	30	> 20	Moderate	Male	yes	NA	1
85	466	uncensored	> 60	33	> 20	Poor	Male	NA	Negative	2
86	1059	uncensored	< 60	15	< 20	Moderate	Female	yes	Negative	2
87	776	uncensored	> 60	38	> 20	Well	Female	yes	Positive	2
88	103	uncensored	> 60	40	> 20	Poor	Male	NA	Negative	1
89	12	uncensored	> 60	30	> 20	Well	Male	NA	Negative	1
90	310	uncensored	> 60	22	> 20	Poor	Female	NA	Negative	1
91	807	uncensored	> 60	35	> 20	Poor	Male	No	Negative	2
92	850	uncensored	> 60	20	< 20	Moderate	Female	yes	Positive	2
93	400	uncensored	> 60	15	< 20	Moderate	Male	yes	Negative	2
94	1824	Censored	> 60	30	> 20	Moderate	Male	yes	Positive	0
95	1221	uncensored	> 60	40	> 20	Well	Female	yes	Negative	3
96	2426	Censored	> 60	20	< 20	Well	Male	No	Negative	2
97	531	uncensored	> 60	22	> 20	Well	Male	yes	NA	2
98	299	uncensored	> 60	27	> 20	Moderate	Male	yes	Positive	0
99	122	uncensored	> 60	30	> 20	Poor	Female	yes	Negative	2
100	300	uncensored	< 60	30	> 20	Well	Male	yes	Positive	2
101	460	uncensored	> 60	40	> 20	Moderate	Female	yes	Negative	2
102	810	uncensored	> 60	35	> 20	Moderate	Female	No	Negative	3
103	289	uncensored	< 60	28	> 20	Well	Female	yes	Negative	2
104	376	uncensored	> 60	35	> 20	Moderate	Male	No	Positive	1
105	1470	Censored	> 60	50	> 20	Moderate	Male	yes	Negative	2
106	15	uncensored	> 60	50	> 20	Poor	Female	yes	Negative	2
107	303	uncensored	> 60	45	> 20	Moderate	Female	yes	Negative	1
108	197	uncensored	> 60	35	> 20	Moderate	Male	yes	Negative	2
109	259	Censored	< 60	30	> 20	Moderate	Female	No	Negative	3
110	475	uncensored	> 60	24	> 20	Well	Female	yes	Negative	1
111	131	uncensored	> 60	25	> 20	Poor	Male	yes	Negative	2
112	340	uncensored	> 60	50	> 20	Moderate	Female	yes	Negative	2
113	903	uncensored	> 60	17	< 20	Moderate	Female	yes	Negative	0
114	575	uncensored	< 60	40	> 20	Moderate	Male	yes	Negative	1
115	253	uncensored	> 60	65	> 20	Poor	Male	yes	Negative	2
116	216	uncensored	> 60	43	> 20	Moderate	Male	yes	Positive	0
117	309	uncensored	> 60	40	> 20	Moderate	Female	yes	NA	3

118	86	uncensored	> 60	40	> 20	Poor	Female	yes	Negative	1
119	367	uncensored	> 60	33	> 20	Well	Female	yes	Negative	2
120	584	Censored	> 60	40	> 20	Moderate	Male	yes	Negative	3
121	100	uncensored	> 60	45	> 20	Poor	Female	yes	Negative	2
122	240	uncensored	> 60	45	> 20	Poor	Male	yes	Negative	1
123	110	Censored	> 60	25	> 20	Poor	Female	yes	Negative	1
124	389	uncensored	< 60	27	> 20	Poor	Female	yes	Negative	2
125	94	uncensored	> 60	45	> 20	Poor	Male	yes	Negative	2
126	310	uncensored	> 60	30	> 20	Moderate	Male	yes	Negative	1
127	76	uncensored	> 60	38	> 20	Poor	Male	yes	Negative	3
128	33	uncensored	> 60	6	< 20	Poor	Male	yes	Negative	2
129	418	uncensored	> 60	30	> 20	Moderate	Female	yes	NA	1
130	262	uncensored	> 60	30	> 20	Poor	Male	yes	NA	1
131	1824	Censored	> 60	30	> 20	Moderate	Male	yes	NA	1
132	645	Censored	> 60	30	> 20	Poor	Female	yes	NA	2

7.2 Appendix 2: Primer design

Primer designs of the targeted sequence in the promoter regions of the *LINE1, RASSF1, CDKN2A, KEAP1*a and *KEAP1*b generated using primer assay design from Qiagen.

LINE-1

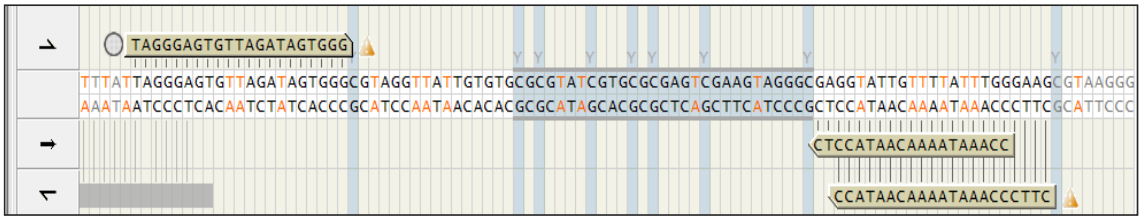

RASSF-1

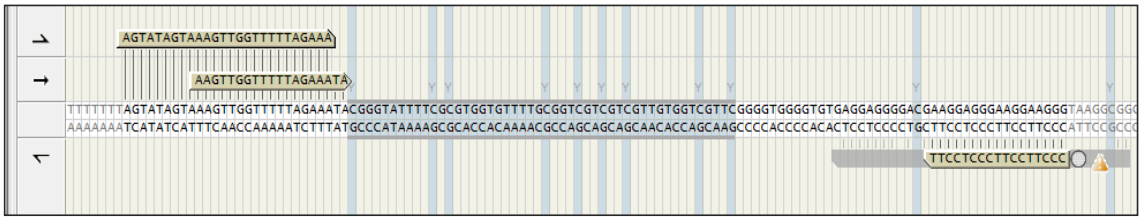

CDKN2A

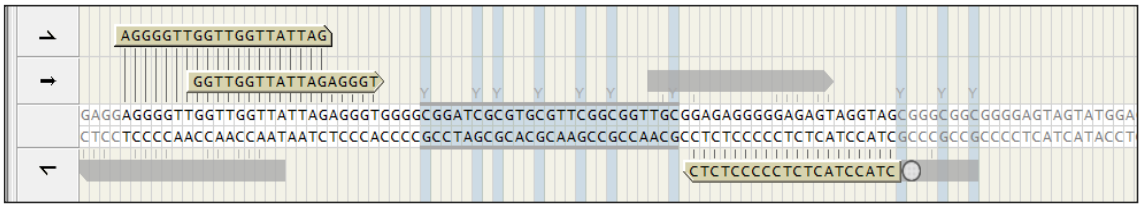

KEAP1 a

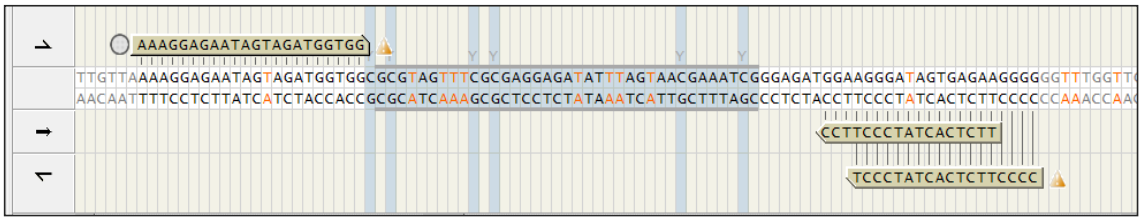

KEAP1 b

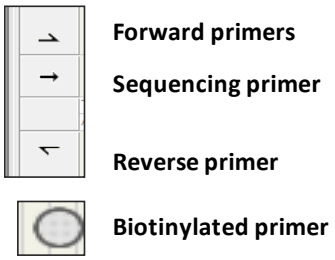

7.3 Appendix 3 :Pyrogram of *LINE-1, RASSF1* and *Alu*-V.

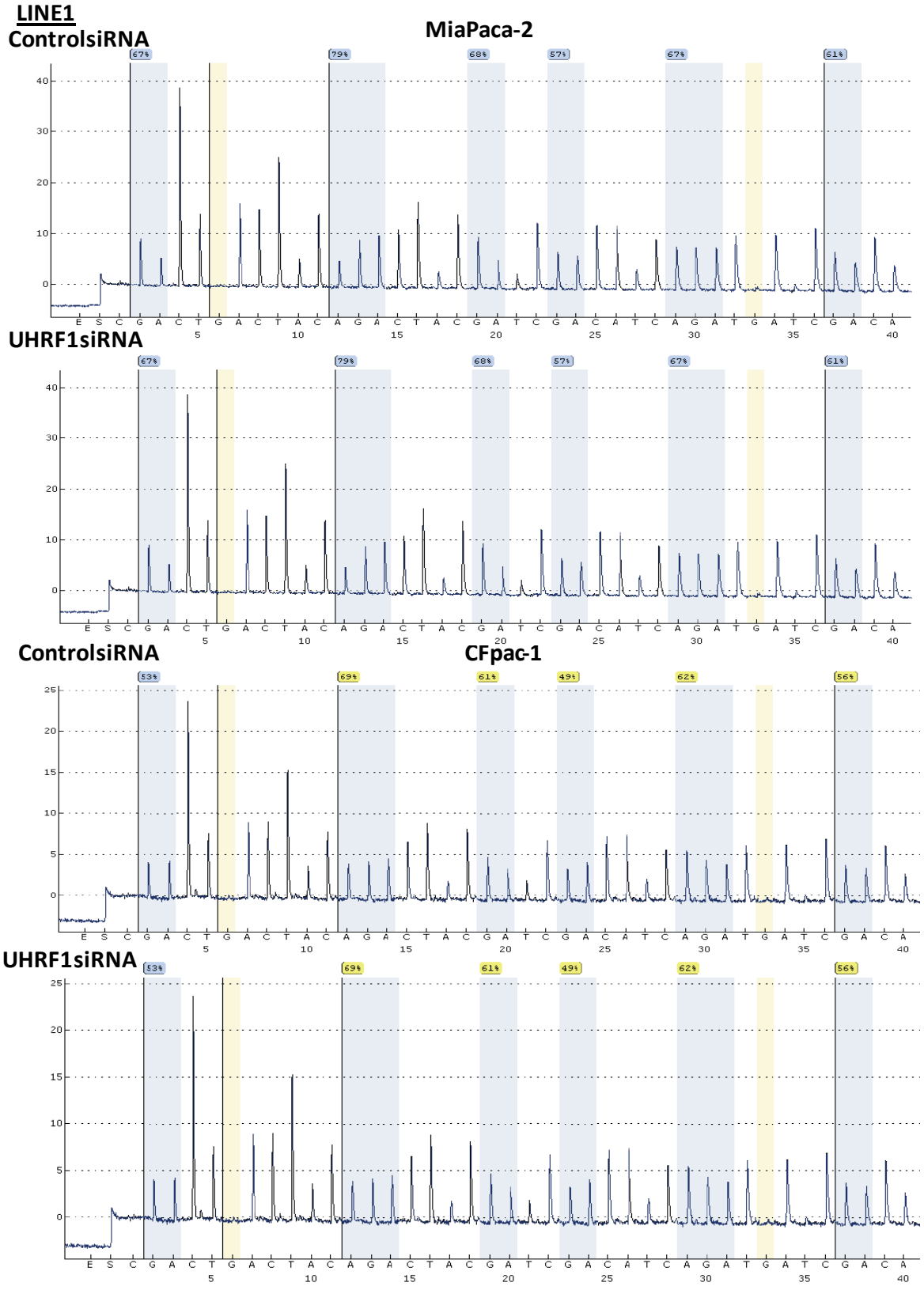

Suit-2

LINE-1

Control siRNA

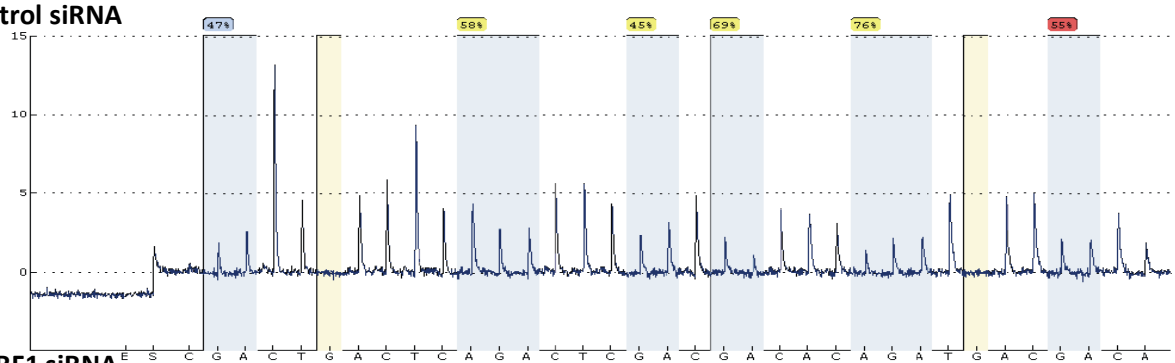

UHRF1 siRNA

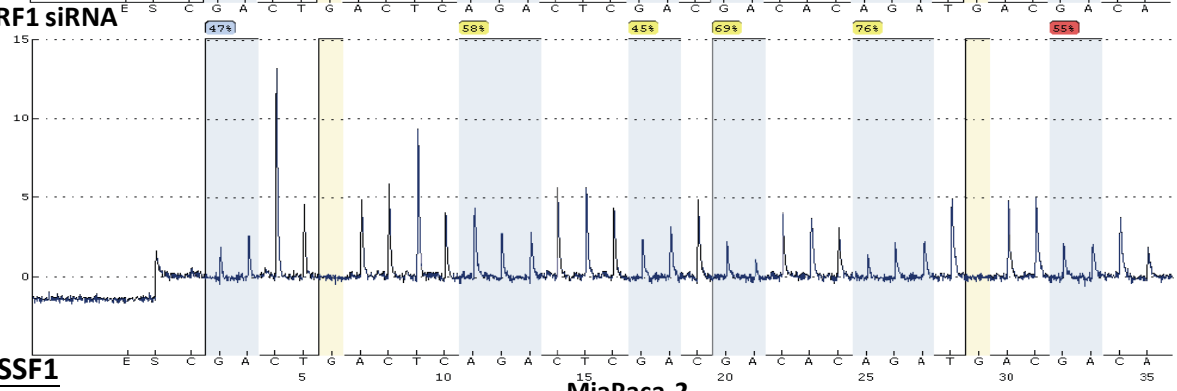

RASSF1

MiaPaca-2

Control siRNA

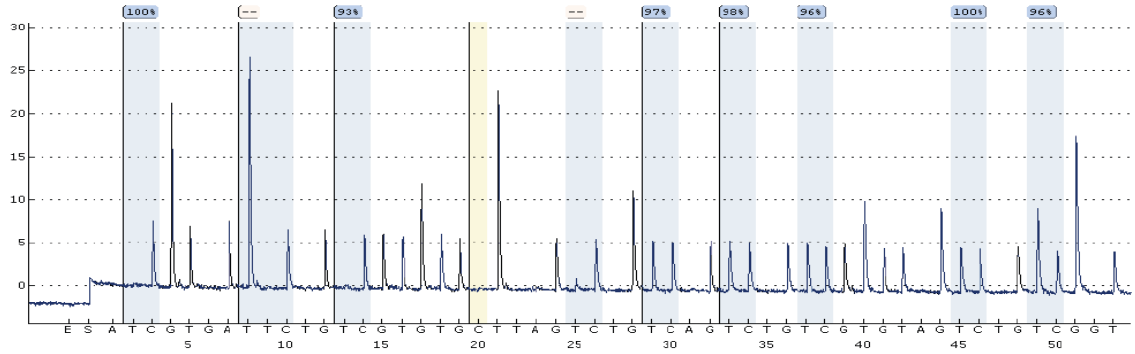

UHRF1 siRNA

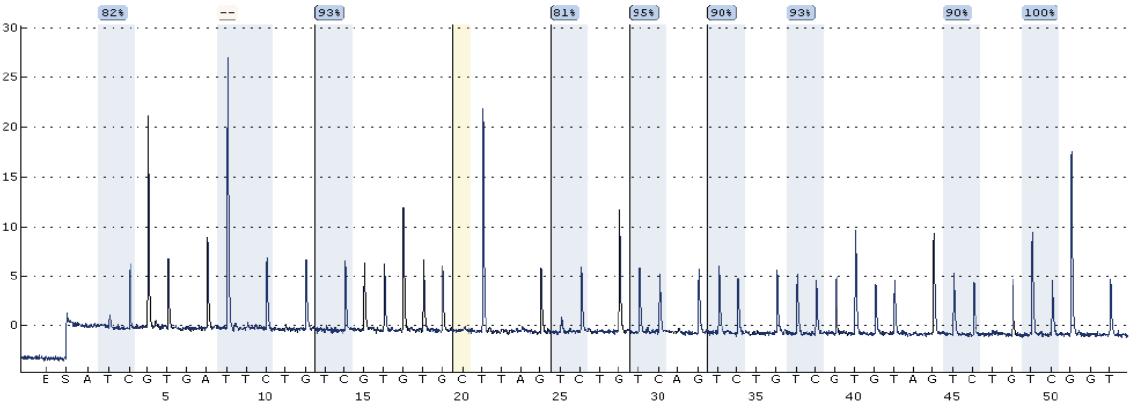

RASSF1

CFpac-1

Control siRNA

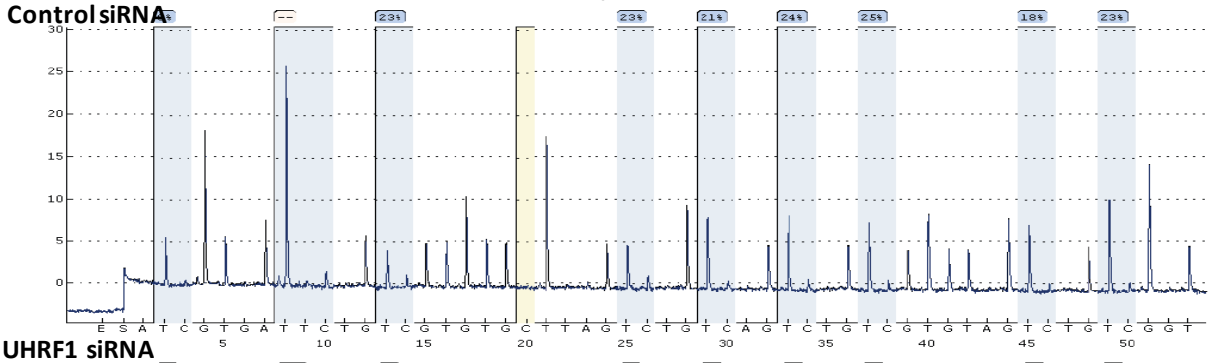

UHRF1 siRNA

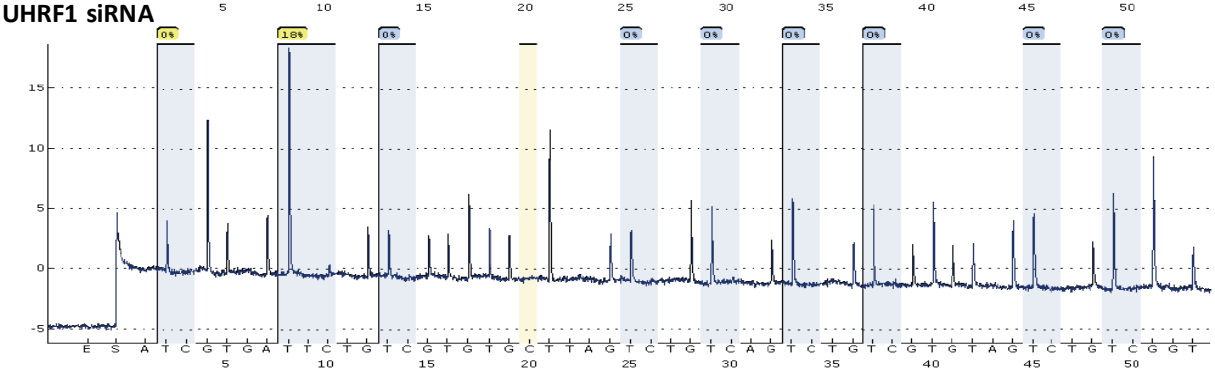

Control siRNA

Suit-2

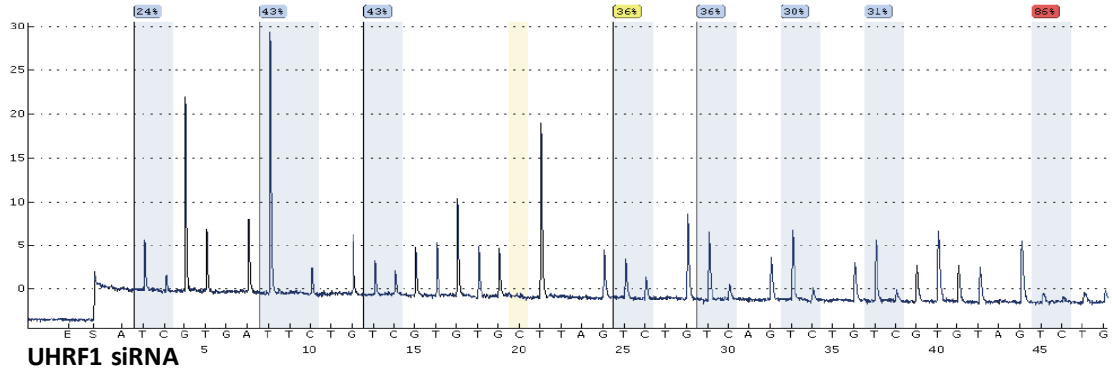

UHRF1 siRNA

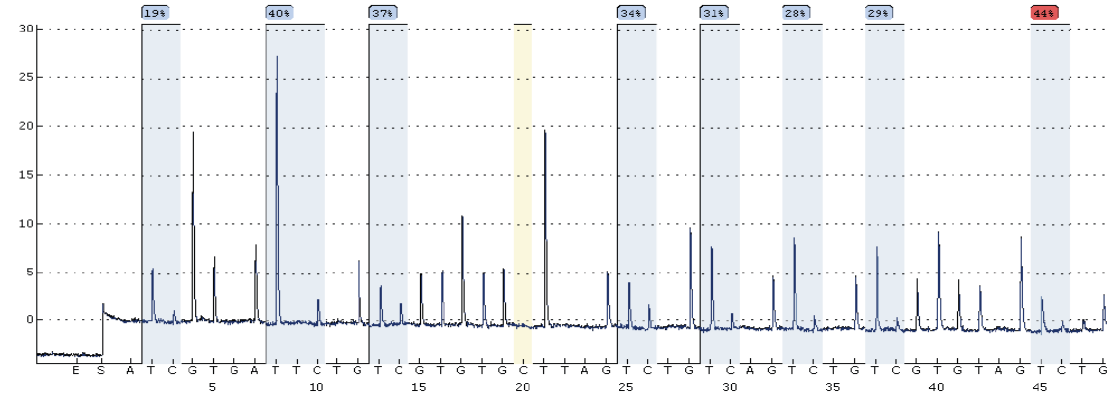

Alu-PV **MiaPaca-2**

ControlsiRNA

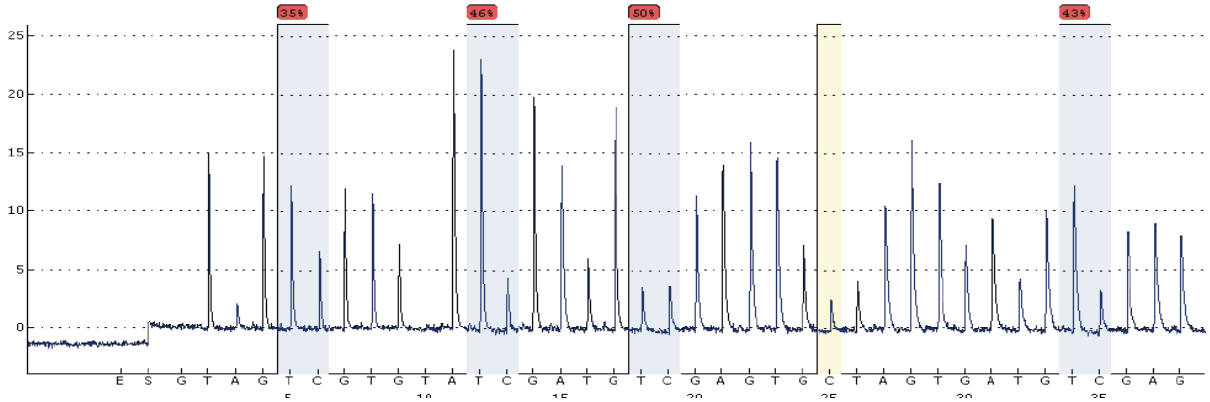

UHRF1 siRNA

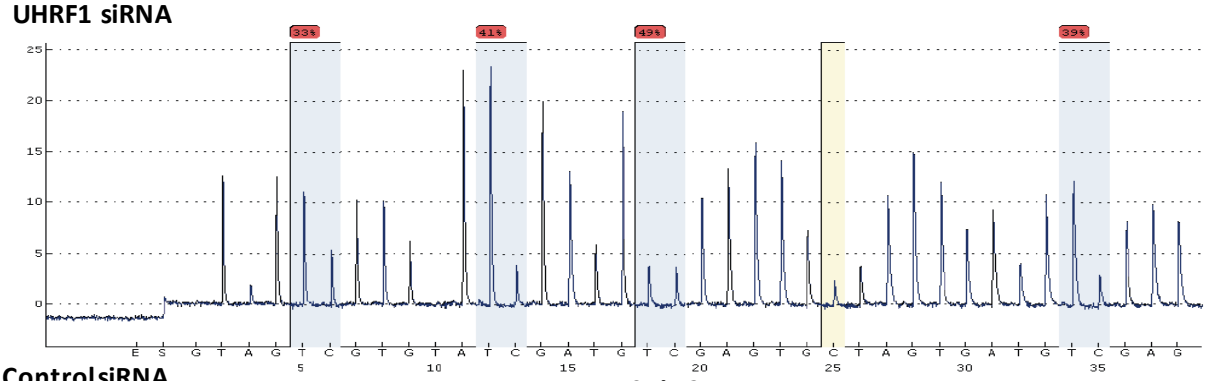

ControlsiRNA **Suit-2**

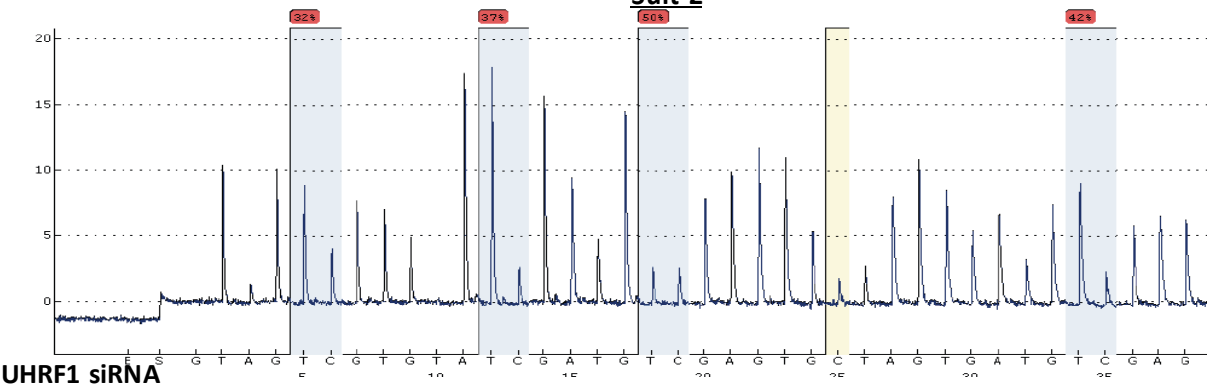

UHRF1 siRNA

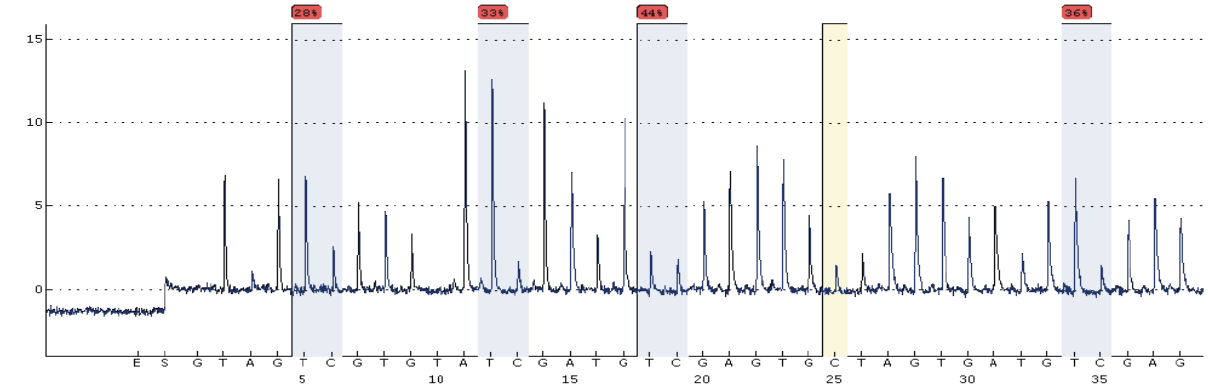

References

References:

1. Hahn, W.C., et al., *Creation of human tumour cells with defined genetic elements.* Nature, 1999. **400**(6743): p. 464-8.
2. Hanahan, D. and R.A. Weinberg, *The hallmarks of cancer.* Cell, 2000. **100**(1): p. 57-70.
3. Colotta, F., et al., *Cancer-related inflammation, the seventh hallmark of cancer: links to genetic instability.* Carcinogenesis, 2009. **30**(7): p. 1073-81.
4. Hanahan, D. and R.A. Weinberg, *Hallmarks of cancer: the next generation.* Cell, 2011. **144**(5): p. 646-74.
5. Yachida, S., et al., *Distant metastasis occurs late during the genetic evolution of pancreatic cancer.* Nature, 2010. **467**(7319): p. 1114-7.
6. Olson, S.H. and R.C. Kurtz, *Epidemiology of pancreatic cancer and the role of family history.* J Surg Oncol, 2012. **107**(1): p. 1-7.
7. Luttges, J., *[What's new? The 2010 WHO classification for tumours of the pancreas].* Pathologe. **32 Suppl 2**: p. 332-6.
8. Jones, S., et al., *Core signaling pathways in human pancreatic cancers revealed by global genomic analyses.* Science, 2008. **321**(5897): p. 1801-6.
9. Cunningham, D., et al., *Phase III randomized comparison of gemcitabine versus gemcitabine plus capecitabine in patients with advanced pancreatic cancer.* J Clin Oncol, 2009. **27**(33): p. 5513-8.
10. Valle, J.W., et al., *Optimal duration and timing of adjuvant chemotherapy after definitive surgery for ductal adenocarcinoma of the pancreas: ongoing lessons from the ESPAC-3 study.* J Clin Oncol, 2014. **32**(6): p. 504-12.
11. Neoptolemos, J.P., et al., *A randomized trial of chemoradiotherapy and chemotherapy after resection of pancreatic cancer.* N Engl J Med, 2004. **350**(12): p. 1200-10.
12. Chen, M.J., et al., *Caffeic acid phenethyl ester induces apoptosis of human pancreatic cancer cells involving caspase and mitochondrial dysfunction.* Pancreatology, 2008. **8**(6): p. 566-76.
13. Stathis, A. and M.J. Moore, *Advanced pancreatic carcinoma: current treatment and future challenges.* Nat Rev Clin Oncol, 2010. **7**(3): p. 163-72.
14. Risch, H.A., *Etiology of pancreatic cancer, with a hypothesis concerning the role of N-nitroso compounds and excess gastric acidity.* J Natl Cancer Inst, 2003. **95**(13): p. 948-60.
15. Wang, F., et al., *The relationship between diabetes and pancreatic cancer.* Mol Cancer, 2003. **2**: p. 4.
16. Wolfgang, C.L., et al., *Recent progress in pancreatic cancer.* CA Cancer J Clin, 2013. **63**(5): p. 318-48.
17. Bowles, M.J. and I.S. Benjamin, *ABC of the upper gastrointestinal tract: Cancer of the stomach and pancreas.* BMJ, 2001. **323**(7326): p. 1413-6.
18. Blattman, J.N. and P.D. Greenberg, *Cancer immunotherapy: a treatment for the masses.* Science, 2004. **305**(5681): p. 200-5.
19. DeVita, V.T., Jr. and S.A. Rosenberg, *Two hundred years of cancer research.* N Engl J Med, 2012. **366**(23): p. 2207-14.
20. Ghosal, G. and J. Chen, *DNA damage tolerance: a double-edged sword guarding the genome.* Transl Cancer Res, 2013. **2**(3): p. 107-129.

21. Conroy, T., et al., *FOLFIRINOX versus gemcitabine for metastatic pancreatic cancer.* N Engl J Med, 2011. **364**(19): p. 1817-25.
22. Costello, E., W. Greenhalf, and J.P. Neoptolemos, *New biomarkers and targets in pancreatic cancer and their application to treatment.* Nat Rev Gastroenterol Hepatol, 2012. **9**(8): p. 435-44.
23. Hidalgo, M., *Pancreatic cancer.* N Engl J Med, 2010. **362**(17): p. 1605-17.
24. Evans, A. and E. Costello, *The role of inflammatory cells in fostering pancreatic cancer cell growth and invasion.* Front Physiol, 2012. **3**: p. 270.
25. Campbell, P.J., et al., *The patterns and dynamics of genomic instability in metastatic pancreatic cancer.* Nature, 2010. **467**(7319): p. 1109-13.
26. Scarlett, C.J., et al., *Precursor lesions in pancreatic cancer: morphological and molecular pathology.* Pathology, 2011. **43**(3): p. 183-200.
27. Iovanna, J., et al., *Current knowledge on pancreatic cancer.* Front Oncol, 2012. **2**: p. 6.
28. Laghi, L., et al., *Common occurrence of multiple K-RAS mutations in pancreatic cancers with associated precursor lesions and in biliary cancers.* Oncogene, 2002. **21**(27): p. 4301-6.
29. Cowan, R.W. and A. Maitra, *Genetic progression of pancreatic cancer.* Cancer J, 2014. **20**(1): p. 80-4.
30. Huang, C., et al., *Oncogenesis and the clinical significance of K-ras in pancreatic adenocarcinoma.* Asian Pac J Cancer Prev. **14**(5): p. 2699-701.
31. Berndt, N., A.D. Hamilton, and S.M. Sebti, *Targeting protein prenylation for cancer therapy.* Nat Rev Cancer, 2011. **11**(11): p. 775-91.
32. McCleary-Wheeler, A.L., et al., *Insights into the epigenetic mechanisms controlling pancreatic carcinogenesis.* Cancer Lett, 2013. **328**(2): p. 212-21.
33. Schutte, M., et al., *Abrogation of the Rb/p16 tumor-suppressive pathway in virtually all pancreatic carcinomas.* Cancer Res, 1997. **57**(15): p. 3126-30.
34. Sato, N., et al., *Discovery of novel targets for aberrant methylation in pancreatic carcinoma using high-throughput microarrays.* Cancer Res, 2003. **63**(13): p. 3735-42.
35. Sharif, J. and H. Koseki, *Recruitment of Dnmt1 roles of the SRA protein Np95 (Uhrf1) and other factors.* Prog Mol Biol Transl Sci, 2011. **101**: p. 289-310.
36. Mohan, K.N. and J.R. Chaillet, *Cell and molecular biology of DNA methyltransferase 1.* Int Rev Cell Mol Biol, 2013. **306**: p. 1-42.
37. Crnogorac-Jurcevic, T., et al., *Proteomic analysis of chronic pancreatitis and pancreatic adenocarcinoma.* Gastroenterology, 2005. **129**(5): p. 1454-63.
38. Jenkins, Y., et al., *Critical role of the ubiquitin ligase activity of UHRF1, a nuclear RING finger protein, in tumor cell growth.* Mol Biol Cell, 2005. **16**(12): p. 5621-9.
39. Hopfner, R., et al., *ICBP90, a novel human CCAAT binding protein, involved in the regulation of topoisomerase IIalpha expression.* Cancer Res, 2000. **60**(1): p. 121-8.
40. Bronner, C., et al., *The UHRF family: oncogenes that are drugable targets for cancer therapy in the near future?* Pharmacol Ther, 2007. **115**(3): p. 419-34.
41. Liang, C., et al., *Identification of UHRF1/2 as new N-methylpurine DNA glycosylase-interacting proteins.* Biochem Biophys Res Commun, 2013. **433**(4): p. 415-9.

42. Arita, K., et al., *Recognition of modification status on a histone H3 tail by linked histone reader modules of the epigenetic regulator UHRF1.* Proc Natl Acad Sci U S A, 2012. **109**(32): p. 12950-5.
43. Zhang, J., et al., *S phase-dependent interaction with DNMT1 dictates the role of UHRF1 but not UHRF2 in DNA methylation maintenance.* Cell Res, 2011. **21**(12): p. 1723-39.
44. Frauer, C., et al., *Recognition of 5-hydroxymethylcytosine by the Uhrf1 SRA domain.* PLoS One, 2011. **6**(6): p. e21306.
45. Citterio, E., et al., *Np95 is a histone-binding protein endowed with ubiquitin ligase activity.* Mol Cell Biol, 2004. **24**(6): p. 2526-35.
46. Kim, J.K., et al., *UHRF1 binds G9a and participates in p21 transcriptional regulation in mammalian cells.* Nucleic Acids Res, 2009. **37**(2): p. 493-505.
47. Lallous, N., et al., *The PHD finger of human UHRF1 reveals a new subgroup of unmethylated histone H3 tail readers.* PLoS One, 2011. **6**(11): p. e27599.
48. Rajakumara, E., et al., *PHD finger recognition of unmodified histone H3R2 links UHRF1 to regulation of euchromatic gene expression.* Mol Cell, 2011. **43**(2): p. 275-84.
49. Xie, S., J. Jakoncic, and C. Qian, *UHRF1 double tudor domain and the adjacent PHD finger act together to recognize K9me3-containing histone H3 tail.* J Mol Biol, 2012. **415**(2): p. 318-28.
50. Hashimoto, H., et al., *UHRF1, a modular multi-domain protein, regulates replication-coupled crosstalk between DNA methylation and histone modifications.* Epigenetics, 2009. **4**(1): p. 8-14.
51. Felle, M., et al., *The USP7/Dnmt1 complex stimulates the DNA methylation activity of Dnmt1 and regulates the stability of UHRF1.* Nucleic Acids Res, 2011. **39**(19): p. 8355-65.
52. Ma, H., et al., *M phase phosphorylation of the epigenetic regulator UHRF1 regulates its physical association with the deubiquitylase USP7 and stability.* Proc Natl Acad Sci U S A, 2012. **109**(13): p. 4828-33.
53. Chen, H., et al., *DNA damage regulates UHRF1 stability via the SCF(beta-TrCP) E3 ligase.* Mol Cell Biol, 2013. **33**(6): p. 1139-48.
54. Muto, M., et al., *The characterization of the monoclonal antibody Th-10a, specific for a nuclear protein appearing in the S phase of the cell cycle in normal thymocytes and its unregulated expression in lymphoma cell lines.* Cell Prolif, 1995. **28**(12): p. 645-57.
55. Mousli, M., et al., *ICBP90 belongs to a new family of proteins with an expression that is deregulated in cancer cells.* Br J Cancer, 2003. **89**(1): p. 120-7.
56. Unoki, M., et al., *UHRF1 is a novel molecular marker for diagnosis and the prognosis of bladder cancer.* Br J Cancer, 2009. **101**(1): p. 98-105.
57. Yang, G.L., et al., *UHRF1 is associated with tumor recurrence in non-muscle-invasive bladder cancer.* Med Oncol, 2012. **29**(2): p. 842-7.
58. Yan, F., et al., *Inhibition effect of siRNA-downregulated UHRF1 on breast cancer growth.* Cancer Biother Radiopharm, 2011. **26**(2): p. 183-9.
59. Li, X., et al., *UHRF1 confers radioresistance to human breast cancer cells.* Int J Radiat Biol, 2011. **87**(3): p. 263-73.
60. Sabatino, L., et al., *UHRF1 coordinates peroxisome proliferator activated receptor gamma (PPARG) epigenetic silencing and mediates colorectal cancer progression.* Oncogene, 2012. **31**(49): p. 5061-72.

61. Wang, F., et al., *UHRF1 promotes cell growth and metastasis through repression of p16(ink(4)a) in colorectal cancer.* Ann Surg Oncol, 2012. **19**(8): p. 2753-62.
62. Babbio, F., et al., *The SRA protein UHRF1 promotes epigenetic crosstalks and is involved in prostate cancer progression.* Oncogene, 2012. **31**(46): p. 4878-87.
63. Unoki, M., et al., *UHRF1 is a novel diagnostic marker of lung cancer.* Br J Cancer, 2010. **103**(2): p. 217-22.
64. Daskalos, A., et al., *UHRF1-mediated tumor suppressor gene inactivation in nonsmall cell lung cancer.* Cancer, 2011. **117**(5): p. 1027-37.
65. Mudbhary, R., et al., *UHRF1 Overexpression Drives DNA Hypomethylation and Hepatocellular Carcinoma.* Cancer Cell, 2014. **25**(2): p. 196-209.
66. Lecker, S.H., A.L. Goldberg, and W.E. Mitch, *Protein degradation by the ubiquitin-proteasome pathway in normal and disease states.* J Am Soc Nephrol, 2006. **17**(7): p. 1807-19.
67. Nurse, P., *Regulation of the eukaryotic cell cycle.* Eur J Cancer, 1997. **33**(7): p. 1002-4.
68. Lim, S. and P. Kaldis, *Cdks, cyclins and CKIs: roles beyond cell cycle regulation.* Development, 2013. **140**(15): p. 3079-93.
69. Bertoli, C., J.M. Skotheim, and R.A. de Bruin, *Control of cell cycle transcription during G1 and S phases.* Nat Rev Mol Cell Biol, 2013. **14**(8): p. 518-28.
70. Kim, J.K. and J.A. Diehl, *Nuclear cyclin D1: an oncogenic driver in human cancer.* J Cell Physiol, 2009. **220**(2): p. 292-6.
71. Androic, I., et al., *Targeting cyclin B1 inhibits proliferation and sensitizes breast cancer cells to taxol.* BMC Cancer, 2008. **8**: p. 391.
72. Xie, X.H., et al., *Loss of Cyclin B1 followed by downregulation of Cyclin A/Cdk2, apoptosis and antiproliferation in Hela cell line.* Int J Cancer, 2005. **116**(4): p. 520-5.
73. Mazumder, S., et al., *Proteolytic cleavage of cyclin E leads to inactivation of associated kinase activity and amplification of apoptosis in hematopoietic cells.* Mol Cell Biol, 2002. **22**(7): p. 2398-409.
74. Kerr, J.F., A.H. Wyllie, and A.R. Currie, *Apoptosis: a basic biological phenomenon with wide-ranging implications in tissue kinetics.* Br J Cancer, 1972. **26**(4): p. 239-57.
75. Cryns, V.L., et al., *Specific cleavage of alpha-fodrin during Fas- and tumor necrosis factor-induced apoptosis is mediated by an interleukin-1beta-converting enzyme/Ced-3 protease distinct from the poly(ADP-ribose) polymerase protease.* J Biol Chem, 1996. **271**(49): p. 31277-82.
76. Orth, K., et al., *The CED-3/ICE-like protease Mch2 is activated during apoptosis and cleaves the death substrate lamin A.* J Biol Chem, 1996. **271**(28): p. 16443-6.
77. Mashima, T., et al., *Actin cleavage by CPP-32/apopain during the development of apoptosis.* Oncogene, 1997. **14**(9): p. 1007-12.
78. Logue, S.E. and S.J. Martin, *Caspase activation cascades in apoptosis.* Biochem Soc Trans, 2008. **36**(Pt 1): p. 1-9.
79. Tien, A.L., et al., *UHRF1 depletion causes a G2/M arrest, activation of DNA damage response and apoptosis.* Biochem J, 2011. **435**(1): p. 175-85.
80. Arima, Y., et al., *Down-regulation of nuclear protein ICBP90 by p53/p21Cip1/WAF1-dependent DNA-damage checkpoint signals contributes to cell cycle arrest at G1/S transition.* Genes Cells, 2004. **9**(2): p. 131-42.

81. Hervouet, E., et al., *Kinetics of DNA methylation inheritance by the Dnmt1-including complexes during the cell cycle.* Cell Div, 2012. **7**: p. 5.
82. Jones, P.A., *Functions of DNA methylation: islands, start sites, gene bodies and beyond.* Nat Rev Genet, 2012. **13**(7): p. 484-92.
83. Herman, J.G. and S.B. Baylin, *Gene silencing in cancer in association with promoter hypermethylation.* N Engl J Med, 2003. **349**(21): p. 2042-54.
84. Robertson, K.D., *DNA methylation and human disease.* Nat Rev Genet, 2005. **6**(8): p. 597-610.
85. Brown, S.E., et al., *Variations in DNA methylation patterns during the cell cycle of HeLa cells.* Epigenetics, 2007. **2**(1): p. 54-65.
86. Kanwal, R. and S. Gupta, *Epigenetic modifications in cancer.* Clin Genet, 2012. **81**(4): p. 303-11.
87. Sharif, J., et al., *The SRA protein Np95 mediates epigenetic inheritance by recruiting Dnmt1 to methylated DNA.* Nature, 2007. **450**(7171): p. 908-12.
88. Arita, K., et al., *Recognition of hemi-methylated DNA by the SRA protein UHRF1 by a base-flipping mechanism.* Nature, 2008. **455**(7214): p. 818-21.
89. Kulis, M. and M. Esteller, *DNA methylation and cancer.* Adv Genet, 2010. **70**: p. 27-56.
90. Wilson, A.S., B.E. Power, and P.L. Molloy, *DNA hypomethylation and human diseases.* Biochim Biophys Acta, 2007. **1775**(1): p. 138-62.
91. Sharma, S., T.K. Kelly, and P.A. Jones, *Epigenetics in cancer.* Carcinogenesis, 2009. **31**(1): p. 27-36.
92. Ohtsubo, K., et al., *Abnormalities of tumor suppressor gene p16 in pancreatic carcinoma: immunohistochemical and genetic findings compared with clinicopathological parameters.* J Gastroenterol, 2003. **38**(7): p. 663-71.
93. Dammann, R., et al., *Frequent RASSF1A promoter hypermethylation and K-ras mutations in pancreatic carcinoma.* Oncogene, 2003. **22**(24): p. 3806-12.
94. Matthaios, D., et al., *Molecular pathogenesis of pancreatic cancer and clinical perspectives.* Oncology, 2011. **81**(3-4): p. 259-72.
95. Patel, K., et al., *Targeting of 5-aza-2'-deoxycytidine residues by chromatin-associated DNMT1 induces proteasomal degradation of the free enzyme.* Nucleic Acids Res, 2010. **38**(13): p. 4313-24.
96. Mossman, D., K.T. Kim, and R.J. Scott, *Demethylation by 5-aza-2'-deoxycytidine in colorectal cancer cells targets genomic DNA whilst promoter CpG island methylation persists.* BMC Cancer, 2010. **10**: p. 366.
97. Dobosy, J.R., et al., *The expanding role of epigenetics in the development, diagnosis and treatment of prostate cancer and benign prostatic hyperplasia.* J Urol, 2007. **177**(3): p. 822-31.
98. Daniel, F.I., et al., *The role of epigenetic transcription repression and DNA methyltransferases in cancer.* Cancer, 2010. **117**(4): p. 677-87.
99. Shames, D.S., J.D. Minna, and A.F. Gazdar, *Methods for detecting DNA methylation in tumors: from bench to bedside.* Cancer Lett, 2007. **251**(2): p. 187-98.
100. Dupont, J.M., et al., *De novo quantitative bisulfite sequencing using the pyrosequencing technology.* Anal Biochem, 2004. **333**(1): p. 119-27.

101. Tost, J., H. El abdalaoui, and I.G. Gut, *Serial pyrosequencing for quantitative DNA methylation analysis.* Biotechniques, 2006. **40**(6): p. 721-2, 724, 726.
102. Tost, J. and I.G. Gut, *DNA methylation analysis by pyrosequencing.* Nat Protoc, 2007. **2**(9): p. 2265-75.
103. Weisenberger, D.J., et al., *Analysis of repetitive element DNA methylation by MethyLight.* Nucleic Acids Res, 2005. **33**(21): p. 6823-36.
104. Yang, A.S., et al., *A simple method for estimating global DNA methylation using bisulfite PCR of repetitive DNA elements.* Nucleic Acids Res, 2004. **32**(3): p. e38.
105. Chalitchagorn, K., et al., *Distinctive pattern of LINE-1 methylation level in normal tissues and the association with carcinogenesis.* Oncogene, 2004. **23**(54): p. 8841-6.
106. Beck, C.R., et al., *LINE-1 elements in structural variation and disease.* Annu Rev Genomics Hum Genet, 2011. **12**: p. 187-215.
107. Kazazian, H.H., Jr., *Mobile elements: drivers of genome evolution.* Science, 2004. **303**(5664): p. 1626-32.
108. Kolomietz, E., et al., *The role of Alu repeat clusters as mediators of recurrent chromosomal aberrations in tumors.* Genes Chromosomes Cancer, 2002. **35**(2): p. 97-112.
109. Perrin, D., et al., *Specific hypermethylation of LINE-1 elements during abnormal overgrowth and differentiation of human placenta.* Oncogene, 2007. **26**(17): p. 2518-24.
110. Florl, A.R., et al., *DNA methylation and expression of LINE-1 and HERV-K provirus sequences in urothelial and renal cell carcinomas.* Br J Cancer, 1999. **80**(9): p. 1312-21.
111. Di, J.Z., et al., *Association of hypomethylation of LINE-1 repetitive element in blood leukocyte DNA with an increased risk of hepatocellular carcinoma.* J Zhejiang Univ Sci B, 2011. **12**(10): p. 805-11.
112. Cho, Y.H., et al., *Aberrant promoter hypermethylation and genomic hypomethylation in tumor, adjacent normal tissues and blood from breast cancer patients.* Anticancer Res, 2010. **30**(7): p. 2489-96.
113. Dauksa, A., et al., *Whole blood DNA aberrant methylation in pancreatic adenocarcinoma shows association with the course of the disease: a pilot study.* PLoS One, 2012. **7**(5): p. e37509.
114. El-Naggar, A.K., et al., *Methylation, a major mechanism of p16/CDKN2 gene inactivation in head and neck squamous carcinoma.* Am J Pathol, 1997. **151**(6): p. 1767-74.
115. Matsuda, Y., et al., *p16(INK4) is inactivated by extensive CpG methylation in human hepatocellular carcinoma.* Gastroenterology, 1999. **116**(2): p. 394-400.
116. Tadokoro, H., et al., *Two distinct pathways of p16 gene inactivation in gallbladder cancer.* World J Gastroenterol, 2007. **13**(47): p. 6396-403.
117. Chan, J.J. and M. Katan, *PLCvarepsilon and the RASSF family in tumour suppression and other functions.* Adv Biol Regul, 2013. **53**(3): p. 258-79.
118. DeNicola, G.M., et al., *Oncogene-induced Nrf2 transcription promotes ROS detoxification and tumorigenesis.* Nature, 2011. **475**(7354): p. 106-9.
119. Bryan, H.K., et al., *The Nrf2 cell defence pathway: Keap1-dependent and -independent mechanisms of regulation.* Biochem Pharmacol, 2013. **85**(6): p. 705-17.
120. Jaramillo, M.C. and D.D. Zhang, *The emerging role of the Nrf2-Keap1 signaling pathway in cancer.* Genes Dev, 2013. **27**(20): p. 2179-91.

121. Hybertson, B.M., et al., *Oxidative stress in health and disease: the therapeutic potential of Nrf2 activation.* Mol Aspects Med, 2011. **32**(4-6): p. 234-46.
122. Rushworth, S.A., D.J. MacEwan, and M.A. O'Connell, *Lipopolysaccharide-induced expression of NAD(P)H:quinone oxidoreductase 1 and heme oxygenase-1 protects against excessive inflammatory responses in human monocytes.* J Immunol, 2008. **181**(10): p. 6730-7.
123. Li, W., et al., *Activation of Nrf2-antioxidant signaling attenuates NFkappaB-inflammatory response and elicits apoptosis.* Biochem Pharmacol, 2008. **76**(11): p. 1485-9.
124. Steel, R., et al., *Anti-inflammatory Effect of a Cell-Penetrating Peptide Targeting the Nrf2/Keap1 Interaction.* ACS Med Chem Lett, 2012. **3**(5): p. 407-410.
125. Surh, Y.J. and H.K. Na, *NF-kappaB and Nrf2 as prime molecular targets for chemoprevention and cytoprotection with anti-inflammatory and antioxidant phytochemicals.* Genes Nutr, 2008. **2**(4): p. 313-7.
126. Kensler, T.W., N. Wakabayashi, and S. Biswal, *Cell survival responses to environmental stresses via the Keap1-Nrf2-ARE pathway.* Annu Rev Pharmacol Toxicol, 2007. **47**: p. 89-116.
127. Shibata, T., et al., *Cancer related mutations in NRF2 impair its recognition by Keap1-Cul3 E3 ligase and promote malignancy.* Proc Natl Acad Sci U S A, 2008. **105**(36): p. 13568-73.
128. Lister, A., et al., *Nrf2 is overexpressed in pancreatic cancer: implications for cell proliferation and therapy.* Mol Cancer, 2011. **10**: p. 37.
129. Zhang, D.D. and M. Hannink, *Distinct cysteine residues in Keap1 are required for Keap1-dependent ubiquitination of Nrf2 and for stabilization of Nrf2 by chemopreventive agents and oxidative stress.* Mol Cell Biol, 2003. **23**(22): p. 8137-51.
130. Shen, G. and A.N. Kong, *Nrf2 plays an important role in coordinated regulation of Phase II drug metabolism enzymes and Phase III drug transporters.* Biopharm Drug Dispos, 2009. **30**(7): p. 345-55.
131. Aleksunes, L.M., et al., *Induction of Mrp3 and Mrp4 transporters during acetaminophen hepatotoxicity is dependent on Nrf2.* Toxicol Appl Pharmacol, 2008. **226**(1): p. 74-83.
132. Das, B.N., Y.W. Kim, and Y.S. Keum, *Mechanisms of Nrf2/Keap1-dependent phase II cytoprotective and detoxifying gene expression and potential cellular targets of chemopreventive isothiocyanates.* Oxid Med Cell Longev. **2013**: p. 839409.
133. Fukutomi, T., et al., *Kinetic, thermodynamic, and structural characterizations of the association between Nrf2-DLGex degron and Keap1.* Mol Cell Biol, 2014. **34**(5): p. 832-46.
134. Tong, K.I., et al., *Keap1 recruits Neh2 through binding to ETGE and DLG motifs: characterization of the two-site molecular recognition model.* Mol Cell Biol, 2006. **26**(8): p. 2887-900.
135. Itoh, K., et al., *Keap1 regulates both cytoplasmic-nuclear shuttling and degradation of Nrf2 in response to electrophiles.* Genes Cells, 2003. **8**(4): p. 379-91.
136. Kobayashi, M. and M. Yamamoto, *Molecular mechanisms activating the Nrf2-Keap1 pathway of antioxidant gene regulation.* Antioxid Redox Signal, 2005. **7**(3-4): p. 385-94.
137. Zhang, D.D., et al., *Keap1 is a redox-regulated substrate adaptor protein for a Cul3-dependent ubiquitin ligase complex.* Mol Cell Biol, 2004. **24**(24): p. 10941-53.

138. Ogura, T., et al., *Keap1 is a forked-stem dimer structure with two large spheres enclosing the intervening, double glycine repeat, and C-terminal domains.* Proc Natl Acad Sci U S A, 2010. **107**(7): p. 2842-7.
139. Brigelius-Flohe, R. and A. Banning, *Part of the series: from dietary antioxidants to regulators in cellular signaling and gene regulation. Sulforaphane and selenium, partners in adaptive response and prevention of cancer.* Free Radic Res, 2006. **40**(8): p. 775-87.
140. Ma, Q., *Role of nrf2 in oxidative stress and toxicity.* Annu Rev Pharmacol Toxicol, 2013. **53**: p. 401-26.
141. Lu, Y., X.H. Zhang, and A.I. Cederbaum, *Ethanol induction of CYP2A5: role of CYP2E1-ROS-Nrf2 pathway.* Toxicol Sci, 2012. **128**(2): p. 427-38.
142. Abu-Bakar, A., et al., *Regulation of CYP2A5 gene by the transcription factor nuclear factor (erythroid-derived 2)-like 2.* Drug Metab Dispos, 2007. **35**(5): p. 787-94.
143. Velichkova, M. and T. Hasson, *Keap1 regulates the oxidation-sensitive shuttling of Nrf2 into and out of the nucleus via a Crm1-dependent nuclear export mechanism.* Mol Cell Biol, 2005. **25**(11): p. 4501-13.
144. Nguyen, T., et al., *Nrf2 controls constitutive and inducible expression of ARE-driven genes through a dynamic pathway involving nucleocytoplasmic shuttling by Keap1.* J Biol Chem, 2005. **280**(37): p. 32485-92.
145. Zhao, R., et al., *Cross-regulations among NRFs and KEAP1 and effects of their silencing on arsenic-induced antioxidant response and cytotoxicity in human keratinocytes.* Environ Health Perspect, 2012. **120**(4): p. 583-9.
146. Lau, A., et al., *Dual roles of Nrf2 in cancer.* Pharmacol Res, 2008. **58**(5-6): p. 262-70.
147. Zhang, M., et al., *Emerging roles of Nrf2 and phase II antioxidant enzymes in neuroprotection.* Prog Neurobiol, 2013. **100**: p. 30-47.
148. Reddy, N.M., et al., *Deficiency in Nrf2-GSH signaling impairs type II cell growth and enhances sensitivity to oxidants.* Am J Respir Cell Mol Biol, 2007. **37**(1): p. 3-8.
149. Kim, H.J. and N.D. Vaziri, *Contribution of impaired Nrf2-Keap1 pathway to oxidative stress and inflammation in chronic renal failure.* Am J Physiol Renal Physiol, 2009. **298**(3): p. F662-71.
150. Yamamoto, T., et al., *Physiological significance of reactive cysteine residues of Keap1 in determining Nrf2 activity.* Mol Cell Biol, 2008. **28**(8): p. 2758-70.
151. Wang, R., et al., *Hypermethylation of the Keap1 gene in human lung cancer cell lines and lung cancer tissues.* Biochem Biophys Res Commun, 2008. **373**(1): p. 151-4.
152. Muscarella, L.A., et al., *Regulation of KEAP1 expression by promoter methylation in malignant gliomas and association with patient's outcome.* Epigenetics, 2011. **6**(3): p. 317-25.
153. Hanada, N., et al., *Methylation of the KEAP1 gene promoter region in human colorectal cancer.* BMC Cancer, 2012. **12**: p. 66.
154. Barbano, R., et al., *Aberrant Keap1 methylation in breast cancer and association with clinicopathological features.* Epigenetics, 2013. **8**(1): p. 105-12.
155. Zhang, P., et al., *Loss of Kelch-like ECH-associated protein 1 function in prostate cancer cells causes chemoresistance and radioresistance and promotes tumor growth.* Mol Cancer Ther, 2010. **9**(2): p. 336-46.

156. Karasek, M., et al., *Melatonin inhibits growth of diethylstilbestrol-induced prolactin-secreting pituitary tumor in vitro: possible involvement of nuclear RZR/ROR receptors.* J Pineal Res, 2003. **34**(4): p. 294-6.
157. Puissegur, M.P., et al., *miR-210 is overexpressed in late stages of lung cancer and mediates mitochondrial alterations associated with modulation of HIF-1 activity.* Cell Death Differ, 2011. **18**(3): p. 465-78.
158. Bostick, M., et al., *UHRF1 plays a role in maintaining DNA methylation in mammalian cells.* Science, 2007. **317**(5845): p. 1760-4.
159. Bronner, C., et al., *UHRF1 Links the Histone code and DNA Methylation to ensure Faithful Epigenetic Memory Inheritance.* Genet Epigenet, 2010. **2009**(2): p. 29-36.
160. Ehrlich, M., *Cancer-linked DNA hypomethylation and its relationship to hypermethylation.* Curr Top Microbiol Immunol, 2006. **310**: p. 251-74.
161. Xu, T., et al., *Dual roles of sulforaphane in cancer treatment.* Anticancer Agents Med Chem, 2012. **12**(9): p. 1132-42.
162. Itoh, K., et al., *Transcription factor Nrf2 regulates inflammation by mediating the effect of 15-deoxy-Delta(12,14)-prostaglandin j(2).* Mol Cell Biol, 2004. **24**(1): p. 36-45.
163. Segura-Pacheco, B., et al., *Reactivation of tumor suppressor genes by the cardiovascular drugs hydralazine and procainamide and their potential use in cancer therapy.* Clin Cancer Res, 2003. **9**(5): p. 1596-603.
164. Chowdhury, S., S. Ammanamanchi, and G.M. Howell, *Epigenetic Targeting of Transforming Growth Factor beta Receptor II and Implications for Cancer Therapy.* Mol Cell Pharmacol, 2009. **1**(1): p. 57-70.
165. Neureiter, D., et al., *Epigenetics and pancreatic cancer: pathophysiology and novel treatment aspects.* World J Gastroenterol, 2014. **20**(24): p. 7830-48.
166. Wang, X.J., et al., *Oxaliplatin activates the Keap1/Nrf2 antioxidant system conferring protection against the cytotoxicity of anticancer drugs.* Free Radic Biol Med, 2014. **70**: p. 68-77.
167. Kubisch, J., et al., *Complex regulation of autophagy in cancer - integrated approaches to discover the networks that hold a double-edged sword.* Semin Cancer Biol, 2013. **23**(4): p. 252-61.
168. Acharya, A., et al., *Redox regulation in cancer: a double-edged sword with therapeutic potential.* Oxid Med Cell Longev, 2010. **3**(1): p. 23-34.